DEPARTMENT OF PHYSICS

TECHNISCHE UNIVERSITÄT MÜNCHEN

MAX-PLANCK-INSTITUT FÜR PHYSIK
(WERNER-HEISENBERG-INSTITUT)

Master's Thesis in Nuclear, Particle and Astrophysics

Simulation, Data Challenge, and Analysis of First KATRIN Tritium Data

Pablo Israel Morales Guzmán

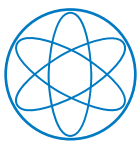

DEPARTMENT OF PHYSICS

TECHNISCHE UNIVERSITÄT MÜNCHEN

MAX-PLANCK-INSTITUT FÜR PHYSIK
(WERNER-HEISENBERG-INSTITUT)

Master's Thesis in Nuclear, Particle and Astrophysics

Simulation, Data Challenge, and Analysis of First KATRIN Tritium Data

Simulation, Datenherausforderung und Analyse der ersten KATRIN Tritium Daten

Author:	Pablo Israel Morales Guzmán
Supervisor:	Dr. Thierry Lasserre (CEA - TUM - IAS)
Chair:	Prof. Susanne Mertens
Submission Date:	02.10.2018

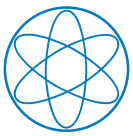

I confirm that this master's thesis in nuclear, particle and astrophysics is my own work and I have documented all sources and material used.

Munich, 02.10.2018 Pablo Israel Morales Guzmán

Acknowledgments

There are several persons and organizations without whom the present work would not have been at all possible, and persons who were of great help and had a significant effect in the improvement of this work. I would like to thank all of them for enabling such an enlightening experience, and in particular:

- Dr. Thierry Lasserre for the careful and extensive support and guidance given during my master's project, and for the teachings in experimental physics.

- Prof. Susanne Mertens for accepting me in the group, first as HiWi and then as master's student, and introducing me to the world of neutrino physics.

- Dr. Martin Slézak, for installing MATLAB® in the MPP server, and maintaining it, and for helpful comments about the statistics of KATRIN.

- All members of the MPP-Container who work in KATRIN/TRISTAN, for showing me the interactions within a physics research group, and letting me learn about experimental physics research through your work. Special thanks to the other member of the SAMAK team, Lisa, for providing the covariance matrices used in this thesis, as well as for the discussions to improve the SAMAK code.

- The Mexican citizens, who enable the development of scientific projects of basic science such as this, by allowing that their taxes are used for granting scholarships by the CONACyT (Consejo Nacional de Ciencia y Tecnología). Explicitly, I was benefited with the DAAD-CONACyT scholarship with number 438642, and registry number 600718.

- The DAAD (Deutsche Akademische Austausch Dienst), which together with CONACyT, provided me the scholarship for my master's studies.

- The MPP (Max-Planck-Institut für Physik) for providing financial support to attend various conferences and meetings in Germany.

- A mis amigos mexicanos en Múnich, en México, y en el resto del mundo, por darme ese esparcimiento y apoyo necesario para poder seguir con la tesis, y hacer sentir a casa un poco más cerca.

- Madlen für die unschätzbare Hilfe, als ich in der Klemme war, y por proveerme constantemente de retos para mi mejoramiento continuo.

- A mi impresionante familia, especialmente mi madre y padre, Isabel y Pablo, y mis hermanas y hermano, Inti, Itzel y Emmanuel, por apoyarme desde siempre y alentarme a perseguir un título en Alemania, a unos 9000 km de casa.

Abstract

The KATRIN Experiment strives to improve the knowledge of the effective electron anti-neutrino mass, by determining it with a sensitivity of 200 meV at 90 % C.L.

This master's thesis gives an insight into a new analysis software for the KATRIN Collaboration, SAMAK, and applies it to analyze the first KATRIN tritium data. Special focus is given to the estimation of tritium gas density in the windowless gaseous tritium source of KATRIN, and the determination of the effective endpoint of the tritium β-decay spectrum, where it is shown that an exhaustive understanding of the systematic uncertainties is critical for the correct interpretation of the experimental results.

Furthermore, SAMAK is used to perform sensitivity studies on the neutrino mass using the most updated information on the background of the experiment. Lastly, SAMAK participated in a series of validation processes called "data challenges", where analysis results where compared among different analysis packages within the KATRIN Collaboration.

Contents

1 Introduction

In this thesis, three concepts are mentioned recurrently throughout: KATRIN, SAMAK and the First Tritium Campaign. I want to introduce them casually to the reader here, so that they become familiar early on and the information presented hereafter can be more fluently followed.

1.1 KATRIN and neutrinos

KATRIN stands for KArlsruhe TRItrium Neutrino (Experiment). It is a large Neutrino Physics Experiment, around 70 m in total length, located very close to Karlsruhe, Germany, whose main objective is to find the effective mass of the electron antineutrino, or set upper limits to it. Parallel to or after the main KATRIN measurements, other goals are to provide new information about sterile neutrinos in the eV and keV range (for a mass smaller than the endpoint of the tritium spectrum), about the tritium spectrum itself (endpoint, Final States Distributions), and to confirm the effectiveness of new technology. This is the experiment whose data I analyze in this thesis. More details about the experimental set-up are in chapter 3.

The neutrino is a neutral particle first proposed by W. Pauli in 1930 [Pau], as a product of the β-decay. It only interacts through gravity and the weak interaction. At first, it seemed convenient to treat is as a massless particle, but relatively recently, around the year 2000, several experiments indicated that neutrinos undergo a phenomenon called "neutrino oscillations" [Ahm+02], which means they have a mass, even if small compared to other elementary particles.

The probability of the neutrino interacting with other particles is relatively low, so that it is possible for a neutrino to go through one light-year[1] of lead without interacting [Dav87]. For this reason, neutrinos have been dubbed the "ghost particles". More on the history and physics of the neutrinos in chapter 2.

Discoveries that have something to do with neutrinos have the potential to be quite important in fundamental physics. At least four Nobel Prizes (as of 2018) have been awarded to research about neutrinos [AB18]; and they are one of the keys to unravel physics beyond the Standard Model.

[1] 9.46×10^{15}m or some 800 times the size of the solar system (average distance Sun to Pluto [NAS15]).

1.2 SAMAK Analysis Software

SAMAK stands for Simulation and Analysis with MATLAB® for KATRIN. It is a software package written in (of course) MATLAB® by Dr. Thierry Lasserre from CEA Saclay. Its purpose is to do analysis for KATRIN. It can simulate the tritium spectrum as well as fit the data generated by KATRIN. SAMAK has been greatly developed since I started working with the code more than one year ago, and every now and then a new feature is added, making it more robust and complex. The coding in MATLAB® is relatively flexible, so it is not hard to implement new corrections and add components. In this way, SAMAK can be used to give results in a short time frame and help guide the experimental procedures and further analytic efforts.

I have assisted in the development of some fragments of the code, which will be mentioned in this thesis. Some of the items I have worked with are the implementation of the Doppler Effect, the display of the Focal Plane Detector view, reading KATRIN data (HDF5 and/or Run Summaries), parallelization, use of a minimizer that can handle more than 150 parameters for multipixel fits, flexibility to change between different analysis types (single-pixel, multipixel, etc.), technical work on the storage and handling of the response function of KATRIN, standardizing the fitting procedure, and some work to move SAMAK to the Git version control system. More details on the tritium model in SAMAK are in chapter 4, on the fitting in chapter 6, and types of analysis in chapter 5.

1.3 First Tritium Campaign

The First Tritium Campaign is a period of two weeks in Spring 2018 where tritium was injected in the KATRIN Source. After many years (the Design Report of KATRIN dates back to 2004) of planning, building, doing simulations, fine-tuning of components, etc., real measurements using tritium were done for the first time. Although the conditions were to some extent different to what is planned for the three-year measurement period, the First Tritium Campaign delivered very nice and useful results; both to test and confirm the correct functioning of the hardware, and to test and further develop the different analysis tools. More material related to the First Tritium Campaign can be found in chapter 9.

1.4 Thesis Outline

First I present a summary of the history and phyiscs of the neutrino. I then explain the KATRIN Experiment, followed by how the tritium β-decay spectrum is built in SAMAK. Afterwards I turn my attention to the explanation of the analysis and statistical methods used in SAMAK. Finally I present some applications of SAMAK, i.e. sensitivity studies, Data Challenges and diverse analysis using the data from the First Tritium Campaign.

2 Neutrino Physics

Since their postulation almost 90 years ago, neutrinos have been involved in the development of new physics, expanding our knowledge of nature, and defying some established physical theories and concepts.

Knowing and understanding something is good, but being actually on the way of understading it, is more interesting. Physicist who study neutrinos are for sure in this path. Dark Matter candidates (through sterile neutrino [Boy+18]), absolute neutrino mass [Col05], multimessenger astronomy[1] and production of cosmogenic neutrinos (recently found by IceCube [Col+18]), and communication using neutrinos [Sta+12] are just some of the unresolved topics relating to neutrino physics.

In the next chapters I follow historically the origins of the development of neutrino physics in sec. 2.1. Afterwards, in sec. 2.2, I expose the mathematical description of neutrino oscillations; and in secs. 2.3 and 2.4 we have a look at the theory of the absolute neutrino mass, and the limits that have been set on it so far.

2.1 Discovery of the neutrino

2.1.1 The particle of Wolfgang Pauli

It all started in the prelude of winter in 1930 near the Alps. There, Wolfgang Pauli wrote the decisive letter that would give the world a new elementary particle to think about [Pau]. Previously, experiments regarding β-decays had shown unexpected results. At that time, the β-decay was thought to be a two-body decay, which would result in a peak in the energy spectrum of the emitted β-electron. It turned out that the spectrum of the β-decay electron was a continuous one, for example that of radium in fig. 2.1 [Sco35]. Wolfgang P. came up with the idea that there was a third particle in the β-decay game, making it a three-body decay. This particle should be electrically neutral, with spin 1/2, should obey the exclusion principle, and could not travel as fast as light. This particle would solve the conundrums posed by the continuous β-decay spectrum, namely the violation of conservation of energy and

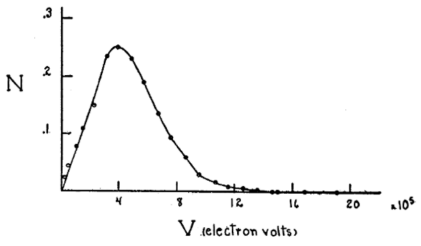

Figure 2.1 | **Radium β-decay.** β-decay energy spectrum of the emitted electron from radium decay, from [Sco35].

[1] Observations done with electromagnetic radiation, gravitational waves, cosmic rays and neutrinos.

spin. He arbitrarily named this particle the "neutron". Two years later a neutral particle was discovered and named neutron, but it was too massive to be the one suggested by Wolfgang P. Two more years passed, and Enrico Fermi coined a new term for that particle: "neutrino" [Fer34], meaning "little neutron" in Italian (probably since it was less massive than the neutron). The formula describing the β-decay is then

$$n \rightarrow p + e^- + \bar{\nu}_e \tag{2.1}$$

where n is the neutron, p the proton, e^- the electron, and $\bar{\nu}_e$ represents the electron anti-neutrino.

2.1.2 Neutrinos Flavors

Electron neutrino

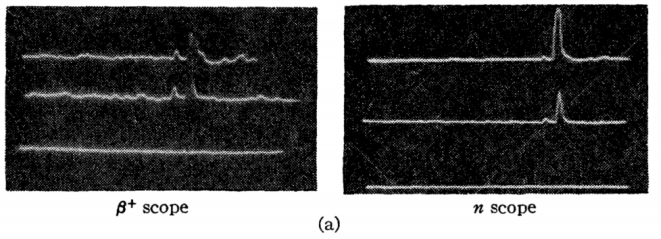

Figure 2.2 | **Cowan and Reines detection of the neutrino.** Events with a delay of 2.5 μs, the first pulse has energies of 0.3 and 0.35 MeV. The second pulse has energies of 5.8 and 3.3 MeV. Figure from [Rei+60].

C. Cowan and F. Reines were the first to detect a neutrino [Cow+56], using the inverse β-decay

$$\bar{\nu}_e + p \rightarrow n + e^+, \tag{2.2}$$

where a neutron and a positron e^+ are produced. The experiment was set near the Savannah river nuclear power plant. The detector they used was a series of liquid scintillator tanks separated by cadmium-loaded water targets. The expected signal was very clear and could not be confused with other events. In the reaction, the positron created annihilates with an electron producing two γ-rays with energy $E_\gamma = 511$ keV each. Between 0.75 and 30 μs later, the neutron thermalizes and is captured by the cadmium, which decays emitting γ-rays. An example of a valid β-decay signal recorded is in fig. 2.2. Reines was awarded the Nobel Prize in 1995 for this experiment, by which time Cowan had already passed away.

Muon neutrino

Using the decay of pions π^+ into muons μ^+ and muon neutrinos ν_μ

$$\pi^+ \rightarrow \mu^+ + \nu_\mu, \tag{2.3}$$

L.M. Lederman, M. Schwartz and J. Steinberger detected the muon neutrino in 1962 at the Brookhaven Alternating Gradient Synchrotron (AGS) [Dan+62]. During several months, around 3.5 $\times 10^{17}$ protons hit a beryllium target, producing pions in the process.

The pions decayed into muons and muons neutrinos. All particles except the neutrinos were stopped by a steel wall, leaving a "neutrino beam" in direction of a spark chamber. Occasionally one of the neutrinos would interact with a proton in an aluminum nucleus, producing a neutron and an electron or muon. Since only muons were detected in the spark chamber, it was concluded that the neutrinos produced in the reaction were different from the electron neutrinos (otherwise, electrons and muons would have been produced in equal quantities). For this finding, the Nobel Prize was awarded in 1988[2].

Tau neutrino

The tau neutrino was quite more elusive than the other two. It was not until the new millennium that it could be found. In 2000 in the DONUT (Direct Observation of Nu Tau[3]) Experiment in Fermilab [Kod+01], a proton beam was fired at a tungsten target, which created a particle shower. Some of the particles were taus, which decayed into, among other particles, tau neutrinos.

All but the tau neutrinos were stopped using a dedicated shield. The tau neutrinos entered an emulsion lead target were they interacted with neutrons to produce protons and taus. The latter leave a short track in the emulsion due to their short half life, producing a characteristic signal with which they can be identified.

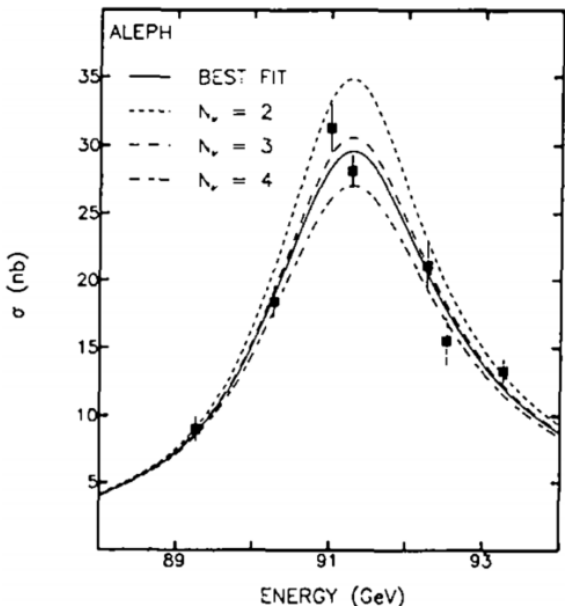

Figure 2.3 | **Z boson 91 GeV resonance.** Cross-section for $e_+ + e_- \rightarrow$ hadron in dependence of center of mass energy. The fitted curve is a result of a three parameter fit. Shown are the curves for one, two and three neutrino species, and the best fit at 3.27 ± 0.3. Figure from [DeC+89].

Just three neutrino flavors

Since 1989, the ALEPH Experiment had already determined that there were only three neutrino flavors [DeC+89]. The proof is the invisible width of the Z Boson resonance at 91 GeV, which is seen as a peak of the total cross section of the electron positron

[2]Curiously 7 years **before** the Nobel Prize for the electron antineutrino.
[3]Clever selection of words.

scattering. It depends on the number of neutrinos flavors available, and the best fit (fig. 2.3) excludes the possibility of more than three neutrino flavors.

2.2 Neutrino oscillations

The fact that neutrinos oscillate, meaning that they can be detected in a different flavor from the one in which they were produced, proves that they are outside of the successful Standard Model. They also invoke the necessity of neutrinos having a non-zero mass, since the mass eigenstates must be different (so not all of them can be zero). First suggested by Pontecorvo in 1957 [Pon57], it was not until 2002 that they were finally confirmed by the SNO Experiment.

Solar neutrino problem

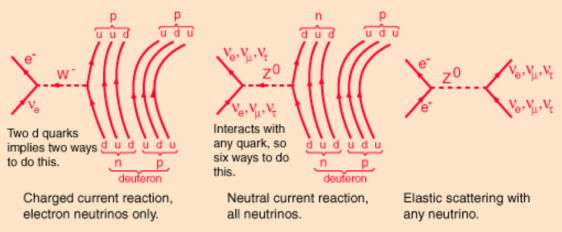

Figure 2.4 | **Neutrino interactions in SNO.** Possible interactions with the charged and neutral current between neutrinos, quarks, and leptons, in the SNO Experiment. Figure from [Nav16b].

Neutrinos are produced in the sun via the pp-chain and CNO-cycle. Since 1970 the neutrino flux from the sun has been measured by several experiments in different time periods. The first one was the Homestake Experiment [Cle+98], which encountered a neutrino rate lower than expected by the Solar Standard Model[4]. These findings were confirmed in the following years by several other experiments, namely (in parenthesis the date of publication) Gallex/GNO (2005) [Alt+05], SAGE (2002) [Abd+02], and Kamiokande (1996) [Fuk+96]. This problem was definitely considered solved by the Sudbury Neutrino Observatory (SNO) [Ahm+02], which contained 1 kiloton of heavy water D_2O. SNO took advantage of the interaction of all neutrinos flavors with deuterium through the neutral current. The measured reactions were

$$\nu_e + n + p \rightarrow e^- + p + p \qquad \text{(charged current)} \tag{2.4}$$

$$\nu_x + n + p \rightarrow \nu_x + n + p \qquad \text{(neutral current)} \tag{2.5}$$

$$\nu_x + e_- \rightarrow \nu_x + e^- \qquad \text{(elastic scattering)}, \tag{2.6}$$

where ν_x is any type of neutrino, p are protons, n are neutrons and e^- are electrons (fig. 2.4). The total measured flux from all three neutrino flavors was consistent with the Solar Standard Model. Thus, neutrino oscillations were confirmed and the solar neutrino problem was solved.

[4]For an overview of the Solar Standard Model, see for example [Tur16].

2.2.1 Brief theoretical description

Neutrino undergo oscillations because their flavor eigenstates and mass eigenstates are not tantamount, and can be represented in either of the two bases. The flavor eigenstates are the ones that participate in the weak interaction through the coupling to the W and Z bosons; the mass eigenstates are the ones traveling through spacetime.

Now, it is appropriate to introduce the famous Pontecorvo-Maki-Nakagawa-Sakata (PMNS) matrix U, that relates the flavor eigensates ν_e, ν_μ, ν_τ to the mass eigenstates ν_1, ν_2, ν_3 of the neutrino,

$$\begin{bmatrix} \nu_e \\ \nu_\mu \\ \nu_\tau \end{bmatrix} = \begin{bmatrix} U_{e1} & U_{e2} & U_{e3} \\ U_{\mu 1} & U_{\mu 2} & U_{\mu 3} \\ U_{\tau 1} & U_{\tau 2} & U_{\tau 3} \end{bmatrix} \begin{bmatrix} \nu_1 \\ \nu_2 \\ \nu_3 \end{bmatrix}. \tag{2.7}$$

It can be parametrized by three mixing angles θ_{ij} and a complex Dirac phase δ_D, and if the neutrinos were Majorana particles (their own antiparticles), there are two extra complex Majorana phases δ_M.

$$U = \begin{bmatrix} 1 & 0 & 0 \\ 0 & c_{23} & s_{23} \\ 0 & -s_{23} & c_{23} \end{bmatrix} \begin{bmatrix} c_{13} & 0 & s_{13}e^{-i\delta_D} \\ 0 & 1 & 0 \\ -s_{13}e^{i\delta_D} & 0 & c_{13} \end{bmatrix} \begin{bmatrix} c_{12} & s_{12} & 0 \\ -s_{12} & c_{12} & 0 \\ 0 & 0 & 1 \end{bmatrix} \begin{bmatrix} e^{i\delta_{M1}} & 0 & 0 \\ 0 & e^{i\delta_{M2}} & 0 \\ 0 & 0 & 1 \end{bmatrix},$$

where $c_{ij} = \cos\theta_{ij}$ and $s_{ij} = \sin\theta_{ij}$.

Concepts are normally made clearer with examples, so let us take the case of the creation of an electron neutrino at time $t = 0$,

$$\left|\nu(t=0)\right\rangle = \left|\nu_e\right\rangle = U_{e1}\left|\nu_1\right\rangle + U_{e2}\left|\nu_2\right\rangle + U_{e3}\left|\nu_3\right\rangle. \tag{2.8}$$

As time progresses $t > 0$, the neutrino evolves as plane waves[5]

$$\left|\nu(t>0)\right\rangle = U_{e1}e^{-iE_1 t}\left|\nu_1\right\rangle + U_{e2}e^{-iE_2 t}\left|\nu_2\right\rangle + U_{e3}e^{-iE_3 t}\left|\nu_3\right\rangle, \tag{2.9}$$

which is no longer an electron neutrino, but a superposition of all flavor states. Therefore, there is a probability of the neutrino interacting weakly (and being detected) as another flavor. This probability P can be used in experiments to determine the oscillation parameters, and it is given by

$$P(\nu_{\alpha\to\beta}(t)) = |\left\langle \nu_\beta \middle| \nu_\alpha \right\rangle|^2, \tag{2.10}$$

where α and β are any two different flavor eigenstates. One can also express the mass eigenstates in terms of the flavor eigenstates

[5] In eq. 2.8, $|\nu_i\rangle$, $i = 1, 2, 3$ are eigenstates of the Hamiltonian, whose eigenvalue is $E_i = \sqrt{\vec{p_i}^2 + m^2}$.

$$|\nu_\alpha\rangle = \sum_i U_{\alpha i} e^{-E_i t} |\nu_i\rangle \tag{2.11}$$

$$= \sum_i U_{\alpha i} e^{-E_i t} \left(\sum_{\beta=e,\mu,\tau} U^*_\beta \left|\nu_\beta\right\rangle \right) \tag{2.12}$$

$$= \sum_\beta \left(\sum_i U_{\alpha i} e^{-E_i t} U^*_{i\beta} \right) \left|\nu_\beta\right\rangle . \tag{2.13}$$

Combining eqs. 2.10 and 2.13, one obtains

$$P(\nu_{\alpha\to\beta}(t)) = P_{\alpha\beta}(t) = |\sum_i U_{\alpha i} e^{-E_i t} U^*_{i\beta}|^2 \tag{2.14}$$

$$= \sum_{ij} U_{\alpha i} U^*_{i\beta} U^*_{\alpha j} U_{j\beta} e^{-i(E_i - E_j)t}. \tag{2.15}$$

If one makes the assumption that the neutrinos travel close to the speed of light, and thus are ultrarelativistic, so $p_i = p = E$ and $t = L$ leaving as a result

$$P_{\alpha\beta}(L/E) = \sum_{ij} U_{\alpha i} U^*_{i\beta} U^*_{\alpha j} U_{j\beta} e^{-i\Delta m^2_{ij} \frac{L}{2E}}. \tag{2.16}$$

Considering only two neutrinos to simplify things, for example ν_e and ν_μ the probability can be given by the uncomplicated form

$$P_{\nu_{e\to\mu}} = \sin^2(2\theta_{12}) \sin^2 \left(\frac{\Delta m^2_{12} L}{4E} \right). \tag{2.17}$$

The above equation shows how the amplitude on the oscillation probability depends on the mixing parameters, and the frequency is given by the difference of the squared neutrino masses. Also important to note is that experiments that study neutrino oscillations can only make an statement on the difference of the squared neutrino masses, but not on the absolute value of them. At most, they can give a lower limit on one of the masses.

Mass hierarchy

From the oscillation experiments, one cannot know the sign of the mass difference Δm^2_{13}. Therefore it is unclear if the masses have a normal hierarchy ($m_1 < m_2 < m_3$) or inverted hierarchy ($m_3 < m_1 < m_2$). This phenomenon will be investigated by the IceCube-PINGU Experiment [Win13].

2.2.2 Neutrino Oscillation Experiments

All parameters of the PMNS matrix have been determined experimentally, except for the Majorana terms. The angle θ_{12} "solar mixing angle" was determined using a mixture of solar and reactor neturinos [Abe+11]; the angle θ_{13} "the reactor mixing angle" was calculated independently by three experiments Double-Chooz [Abe+12a], Daya bay [Abe+12b] and RENO [Ahn+12]; and the angle θ_{23} ("atmospheric mixing angle") was determined by the Super-Kamiokande Experiment [Wen+10].

The most recent fit results provided in NuFIT (supported by the European Union's Horizon 2020 research and innovation programme under the Marie Sklodowska-Curie grant agreement No 674896 "ELUSIVES") is given in [Est+17], and can be seen in fig. 2.5.

	Normal Ordering (best fit)		Inverted Ordering ($\Delta\chi^2 = 0.83$)		Any Ordering
	bfp $\pm 1\sigma$	3σ range	bfp $\pm 1\sigma$	3σ range	3σ range
$\sin^2\theta_{12}$	$0.306^{+0.012}_{-0.012}$	$0.271 \to 0.345$	$0.306^{+0.012}_{-0.012}$	$0.271 \to 0.345$	$0.271 \to 0.345$
$\theta_{12}/^\circ$	$33.56^{+0.77}_{-0.75}$	$31.38 \to 35.99$	$33.56^{+0.77}_{-0.75}$	$31.38 \to 35.99$	$31.38 \to 35.99$
$\sin^2\theta_{23}$	$0.441^{+0.027}_{-0.021}$	$0.385 \to 0.635$	$0.587^{+0.020}_{-0.024}$	$0.393 \to 0.640$	$0.385 \to 0.638$
$\theta_{23}/^\circ$	$41.6^{+1.5}_{-1.2}$	$38.4 \to 52.8$	$50.0^{+1.1}_{-1.4}$	$38.8 \to 53.1$	$38.4 \to 53.0$
$\sin^2\theta_{13}$	$0.02166^{+0.00075}_{-0.00075}$	$0.01934 \to 0.02392$	$0.02179^{+0.00076}_{-0.00076}$	$0.01953 \to 0.02408$	$0.01934 \to 0.02397$
$\theta_{13}/^\circ$	$8.46^{+0.15}_{-0.15}$	$7.99 \to 8.90$	$8.49^{+0.15}_{-0.15}$	$8.03 \to 8.93$	$7.99 \to 8.91$
$\delta_{CP}/^\circ$	261^{+51}_{-59}	$0 \to 360$	277^{+40}_{-46}	$145 \to 391$	$0 \to 360$
$\frac{\Delta m^2_{21}}{10^{-5}\ \mathrm{eV}^2}$	$7.50^{+0.19}_{-0.17}$	$7.03 \to 8.09$	$7.50^{+0.19}_{-0.17}$	$7.03 \to 8.09$	$7.03 \to 8.09$
$\frac{\Delta m^2_{3\ell}}{10^{-3}\ \mathrm{eV}^2}$	$+2.524^{+0.039}_{-0.040}$	$+2.407 \to +2.643$	$-2.514^{+0.038}_{-0.041}$	$-2.635 \to -2.399$	$\begin{bmatrix} +2.407 \to +2.643 \\ -2.629 \to -2.405 \end{bmatrix}$

Figure 2.5 | **Oscillation parameters.** Three-flavor oscillation parameters from the fit to global data after the NOW 2016 and ICHEP-2016 conference from [Est+17]. Table from [Est+17].

2.3 Neutrino mass

With the discovery of neutrino oscillations it was confirmed that neutrinos should have a mass, but the mechanisms through which it can be obtained it are yet unclear. As a reminder, the upper limit on the neutrino mass [Lob+01] [Kra+05] is in the order of a few eV, five orders of magnitude smaller than the lightest charged lepton. To have the neutrino gain mass via the Higgs mechanism like the rest of the particles in the Standard Model, one would have to fine tune the parameters in the Yukawa coupling, which might be suspicious and is normally avoided in the physics community, but still possible. One should also introduce a right-handed neutrino ν_R, which could only

interact through gravity, also called "sterile neutrino". If the neutrino gets its mass this way, it would be called a Dirac particle.

Another popular possibility is the "Seesaw mechanism", in which the neutrino is assumed to be its own antiparticle, otherwise known as Majorana fermion. In that case, after introducing a right handed neutrino field with the mass term in the Lagrangian, the mass eigenstates from the matrix

$$\begin{bmatrix} 0 & m_D \\ m_D & M \end{bmatrix}, \tag{2.18}$$

have eigenvalues $m_1 \approx M$ and $m_2 \approx m_D^2/M$, if $M \gg m_D$. If m_1 is larger, m_2 turns smaller. For a neutrino mass in the eV range, the right handed neutrino mass should be of the order of GeV.

2.4 Limits on the neutrino mass

There are several procedures through which one can constrain the absolute value of the neutrino mass. Some depend on physical models, and some are independent, working only with kinematics. In this section I give an overview of the current limits set using different approaches.

2.4.1 Cosmology

The ΛCDM-Model dictates that the universe started out as an incredible dense and hot mix of particles confined in a small space. It started expanding at the Big Bang, and has not stopped since then, cooling down in the process. The particles in the mix can interact as long as their mean free path is smaller than the horizon size of the universe. As the universe expands and cools, the mean free path of all particles gets larger, at different rates. Each time the mean free path of a particle reaches and surpasses the horizon size of the universe, a process called "decoupling" occurs, in which the particles can stream freely.

The decoupling with the strongest evidence is the photon decoupling, leaving an important imprint known as the Cosmic Microwave Background Radiation (CMB) first discovered by Penzians and Wilson in 1965 [PW65]. That imprint of electromagnetic radiation in the microwave length which has a mean temperature of 2.7 K, with differences in the order of tens of μK.

Similarly, the neutrinos also had a decoupling, about 1 second after the Big Bang. The estimated density of this "relic neutrinos" is about 336 cm^{-3}, making it the second most abundant particle in the universe. Even if they had small masses, due to their density, the relic neutrinos could have an impact in the energy density of the universe [LP06].

The energy density Ω_ν from neutrinos can be expressed as

$$\Omega_\nu = \frac{\sum_i m_{\nu,i}}{93.14h^2\,\mathrm{eV}}, \tag{2.19}$$

where h is the dimensionless Hubble parameter [LP12]. The upper limit calculated fro this energy density by [Col+14] is

$$\sum_i m_{\nu,i} \leq 0.23\,\text{eV} \quad (95\%\text{C.L.}). \tag{2.20}$$

One should be careful with this result though, as it is based on cosmological models, which, even if carefully thought and analyzed, could be inaccurate.

2.4.2 Double-beta decay

If the neutrinos are Majorana particles, then in principle it is possible for the following reaction to occur

$$2n \rightarrow 2p + 2e^- \tag{2.21}$$

where the two neutrinos that should have been created, interacted as shown in fig. 2.6. This rare decay process is called neutrinoless double β-decay ($0\nu\beta\beta$). If measured, besides proving that the neutrino is its own antiparticle, it would also show that lepton number conservation is violated, which is definitely outside the realm of the Standard Model.

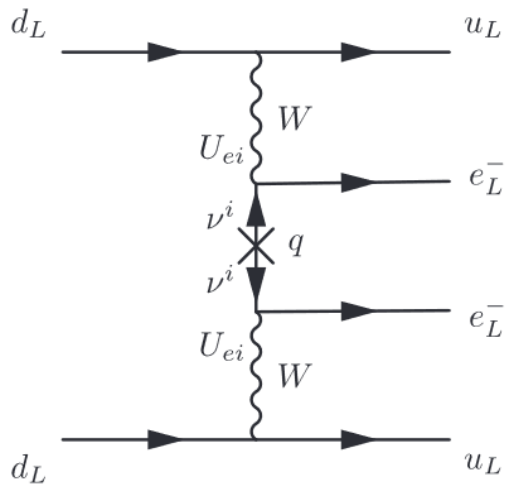

Figure 2.6 | $0\nu\beta\beta$. Feynman diagram for the standard mechanism of neutrinoless double β-decay. Figure from [PR15].

There are several experiments looking for a signal for this kind of decay [Hen16], for example GERDA or the MAJORANA DEMONSTRATOR using ^{76}Ge, or KamLAND-Zen using ^{136}Xe. An effective neutrino mass could be extracted from the results of this experiment by the relation

$$\Gamma_{0\nu\beta\beta} \propto m_{\beta\beta} = |\sum_i E_{ei}^2 m_i|, \tag{2.22}$$

where $\Gamma_{0\nu\beta\beta}$ is the rate of this decay process.

The lifetime of this decay was been measured by GERDA to be 3×10^{25} years (90 % C.L.), which entails a $m_{\beta\beta}$ of 0.2 to 0.4 eV [Ago+13]. Again, this value relies on decay models and the assumption that the neutrino is a Majorana particle, so one should be cautious with it.

2.4.3 Single-beta decay

The single beta decay relies only on kinematics and energy-momentum conservation, therefore it is the least model dependent method to estimate the value for the neutrino mass. The latest reported values are the ones by Troitsk and Mainz where the upper limit for the neutrino mass was established at 2.3 eV at 95 % C.L by Mainz. A detailed description of how the neutrino mass can be extracted from the single β-decay of tritium can be found in sec. 4.1.

3 The KATRIN Experiment

The main objective of the KATRIN (**KA**rlsruhe **TRI**tium **N**eutrino) Experiment is to determine or set new upper limits to the effective electron antineutrino mass. It will do so by using high precision spectroscopy in the zone near the endpoint E_0 of the tritium β-decay spectrum, where the distortion of the spectrum by the neutrino mass is most prominent, see fig. 3.1.

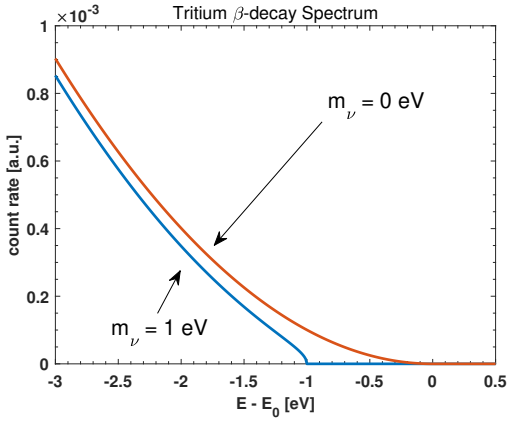

Figure 3.1 | **Tritium β-decay spectra with two different neutrino masses.** Two tritium β-decay spectra near the endpoint are shown. The red line is the spectrum with a neutrino mass of 0 eV, and the blue line is the spectrum with a neutrino mass of 1 eV.

The original design for KATRIN in 2004 envisioned a sensitivity for the neutrino mass of 200 meV with 90 % confidence level after three years of data taking [Col05], improving the last value found in the literature [Kra+05] [Lob+01] by one order of magnitude. This number was set assuming a background level of 10 mcps, and a systematic budget of 0.017 eV^2 attributed to the neutrino mass squared.

In the next sections I will give an overview of the workings of the KATRIN Experiment. Given that the KATRIN Experiment has been thoroughly explained in the Design Report [Col05] and in countless master's and PhD theses, I rather give the reader a leisure walk through the experiment from back to front (source to detector), seen in fig. 3.2, and focus on the most relevant elements for the present work.

3.1 Measurement principle and set-up

The measurement technique used in KATRIN is the MAC-E filtering, short for **M**agnetic **A**diabatic **C**ollimation with **E**lectrostatic filtering. The MAC-E Filter uses an electrostatic filter to only allow electrons from the source, with energies higher than a given retarding potential, to reach the detector. In this sense it is a high-pass filter. The "magnetic" part of the name comes from the fact that the β electrons are guided magnetically through the experiment by superconducting magnets. The magnetic fields also help to increase the count rate by adiabatically changing the direction of the momentum of the β-electrons

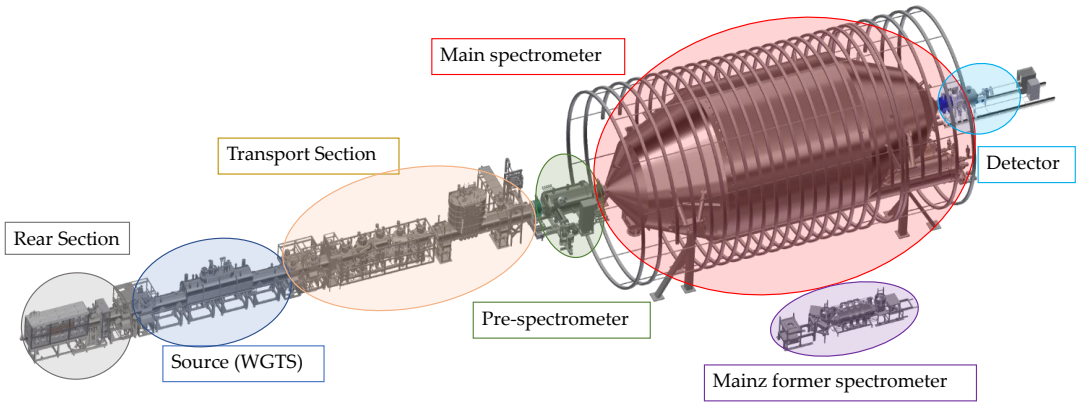

Figure 3.2 | **KATRIN Experimental set-up 2018.** Depiction of the complete KATRIN setup as of 2018. The main sections are highlighted. Figure from the KATRIN Collaboration.

(sec. 4.4.1). This technique allows for a good energy resolution near the endpoint. Since it only relies on the kinematics of the tritium β-decay, it is considered as **model independent**.

3.1.1 Rear Section

The rear section will house two Differential Pumping Sections to return the gaseous tritium to the outer loops. Furthermore, this section will have a Calibration and Monitoring System (CMS). The CMS will accomplish the tasks described in the following:

- Calibrate the detectors with the use of a ^{83m}Kr source.
- Investigate the transmission function (sec. 4.4.1) of the system and the energy dependence of the inelastic scattering cross section by the use of an electron gun with high resolution (around 0.2 eV).
- Define the electric potential of the source.
- Determine the β-electron flux with a monitor detector.

3.1.2 Windowless Gaseous Tritium Source

As the "TRI" in KATRIN indicates, tritium, the isotope of hydrogen with two neutrons, was chosen as the β-electron emitter. The decay for atomic tritium is as follows

$$^3_1\mathrm{H} \rightarrow ^3_2\mathrm{He}^+ + e^- + \bar{\nu}_e. \tag{3.1}$$

In KATRIN, however, molecular tritium is used, so the decay can be one of the following three

$$\mathrm{TT} \rightarrow (^3_2\mathrm{HeT})^+ + e^- + \bar{\nu}_e, \tag{3.2}$$

$$\mathrm{TD} \rightarrow (^3_2\mathrm{HeD})^+ + e^- + \bar{\nu}_e, \tag{3.3}$$

$$\mathrm{TH} \rightarrow (^3_2\mathrm{HeH})^+ + e^- + \bar{\nu}_e, \tag{3.4}$$

where T represents ^3_1H (tritium), D represents ^2_1H (deuterium), and H is just hydrogen. Each molecule produces a slightly different spectrum with a different endpoint due to different Final States Distributions, atomic masses and binding energies (see sec. 4.2). The plan is to have a molecular concentration of 90 % of TT, 5 % of DT and 5 % of HT [Col05]. This means that the atomic concentration (ratio of atoms of tritium to the total number of atoms) of tritium in the gas composition will be of 95 %, as DT and HT only contribute with half of tritium.

Tritium has already demonstrated in the past to be a good candidate for the determination of the neutrino mass [Kra+05] [Lob+01], and there are several good reasons for this choice. First of all, from the differential decay rate (eq. 4.16), one can see that the relative number of electrons with energies close to the endpoint decreases with the value of the endpoint. The rate scales as E_0^{-3}. Moreover, a low endpoint energy facilitates the technical implementation of the high voltage in the electrostatic filter. Molecular tritium has the second lowest endpoint of the β-electron emitters [Sle16] at $E_0 \approx 18.6$ keV.

Tritium can be kept in a gaseous form at the operating temperature of KATRIN, which is around 30 K [Col05]. One of the reasons this low temperature was chosen is to diminish the influence of the Doppler Effect, that would alter the energy resolution. Also gaseous tritium has lower systematic uncertainties in general.

Tritium β-decay is a superallowed transition[1], consequently the nuclear matrix element is independent from β-electron energy and the half-life of tritium is short, compared to other decaying elements, at 12.3 years. The latter allows to have a high luminosity[2] with relatively low density. The molecular density in the source impacts the scattering probabilities of the electrons traveling through the tube: as the density increases, the scattering probabilities also increase. The atomic number also affects the scattering probabilities but in an inverse fashion. In that sense, tritium has relatively less scattering, a consequence of the atomic number being equal to one. More scatterings lead to more energy loss and hence less electrons can go through the spectrometer, decreasing the statistics.

Finally the low Z value of tritium leads to a less complex nuclear structure compared to elements with more nucleons (which are almost all of the rest in the periodic table). This in turn makes the electronic final states relatively easy to obtain, and other atomic corrections affecting the tritium β-decay spectrum can be computed to a high precision (sec. 4.2).

[1] This happens when the mother and daughter are mirror nuclei of the same isospin doublet, where a large overlap of initial and final wave functions occur.

[2] One should have in mind that the number of decays is $N(t) = N_0(\frac{1}{2})^{\frac{t}{t_{1/2}}}$, so a smaller half-life leads to more decays on a shorter period of time.

Windowless Gaseous Tritium Source

The tritium gas is injected in the KATRIN Experiment through the middle of a section named **Windowless Gaseous Tritium Source (WGTS)**. The WGTS is a 10 m long tube with an inner diameter of 90 mm, in which the tritium molecules diffuse to both extrema, and are collected at both ends by Differential and Cryogenic Pumping Sections. These pumps take the gas out of the experiment, clean it, and return it to the WGTS, thus creating a closed loop.

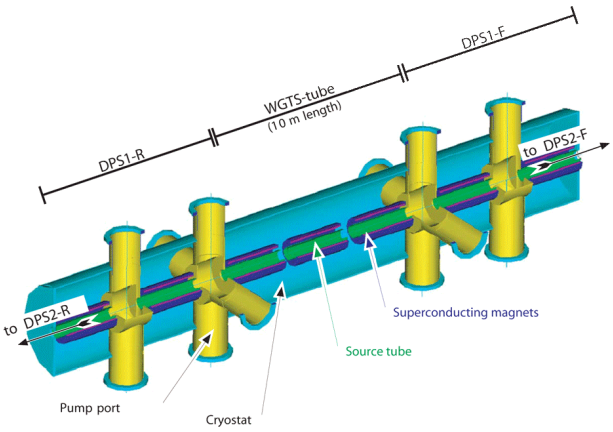

Figure 3.3 | **Schematic view of the WGTS.** The gas entres from the middle, indicated as "source tube", and goes to the pumping sections at both ends. Figure from [KAT99].

The density of the gas inside the WGTS is commonly referred as the **column density** or ρd. The column density is the non-linear gas density, integrated over the length of the tube [Sle16]. It is given in units of molecules/area.

One of the main challenges of the WGTS is to provide an ultra-stable source of β-decays, both in space and time. This enables a much more precise analysis of the data, by decreasing the systematic uncertainties. Let us list some of the most important elements that have to be stable.

- The column density of $5 \times 10^{17} \frac{\text{molecules}}{\text{cm}^2}$ enables a β-decay rate of 10^{11} decays/s, and has to be stable to a 0.01 % level, in relative.
- The temperature, once it acquires a value between 27 and 33 K, has to be kept in a permille level, relative. This has already been achieved using a novel 2 phase liquid neon thermosyphon [Gro+11].
- The pressure inside the WGTS affects directly the column density and also must not have relative changes larger than 1 in 1000. A specialized pressurized control vessel is used for this purpose.
- The isotopic purity of tritium should be high (>95 %) and be kept constant. The spectra of the different isotopologues of the tritium molecule are slightly different, so the isotopic composition of the gas should be very well known. The LARA (LAser-RAman) system measures the relative concentrations of the isotopomers in the gas every 200 seconds with a 0.1 % relative precision.
- The activity of the gas can also be measured independently by detecting the low energy β-electrons from the source using the **Forward Beam Monitor Detector**

(FBM), again with 0.1 % relative precision. The FBM is a small pin diode that lies close to the edge of the magnetic flux tube. A X-ray detector behind the rear plate will measure the Bremsstrahlung of the electrons hitting the plate, giving another handle on the source activity.

3.1.3 Transport Section

The transport section is in charge of retaining as much of the tritium gas as possible and not letting it to the spectrometer section, while at the same time letting all β-electrons go through with an adiabatic magnetic guidance. It achieves this goal by the use of two different pumping sections, and a "chicane" structure[3]. The goal is to reduce the tritium flow by at least 12 orders of magnitude, since tritium in the main spectrometer would be translated into background, which has to be kept as low as possible.

The first pumping section, also used in the rear of the experiment, is the **Differential Pumping Section (DPS)**. The neutral tritium molecules will hit the walls of the tube because of the chicane structure, formed by five tubes (each measuring 1 m) that turn 20° each time, as seen in fig. 3.4. The neutral molecules are then taken into the outer loop by the use of **turbomolecular pumps (TMP)**. This already reduces the flow by five orders of magnitude, approximately, from $\approx 3 \times 10^{17}$ to $\approx 3 \times 10^{12}$ molecules/s [KAT99]. Positively charged ions produced mainly in the tritium decay (eq. 3.1) are invulnerable to the chicane and the TMB as they follow the magnetic lines. That is why at the end of the DPS a slightly more positive potential is set.

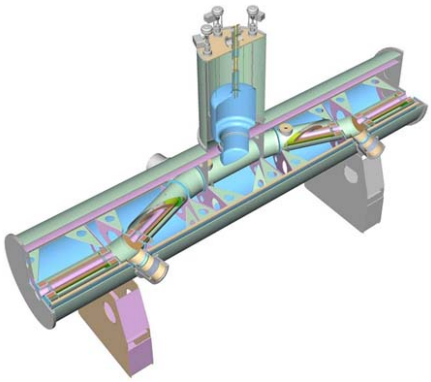

Figure 3.4 | **Differential Pumping Section.** The chicane can be clearly seen. Figure from [KAT99].

After the DPS comes the **Cryogenic Pumping Section (CPS)**, also following the chicane set-up, but this time the angle is 15°. This section uses the cryo-sorption principle to trap the remaining tritium that went through the DPS. Argon frost at 6 K covers the gold plated beam tube and the T_2 are stuck to it. The argon is saturated in around 60 days of operation, after that the valve to the main spectrometer is closed and the tube is set to 100 K to release all of the trapped tritium, which is taken back to the outer loop by the TMPs. This process gives an additional 7 orders of magnitude reduction of the tritium flow (3×10^5 molecules/s).

By the end of the pumps, then, the pressure in the pre-spectrometer and main spectrometer is approximately 10^{-11} mbar.

[3] Chicane (from French) originally refers to a curvy part of a road used to slow down traffic.

3.1.4 Pre-spectrometer

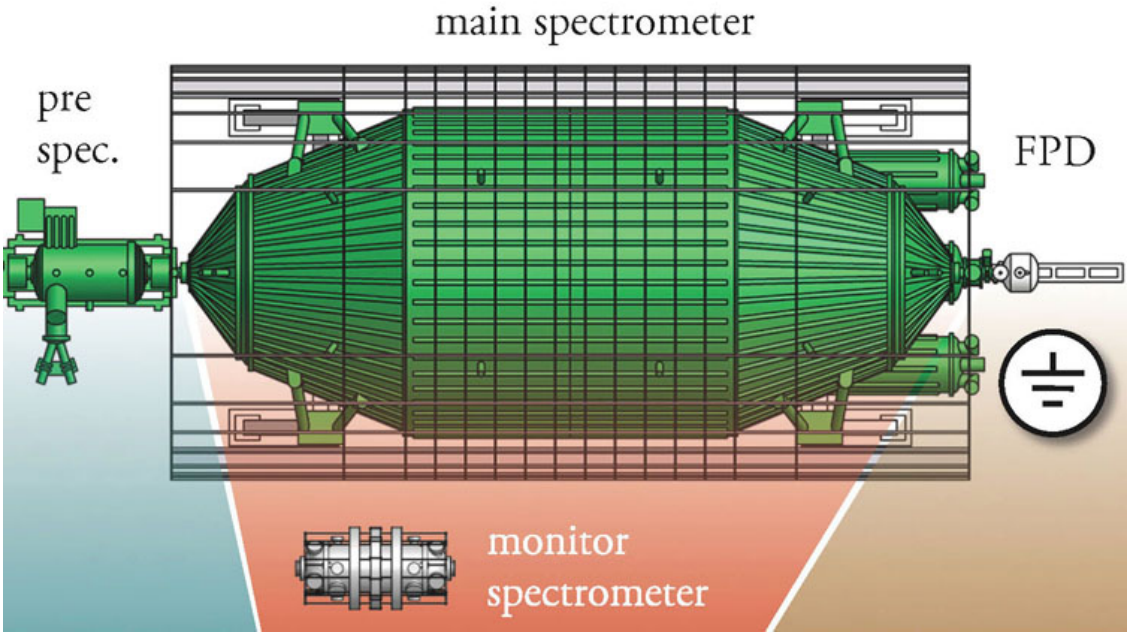

Figure 3.5 | **Schematic view of all spectrometers in KATRIN.** Detailed descriptions of each spectrometer are in the text. Important to note are the sizes of each. Figure taken from [KAT99].

The main task of the pre-spectrometer is to stop the large bulk of low energy electrons that carry no information on the neutrino mass. In principle, those electrons would be anyways rejected by the main spectrometer, but a problem arises if they collide with residuals molecules in the main spectrometer, because then the molecules could become ionized and would contribute to the background. It is made by a 3.4 m long vessel with 1.7 m as diameter (fig. 3.5), and is set to a potential of about -18.3 keV, rejecting electrons with energies lower than around 300 eV from the endpoint.

The pre-spectrometer is in many regards similar to the main spectrometer. Therefore some tests, including the ultra high vacuum and the high voltage stabilization, were done in the pre-spectrometer as early as 2003, before being applied to the main spectrometer.

3.1.5 Main Spectrometer

The main spectrometer is where electrons with neutrino mass information will be finally rejected or accepted. This is the part where the spectrum with high definition is built by the MAC-E Filter principle. The vessel measures 23.3 m in length and has a diameter of 9.8 m, with a vacuum of 10^{-11} mbar set by TMPs. The size corresponds to the goal of KATRIN of improving the energy resolution by one order of magnitude in comparison to similar experiments performed before.

Only the parallel component of the momentum of the β-electron, with respect to the

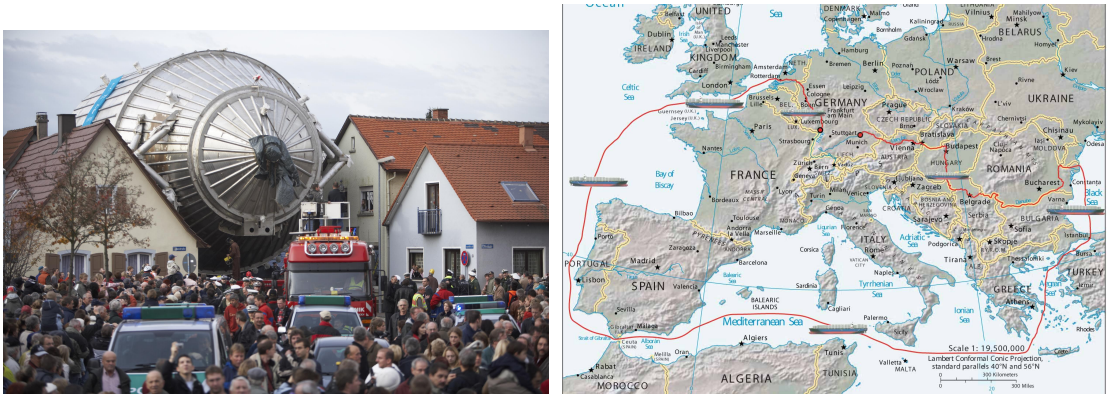

(a) (b)

Figure 3.6 | **Journey of the KATRIN's main spectrometer.** (a) Classical picture of the KATRIN main spectrometer being transported between the houses of Leopoldshafen, already just a few kilometers from its final destination. (b) Map showing the route taking by the spectrometer. Both images from [KAT99].

magnetic lines, is filtered by the potential barrier. Since the β-electrons are produced isotropically, the momentum of almost all of them will contain a perpendicular component, which will not interact with the potential barrier. That is the reason why it is necessary to adiabatically transform the perpendicular component of the momentum of the electron to a parallel component. This is done by decreasing the magnetic field by around four orders of magnitude from the beginning to the center of the vessel, where the highest electrostatic potential is located. This potential is present along a plane perpendicular to the magnetic lines, called the "analyzing plane". If the electrons cross this plane, they will reach the detector; if not, they will return to the source. To conserve the magnetic flux[4], the area of the flux tube of the analyzing plane should be four orders of magnitude larger than the area of the flux tube at entrance of the vessel. The latest input gives a magnetic field at the WGTS of $B_s = 3.6$ T, a magnetic field close to the detector of $B_{max} = 6$ T, and one more at the analyzing plane of $B_{ana} = 9 \times 10^{-4}$ T. The magnetic field in the analyzing plane is fine tuned by an advanced system of air coils, which also correct for the Earth's magnetic field.

The electrostatic field in the main spectrometer is given by a set of two layers of wire electrodes, placed in the inner wall of the vessel, along the beamline. The vessel itself is also set to a high voltage, but the wires are slightly more negative to reject electrons coming from the walls and reduce the background. This electrostatic potential is changed by steps of 0.5 to 1 V at the analyzing plane.

Fun Fact: If you work in the KATRIN Collaboration you know for sure the story. In summary, the vessel for the main spectrometer was produced in Deggendorf, some 400 km away from where the experiment takes place, in Karlsruhe. But transporting the vessel through the streets of the highway was apparently too expensive, because

[4] $B_1 A_1 = B_2 A_2$, where B is magnetic field and A is area, so, $\frac{B_1}{B_2} = \frac{A_2}{A_1}$

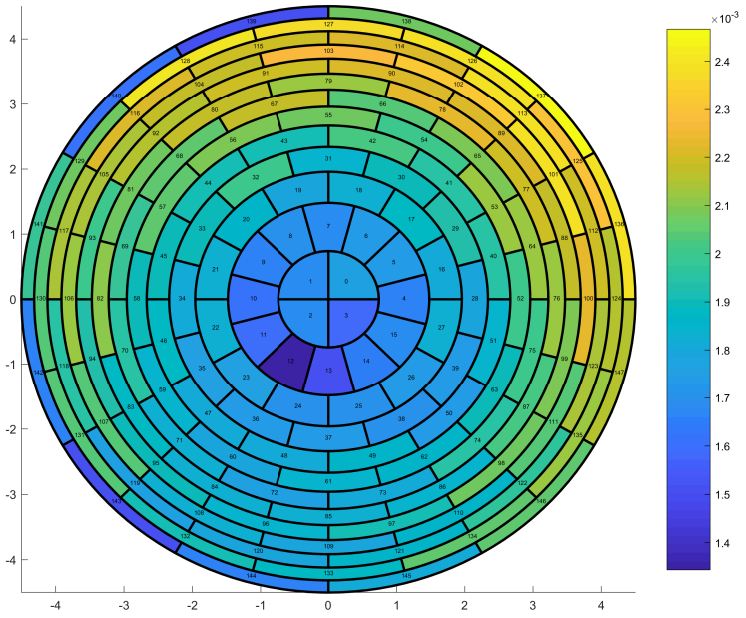

Figure 3.7 | **FPDViewer in SAMAK.** The view of the Focal Plane Detector, given as an output in SAMAK. One can distinguish the ring-wise configuration of the pixels. In this example a simulation of the background is shown.

the highway was not prepared for a tank of such a big size, and (if I heard correctly) some bridges where blocking the way. So instead the vessel was transported by the Danube River, through the Mediterranean Sea, around the Iberian Peninsula and down to Karlsruhe by the Rhine River; a journey of around 9000 km (fig. 3.6).

3.1.6 Monitor Spectrometer

The spectrometer from the former Mainz Experiment is used in KATRIN as a "monitor spectrometer". It measures about 4 m in length and 1 m in diameter. Its role is to measure the high voltage used in the main spectrometer, and in particular its stability. It does so by analyzing the narrow 17.8 keV peak of the ^{83m}Kr energy spectrum with its own MAC-E Filter. Since both vessels are connected to exactly the same high voltage, any perturbation of the high voltage would be equally transmitted and observed in the two spectrometers. In this way, even changes in the ppm level of the high voltage can be detected.

3.1.7 Focal Plane Detector

The detector used in KATRIN is a semi-conductor based silicon PIN diode, called **Focal Plane Detector (FPD)**. It has a circular shape, with 9 cm in diameter, and is divided in 148 pixels, each detecting the same fraction of the flux tube. Furthermore, the pixels are arranged in 13 concentrical rings. The ring in the center has 4 pixels, and the rest are composed of 12 pixels each. The exact positioning of the pixels can be seen in fig. 3.7, and a picture of the detector in real life is in fig. 3.8. The pixel configuration is used to distinguish between inhomogeneities in the magnetic and electric fields in the analyzing plane. Consequently, 148 independent spectra are measured, leading to different analysis types[5], discussed further in chapter 5.

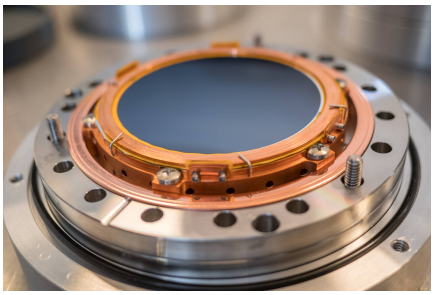

Figure 3.8 | **KATRIN Detector.** The detector for the KATRIN Experiment.

The detector has a resolution of about 2 keV, relevant mainly for the Region of Interest cuts of the data. The resolution of the experiment is actually provided by the main spectrometer and the role of the detector is not to provide information of the energy of each electron, but rather just to count them. The detection efficiency is about 95 %.

[5] . . . and demanding a lot of creativity from the analysis team in KATRIN!

4 Tritium Beta Decay Spectrum Model in SAMAK

In this chapter I explain the process taking place in SAMAK to obtain the integrated β-decay spectrum of the tritium molecule, following the theory. The production of tritium spectra in SAMAK is rather "object-oriented". All the variables and most of the functions to create the spectra are embedded inside classes[1]; the code used to fit the model to the data along with the code to analyze the runs of the First Tritium Campaign are also written as classes.

In SAMAK there are five main superclasses[2]. I list them here in a hierarchical way from top to bottom, together with the main contents of each:

- **KATRIN**: KATRIN general settings including the measuring time distribution and its related parameters are set.
- **FPD**: (Focal Plane Detector) the segmentation (see chapter 5) and its background are chosen; other parameters regarding the detector are set too, like the efficiency for example.
- **WGTSMACE**: this class relates to both the source (WGTS) and the main spectrometer (MACE). It includes the information about the main magnets in KATRIN, density and composition of the gas in the source, and information to construct the response function, among other things.
- **TBD**: (Tritium Beta Decay) this class (actually not a superclass) contains the theoretical information to build the differential and integral spectra of tritium, including all corrections to the Fermi Theory identified so far.
- **Kr**: (Krypton) the purpose of this class (also not a superclass) is similar to TBD, but for krypton.

The first three classes correspond to KATRIN settings and the response function, while the last two are related to the physics of the experiment.

[1] In MATLAB®, classes are templates to create objects that enclose data and the functions to operate on that data. In other words, a class is a collection of variables and functions that ideally are related in some way. Within classes, variables are called properties and functions are called methods.

[2] Classes can inherit all the properties and method from another class. When this happens, the class giving the properties and methods is a superclass, and the class receiving them is a subclass. A class can be a superclass and subclass at the same time, as is sometimes the case in SAMAK.

4.1 Tritium beta-decay

In this section I will explain the theory behind the β-decay spectrum of tritium. This section is influenced by the works of [Nav16a], [Dre+13], and [Roc18].

Enrico Fermi in 1934 proposed a relationship to include the neutrino in the explanation of the distribution of energy of the electrons emitted in β-decay [Fer50]. This relationship is now called "Fermi's Golden Rule".

$$\Gamma = (2\pi) \sum \int |M|^2 \mathrm{d}f \tag{4.1}$$

where $\hbar$, the reduced Planck's constant is taken to be one for simplicity. Γ is the decay rate, $|M|^2$ is the transition matrix element, or the strength of the coupling between initial and final states, and $\sum \int \mathrm{d}f$ is the sum and integration of all discrete and continuous final states, otherwise known as density of final states. Let us have a look at that first.

The number of outgoing particles $\mathrm{d}n$ with momenta between p and $\mathrm{d}p$, within a normalization volume V and into a solid angle $\mathrm{d}\Omega$ is

$$\mathrm{d}n = Vp^2 \mathrm{d}p \mathrm{d}\Omega/(2\pi)^3 = VpE_{\mathrm{tot}} \mathrm{d}E_{\mathrm{tot}} \mathrm{d}\Omega/(2\pi)^3, \tag{4.2}$$

where the 2π in the denominator is the Planck's constant in natural units, and E_{tot} is the total energy of state n. Rearranging terms, one can obtain the state density per energy interval and solid angle.

$$\frac{\mathrm{d}n}{\mathrm{d}E_{\mathrm{tot}} \mathrm{d}\Omega} = \frac{VpE_{\mathrm{tot}}}{(2\pi)^3} \tag{4.3}$$

If one considers the mass of the nucleus much larger than the energies of the emitted electron and neutrino, then it receives no energy and balances the momenta. The correction due to the recoil of the nucleus will be discussed later (sec. 4.3). Then the density of states include only those of the neutrino and electron. Using eq. 4.3 for the energy of the electron E_e and the energy of the neutrino E_ν

$$\rho(E_e, E_\nu, \mathrm{d}\Omega_e, \mathrm{d}\Omega_\nu) = \frac{\mathrm{d}n_e}{\mathrm{d}E_e \mathrm{d}\Omega_e} \frac{\mathrm{d}n_\nu}{\mathrm{d}E_\nu \mathrm{d}\Omega_\nu} \tag{4.4}$$

$$= V^2 p_e E_e p_\nu E_\nu / (2\pi)^6 \tag{4.5}$$

$$= V^2 \sqrt{E_e^2 - m_e^2} E_e \sqrt{E_\nu^2 - m_\nu^2} E_\nu \tag{4.6}$$

That is all, for now, regarding the density of states. Let us turn our attention to the matrix element. Normally it is divided into the leptonic and nuclear parts, and normalized by Fermi's coupling constant and the Cabibbo angle

$$M = G_F \cos(\Theta_C) M_{\mathrm{lep}} M_{\mathrm{nucl}}. \tag{4.7}$$

The decay of tritium is superallowed, which means that the leptonic matrix element is just the probability of finding the neutrino in the nucleus multiplied by the probability

of finding the electron in the nucleus. The latter happens because none of the leptons takes away angular momentum. The probability of finding the neutrino is $1/V$ and the probability of finding the electron is $(1/V)F(E,Z')$, where $F(E,Z')$ is the **Fermi function** [Wil91b]

$$F(Z,W) = 4(2pR)^{-2(1-\gamma)}|\Gamma(\gamma+iy)|^2(\Gamma(2\gamma+1))^{-2}e^{\pi y} \tag{4.8}$$

where $p = \sqrt{E^2-1}$, $\alpha \approx 1/137$ is the fine-structure constant, R is the nuclear radius, $\gamma = \sqrt{1-(\alpha Z)^2}$ and Z is the atomic number, $y = \alpha ZW/p$, and Γ is the Gamma Function $\Gamma(z) = \int_0^\infty t^{z-1}e^{-t}\mathrm{d}t$. The Fermi function takes into account the electromagnetic interaction of the β-electron with the daughter nucleus. The leptonic matrix element is then $|M|^2 = \frac{F(W,Z)}{V^2}$.

The nuclear matrix element, when part of a superallowed transition, is independent of the kinetic energy of the electron. It is normally divided into a vector current or Fermi part (where the change in angular momentum $\Delta I_{\mathrm{nucl}} = 0$ and a coupling of the spins of the electron and neutrino to $S = 0$) and a axial current or Gamow-Teller part ($\Delta I_{\mathrm{nucl}} = 0$ or ± 1, excluding $I_{\mathrm{nucl}} = 0 \to I_{\mathrm{nucl}} = 0$, with the electron and neutrino spin coupling to $S = 1$). Then what is left is an angular correlation of the electron and neutrino. Charge current weak interactions maximally violate parity, so the preferred helicity of particles is positive and for antiparticles is negative (depending on the velocity). The angular correlation factor is, considering the velocity as $\beta = v/c$, then $1 + a(\vec{\beta_e}\vec{\beta_\nu})$. In pure Fermi transitions, the coefficient a is 1, and in Gamow-Teller transitions the coefficient is -1/3 [SBN06].

The density of states, now transformed into a density of phase space (eq. 4.6), is distributed in the two-particle phase space, defined by a δ-function forcing energy conservation. The decay rate Γ is actually a sum over each of the decay channels weighted by its probability P

$$\Gamma = \sum_i P_i \Gamma_i \tag{4.9}$$

Let us compute the decay rate for Γ_0.

$$\Gamma_0 = 2\pi P_0 \int_{E_e,E_\nu,\Omega_e,\Omega_\nu} |G_F \cos\Theta_C M_{\mathrm{lep}} M_{\mathrm{nucl}}|^2 \mathrm{d}n_e \mathrm{d}n_\nu \tag{4.10}$$

$$= \frac{P_0}{(2\pi)^5} \int_{E_e,E_\nu,\Omega_e,\Omega_\nu} G_F^2 \cos^2\Theta_C F(E,Z')|M_{\mathrm{nucl}}|^2 \cdot \tag{4.11}$$

$$\sqrt{E_e^2 - m_e^2}E_e\sqrt{E_\nu^2 - m_\nu^2}E_\nu(1 + a(\vec{\beta_e}\vec{\beta_\nu})) \cdot$$

$$\delta(Q - (E_e - m_e) - E_\nu - E_{\mathrm{rec}})\mathrm{d}E_e\mathrm{d}\Omega_e\mathrm{d}E_\nu\mathrm{d}\Omega_\nu,$$

where Q (or rather Q-value) is the energy released in the decay, given as the differences of the atomic masses and the binding energies $Q = \Delta M(\mathrm{T}-\mathrm{He}) - \Delta E_b$. This ΔE_b is the difference of the electronic binding energy, and can be calculated by a combination of

molecular dissociation and ionization energies [Las18]. The Q-value is distributed in three elements, the kinetic energy of the electron, the total energy of the neutrino, and the recoil energy. If molecular tritium is used, a fourth element is introduced: the Final States. In the range of interest for neutrino mass search, the recoil energy is taken to be constant at a value of $E_{\text{rec}} = 1.72$ eV for TT, with a variation of 3.5 meV in the last 30 eV below the endpoint [Mas+07].

The **endpoint** energy of the β-decay spectrum is defined as the maximal energy the electron takes with a vanishing neutrino mass[3].

$$E_0 = Q - E_{\text{rec}} \tag{4.13}$$

If one performs an integration over the angles, what comes out is an average nuclear matrix element. The next step would be to sum over all final states. This is done two-fold, first over the neutrino mass eigenstates m_i, each with probability $|U_{ei}|^2$; and then over the electronic final states of the daughter system. I discuss the latter in the next section.

4.2 Ground and Excited Molecular Final States

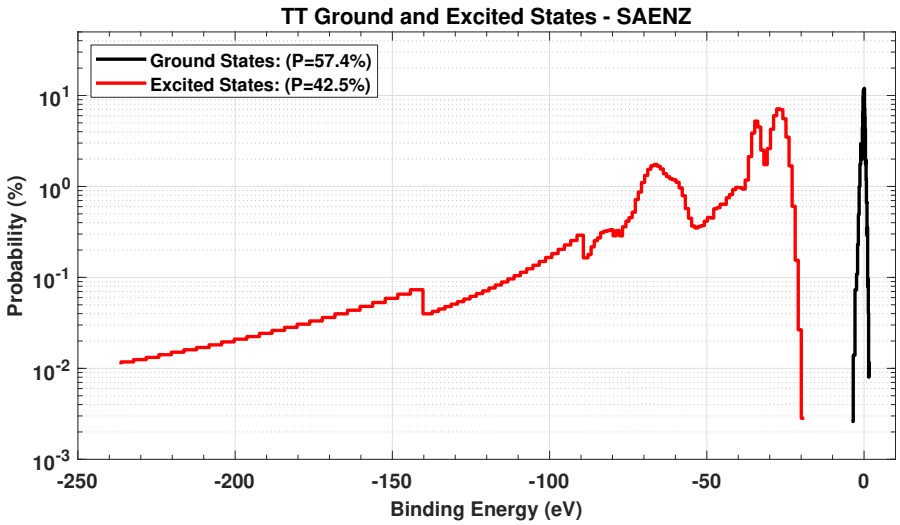

Figure 4.1 | **FSD TT.** Ground and Excited Molecular Final States for the TT molecule used in SAMAK, data from A. Saenz [SJF00].

[3] In the KATRIN Experiment, additionally, there is a work function in the rear wall of the apparatus, which is not yet defined. So the endpoint is like

$$E_0(DT, W) = E_0(DT) + W \tag{4.12}$$

At the time of the First Tritium Campaign, this work function was unknown, but believed to be in the few hundreds of millivolts range [Las18].

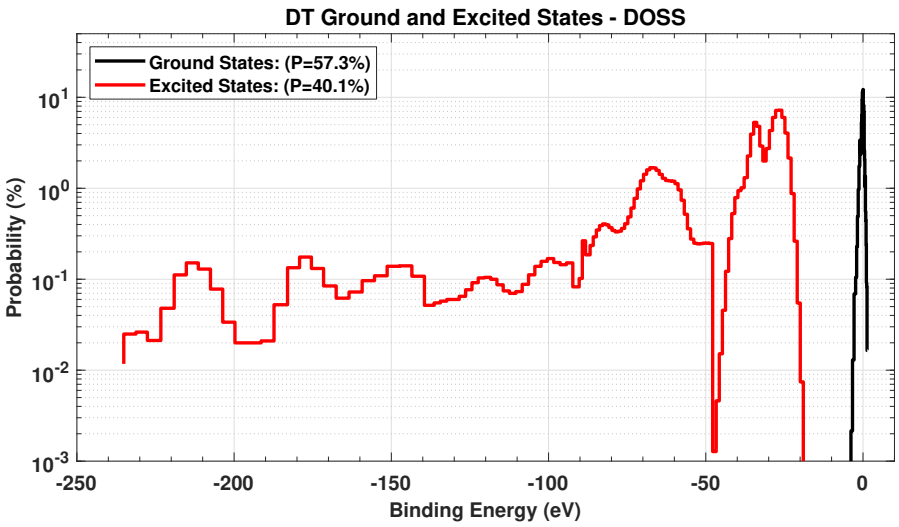

Figure 4.2 | **FSD DT.** Ground and Excited Molecular Final States for the DT molecule used in SAMAK, data from N. Doss [DT08].

These states include both excitations in the electron shells, as well as molecular rotational and vibrational excitations, as the tritium in KATRIN is in molecular form. This motions occur because of the rearrangement of the electronic orbitals in the daughter molecule, consequence of the sudden change of nuclear charge during the decay. The final states shift the endpoint energies.

The Final States Energies and Probabilities for the KATRIN collaboration are provided by A. Saenz for TT and HT [SJF00], fig. 4.1; and N. Doss for DT [DT08], fig. 4.2.

In SAMAK they are included in a matrix, to benefit from MATLAB® vectorization capabilities, making the process faster as there are no loops involved.

```
Ground/Excited State
          TexP_M = repmat(TexP,obj.nTe,1);
          TexE_M = repmat(TexE,obj.nTe,1);
          Q_M = obj.Q*ones(obj.nTe,numel(TexP));
          Te_M = repmat(obj.Te,1,numel(TexP));
          pe_M = repmat(obj.pe,1,numel(TexP));
          me_M = obj.me*ones(obj.nTe,numel(TexP));
          mnuSq_M = obj.mnuSq*ones(obj.nTe,numel(TexP));

          GES = 0 + sum(...
              ((Q_M-Te_M-TexE_M)>=0)...
              .*pe_M.*(Te_M+me_M).*(Q_M-TexE_M-Te_M)
              .*(((ones(obj.nTe,numel(TexP))-sin2T4_M)....
              .*(((Q_M-Te_M-TexE_M).^2-mnuSq_M)>=0)...
              .*((Q_M-TexE_M-Te_M).^2-mnuSq_M).^.5),2);
```

4.2.1 Differential Spectrum

The differential energy spectrum

$$\frac{\mathrm{d}N}{\mathrm{d}t\mathrm{d}E} = \frac{\mathrm{d}\Gamma}{\mathrm{d}E} \tag{4.14}$$

gives the decay rate per energy, and is the seed to compute the integral spectrum, which is what is actually measured in KATRIN. More about the integral spectrum comes later in sec. 4.4.5.

The differential spectrum can be obtained from eq. 4.11 when the second integration over E is not executed. Already summing over the final states, the differential spectrum is

$$\begin{aligned}\frac{\mathrm{d}\Gamma}{\mathrm{d}E} &= CF(E,Z')p_e(E+m_e)\sqrt{(E+m_e)^2-m_e^2} \\ &\sum_{i,j}|U_{ei}|^2 P_j(E-E_0-X_j)\sqrt{(E-E_0-X_j)^2-m_i^2}\end{aligned} \tag{4.15}$$

Where E is the energy of the electron, and X_j are the final state excitation energies, together with their probability P_j. The factor C should be $C = G_F^3 \cos^2\Theta_C |M_{\mathrm{nucl}}|^2/(2\pi)^3$, but in SAMAK it is treated as a normalization factor and is obtained through the experimental half-life of tritium (sec. 4.2.3).

4.2.2 Effective electron anti-neutrino mass

The differences of the squared neutrino masses are in the order of 10^{-3} eV^2 [Ada+11] and 10^{-4} eV^2 [Ara+05], whereas the sensitivity of KATRIN is about $(0.2)^2$ eV^2, so it cannot resolve between the different mass values, as the energy resolution of the MAC-E Filter (~ 1 eV) is much greater than the mas difference. The differential spectrum can be parametrized as

$$\begin{aligned}\frac{\mathrm{d}\Gamma}{\mathrm{d}E} &= CF(E,Z')p_e(E+m_e)\sqrt{(E+m_e)^2-m_e^2} \\ &\cdot\sum_j P_j(E-E_0-X_j)\sqrt{(E-E_0-X_j)^2-m_\beta^2}\end{aligned} \tag{4.16}$$

where the neutrino mass term is represented as $m_\beta^2 = \sum_i |U_{ei}|^2 m_i^2$, an incoherent sum of neutrino masses, and is called the **effective electron anti-neutrino mass**.

4.2.3 Normalization

The normalization in SAMAK is done based on the decay constant of tritium, taken as $\lambda = 1.78283 \times 10^{-9} s^{-1}$ (from the half life of 4500 ± 8) days [LU00]. This decay constant is the total number of decays per second, meaning it is an integral over all energies of

the differential spectrum. For the normalization, one has to find the fraction of decays occurring in the last eVs close to the endpoint (depending on the energy range analyzed, for example -30 eV from the endpoint). This is called the **Cumulative Fraction**, C_{frac} (dimensionless). The product λC_{frac} is the decays per second per tritium atom above a given threshold. That number is then multiplied by two times the total number of tritium molecules, because there are two tritium atoms per tritium molecule. That number can be obtained from the column density which has units $\frac{\text{molecules}}{\text{cm}^2}$ (see sec. 3.1.2) times the area (cm^2) of the flux tube in the WGTS. This assumes that all molecules are TT. To account for DT and HT, the tritium purity factor is also included, which is the atomic fraction of tritium in the gas (dimensionless) as $T_{\text{pur}} = A_{\text{TT}} + 0.5A_{\text{DT}} + 0.5A_{\text{HT}}$ where T_{pur} is the tritium purity and A_{iT} is the molecular fraction of each isotopologue (the amount of isotopologue relative to the total amount of gas) with $i = T, D, H$. Only half of those β-electrons can reach the detector, since the other half go to the rear wall. From that half, only those within the acceptance angle of KATRIN will go through the filter, the rest will be reflected. The last piece is the ability of the detector to detect (forgive the redundancy) the incoming β-electrons, known as detector efficiency.

The equation for the normalization factor N takes then the form

$$N = \lambda \cdot 2\pi r_{\text{flux}} \rho d \cdot 0.5 \left(1 - \cos\left(\sin^{-1}(\sqrt{B_s / B_{\text{max}}})\right)\right) \cdot \epsilon C_{\text{frac}} T_{\text{pur}} \tag{4.17}$$

Where r_{flux} is the radius of the flux tube, ρd is the column density, B_s and B_{max} are the source and pinch magnet respectively, and ϵ is the detector efficiency.

This normalization parameter is almost always fitted anyways, so it is important that it lies relatively close to the real value, but a high precision is not necessary, and actually not possible since the tritium activity is not known precisely.

4.3 Theoretical Corrections

I present in this section the theoretical description of the corrections applied to the differential tritium β-decay spectrum in SAMAK. After these corrections, the Doppler effect is applied as a convolution to the spectrum, while the rest are called "multiplicative corrections", as the correction consists in multiplying the differential spectrum by a corrective function, which depend on the β-electron energy. Depending on the precision wished for the simulated spectrum in SAMAK, one could opt to turn on or off any of these corrections.

4.3.1 Doppler Effect

In the WGTS, there is a Doppler broadening of the differential energy spectrum due to the random thermal motion of the tritium molecules and the bulk gas flow. It is expressed as a convolution of the differential spectrum with a broadening kernel g, as

shown in [Kle+18a],

$$(g \circledast \frac{\mathrm{d}N}{\mathrm{d}E})(E) = \int_{-\infty}^{\infty} g(E-\epsilon)\frac{\mathrm{d}N}{\mathrm{d}E}(\epsilon)\,\mathrm{d}\epsilon, \tag{4.18}$$

with ϵ being the kinetic energy from the β-electron measured in the rest frame of the emitter[4], and E is that energy but in the laboratory frame.

Kernel

The first step to include the Doppler effect is to calculate the kernel, which is given by the Maxwell-Boltzmann distribution. If one considers only the component of the thermal velocity of the tritium molecule $v_{||}$ which is parallel to the electron emission direction, the broadening kernel thereof is a Gaussian centered at $v_{||} = 0$ and with a standard deviation of $\sigma_v = \sqrt{K_B T/M}$, where k_B is the Boltzmann constant, T the temperature of the gas, and M the mass of the emitting tritium molecule,

$$g(v_{||}) = \frac{1}{\sigma_v\sqrt{2\pi}} e^{-\frac{1}{2}(\frac{v_{||}}{\sigma_v})^2}. \tag{4.19}$$

Now one has to consider the bulk velocity u, which in average is 13 m/s. Dealing only with the component parallel to the electron emission direction with polar angle θ, the Gaussian would be now centered at $u\cos\theta$. We integrate then over all emission angles until the maximal acceptance angle $\theta_{\max}$

$$g(v_{||}) = \frac{1}{1-\cos\theta_{\max}} \int_i^{\cos\theta_{\max}} \frac{1}{\sigma_v\sqrt{2\pi}} e^{-\frac{1}{2}(\frac{v_{||}-u\cos\theta}{\sigma_v})^2} \mathrm{d}\cos\theta. \tag{4.20}$$

It is necessary to write the $v_{||}$ in terms of E and ϵ, to incorporate it into the convolution in eq. 4.18. In the non-relativistic approximation

$$E = \frac{1}{2}m_e(v_e + v_{||})^2 = \frac{1}{2}m_e(v_e^2 + 2v_{||}v_e + v_{||}^2), \tag{4.21}$$

where v_e and m_e are the electron velocity and mass, respectively. Considering that $v_e \approx 10^7$ m/s and $v_{||}$ is in the order of 10^2 to 10^3 m/s, the last term in the quadratic expansion is negligible. The approximated difference is then

$$\Delta E = E_{\mathrm{lab}} - E = \frac{1}{2}m_e(v_e^2) - \frac{1}{2}m_e(v_e^2 + 2v_{||}v_e) = m_e v_e v_{||} \tag{4.22}$$

in which $v_{||}$ can be rewritten as $\sqrt{2\epsilon/m_e}$. Finally the kernel has the form

$$g(E,\epsilon) = \frac{1}{m_e v_e}\frac{1}{1-\cos\theta_{\max}} \int_i^{\cos\theta_{\max}} \frac{1}{\sigma_v\sqrt{2\pi}} e^{-\frac{1}{2}(\frac{\frac{E-\epsilon}{m_e v_e}-u\cos\theta}{\sigma_v})^2} \mathrm{d}\cos\theta. \tag{4.23}$$

[4] Which is almost the same as the center of mass energy, owing to the huge difference in the mass of the electron and the mass of the nucleus.

The new standard deviation of eq. 4.23 is $\sigma_E = \sqrt{2\epsilon m_e}\sigma_v$. In SAMAK, it has a standard value of $\sigma_E \approx 95$meV, with standard parameters of bulk velocity $u = 0$ and tritium temperature $T = 30$ K, fig. 4.3. The convolution with the Doppler effect kernel can be seen as a smearing of the energy scale. It can be recalculated with the function computeKernel().

Convolution edge artifacts

Doing a convolution computationally in SAMAK can lead to some complications. The convolution is done on a finite part of the spectrum, causing an undesirable edge effect. This can be avoided by enlarging the energy range of the spectrum, doing the convolution, and then returning the range to its original size.

The convolution is not done explicitly, but rather by doing a matrix multiplication, or using the numerical convolution function from MATLAB® conv [MAT18].

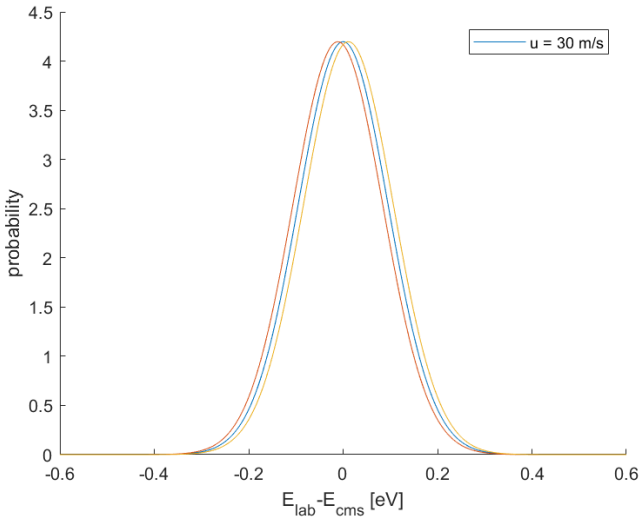

Figure 4.3 | **Doppler effect gaussian kernel.** Kernels for different bulk velocities, but the same temperature $T = 30$ K.

Visualizing the effect

The difference in the differential spectra is minimal for the naked eye, fig. 4.4. A relative difference involving the integral spectra shows more clearly the Doppler effect, fig. 4.5. It shows how the Doppler effect (at different standard deviations) for three years of measurements can have the same magnitude as the effect of the neutrino mass in the spectrum.

4.3.2 Multiplicative Corrections to the Fermi function

In this section I give an overview of the energy-dependent multiplicative corrections applied in SAMAK, summarized in [Mer+15]. The radiative correction has the greatest impact in the spectrum. The relative change in the spectrum caused by the rest is only 0.4 permille in the long First Tritium range (-1600 eV from E_0), and 0.02 permille in the extended neutrino search range (-60 eV from E_0), fig. 4.7.

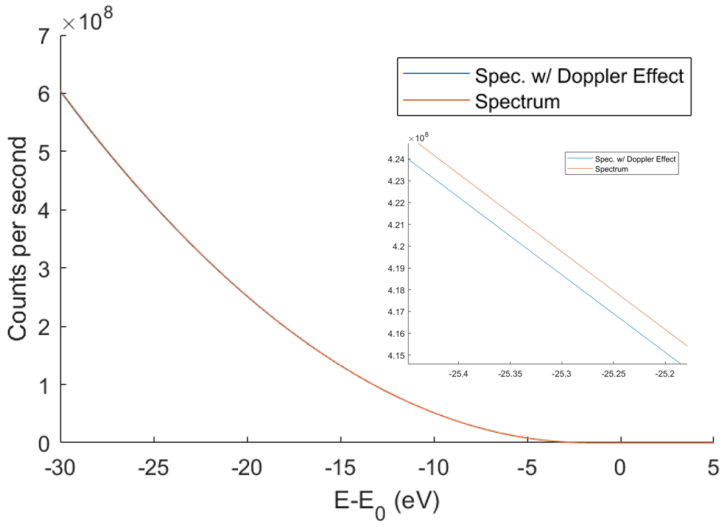

Figure 4.4 | **Doppler effect (relative difference diff. spectrum).** Difference in the differential spectra with and without Doppler effect. The inset shows a zoomed in version, so that the difference is more appreciable.

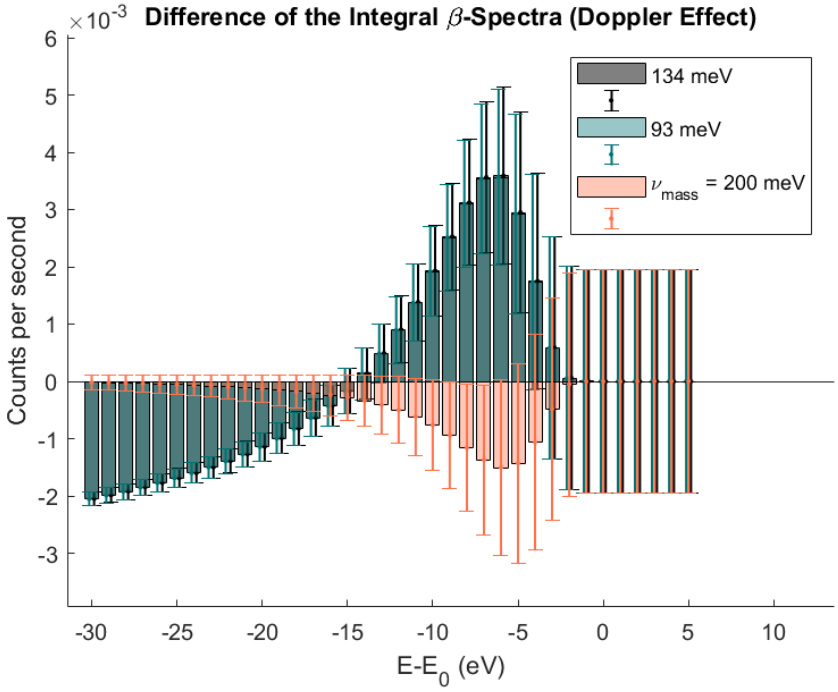

Figure 4.5 | **Doppler effect (relative difference int. spectrum).** Relative difference in the integral spectra showing three cases: Doppler effect with an standard deviation in the kernel of 93 meV and 134 meV, and a neutrino mass of 0; and a spectrum with a neutrino mass of 200 meV and no Doppler effect. The Doppler effect could cancel the neutrino mass effect.

Radiative Correction

Both virtual and real photons interact with the emitted β-electron, prompting corrections to the shape of the β-decay spectrum, the so-called radiative corrections. In SAMAK there are three formulas available to compute them. The first and second ones, are the approximated and general formulas from [RW83], respectively. For the approximation it is taken into account that for tritium $v_e \ll c$ where v_e is the velocity of the emitted β-electron and c the speed of light.

The third option is obtained from [Sir67], but has the issue that the correction has complex values at the endpoint of the spectrum.

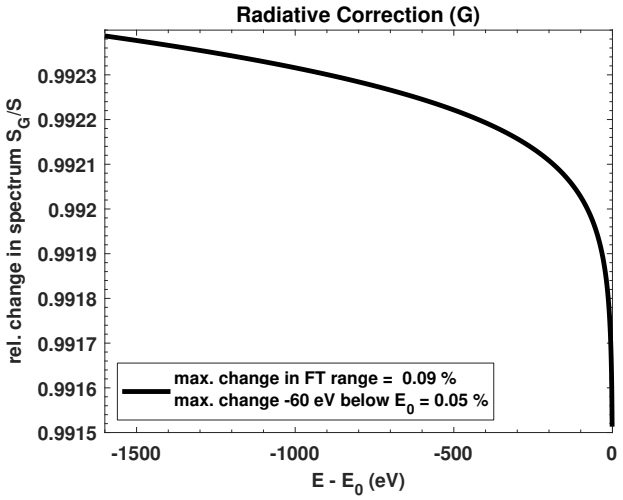

Figure 4.6 | **Impact of radiative correction.** Impact of the radiative correction in the β-decay spectrum, shown as the ratio of the spectra with and without the correction.

Using the the general formula from [RW83], the impact of the radiative correction can be seen in fig. 4.6. In the energy range of interest for the First Tritium campaign, the maximal relative change in the differential spectrum is 0.09 %, meanwhile in the extended region of interest for neutrino mass search (i.e. -60 eV below the endpoint) the same concept has a value of 0.05 %.

Recoil corrections

For the computation of the differential spectrum, it was originally assumed that the momentum taken by the nucleus was negligible. Taking it into account leads to four additional corrections [Wil91a], three of which are handled together: the transformation of the system from a two-body phase space to a three-body phase space, the weak magnetism, and the V-A interface. The correction left is due to the electron interacting with the moving E-field of the daughter nucleus.

Electron-electron exchange correction

Since both the outgoing β-electron and the electron in the orbital of the nucleus are the same, there is the possibility that a quantum mechanical exchange takes place during the emission.

Finite Extension of the Nucleus

So far for the analysis the nucleus of the daughter molecule ^{3}He has been assumed to be point-like, but in reality it has a finite size. Assuming the nucleus has some finite size, the electric field is no longer decreasing quadratically with distance inside the nucleus, leading to a multiplicative factor. Furthermore, the evaluation of the electron and neutrino wavefunctions inside the volume of the nucleus also gives a correction factor.

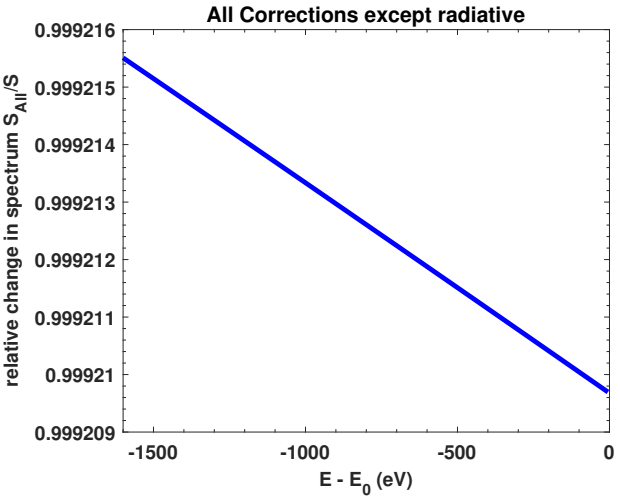

Figure 4.7 | **Impact of theoretical corrections except radiative.** Impact of the all theoretical correction except for the radiative one in the β-decay spectrum, shown as the ratio of the spectra with and without the corrections.

4.4 Response Function

The integral β-decay spectrum measured at the detector is affected by the experimental setup in KATRIN. This is encoded in the response function. It includes the transmission function from the main spectrometer as well as scatterings of β-electrons off tritium molecules, that induce energy losses.

All in all, the response function gives the probability of an electron with certain starting energy to go through the whole apparatus, while the MAC-E Filter is at a certain retarding potential. A detailed derivation of the response function is given in [Kle+18b], to which I will adhere.

4.4.1 MAC-E Transmission Function

The transmission function includes only the probability of crossing the MAC-E Filter. In general, the β-electrons will reach the detector only if the momentum portion perpendicular to the magnetic field lines is positive during the complete journey, or equivalently, the kinetic energy corresponding to that perpendicular momentum $E_{||} \geq 0$, when the electron arrives at the analyzing plane. It means that not all of the longitudinal kinetic energy was transformed into potential energy by the retarding potential.

In this section I make the assumption that the electrons that enter the MAC-E Filter have an isotropic angular distribution and are transported adiabatically (i.e. the electron orbital magnetic moment stays constant) to the detector. In that case, the transfer of perpendicular momentum $p_\perp$ to parallel momentum $p_{||}$ and vice-versa (all with respect

to the magnetic field lines) conserves the adiabatic invariant

$$\frac{p_\perp^2}{B} = \text{const.}, \tag{4.24}$$

in which B is the slowly varying magnetic field in which the electron moves. The transverse momentum of the electron has the relativistic relationship with the perpendicular energy $E_\perp$

$$p_\perp^2 = E_\perp(\gamma+1)m_e, \tag{4.25}$$

where $E_\perp = E\sin^2\theta$, θ is the angle between the momentum of the β-electron and the magnetic field $\theta = \cos^{-1}(\frac{\vec{p}\cdot\vec{B}}{|\vec{p}\cdot\vec{B}|})$, and γ is the relativistic gamma factor $\gamma = \frac{E}{m_e} + 1$. Similarly, the energy corresponding to $p_{||}$ is $E_{||} = E\cos^2\theta$.

Starting at the source with a position z_S, with a magnetic field $B_S = B(z_S)$ and an electrostatic potential $U_S = U(z_S)$, a kinetic energy $E = E(z_S)$, and a polar angle $\theta = \theta(z_S)$, the transmission condition for an electron is

$$\begin{aligned} 0 \leq E_{||}(z) &= E + qU_S - E_\perp(z) - qU(z) \\ &= E + qU_S - E\sin^2\theta\frac{B(z)}{B_S}\frac{\gamma(z_S)+1}{\gamma(z)+1} - qU(z), \end{aligned} \tag{4.26}$$

where q is the electric charge of the β-electron. I also assume that at the analyzing plane of the MAC-E Filter (position $z = z_A$), the retarding potential is maximal, therefore the kinetic energy is minimal and $\gamma(z_A) = 1$. The magnetic field B_A is also minimal. I further assume that the electric potential is zero at the source, so that the transmission condition is now

$$0 \geq E - E\sin\theta\frac{B_A}{B_S}\frac{\gamma+1}{2} - qU. \tag{4.27}$$

The transmission function $\mathcal{T}$ is then given as function of the starting β-electron energy E, angle θ and potential U for a certain magnetic configuration of KATRIN

$$\mathcal{T}(E,\theta,U) = \begin{cases} 1, & \text{if } E(1-\sin^2\theta\frac{B_A}{B_S}\frac{\gamma+1}{2}) - qU > 0 \\ 0, & \text{otherwise} \end{cases} \tag{4.28}$$

To get rid of the angular dependence, one can integrate over the isotropic angular distribution $\omega(\theta) = \sin\theta d\theta$. In KATRIN the magnetic field at the detector $B_{\max}$ is larger than that of the source so electrons emitted at an angle larger than the maximal acceptance angle are reflected magnetically before reaching the detector. This angle is given by

$$\theta_{\max} = \arcsin\left(\sqrt{\frac{B_S}{B_{\max}}}\right). \tag{4.29}$$

One benefit if this, is that the β-electrons emitted at a large angle, therefore traveling through a longer path in the source, scattering more times, and losing more energy, are discarded.

So, after integrating

$$\mathcal{T}(E,\theta,U) = \int_{\theta=0}^{\theta_{max}} \mathcal{T}(E,\theta,U)\sin\theta \mathrm{d}\theta, \tag{4.30}$$

finally the transmission function acquires the relativistic form

$$\mathcal{T}(E,U)_p = \begin{cases} 0, & \text{if } E - qU_p < 0 \\ 1 - \sqrt{1 - \frac{E-qU_p}{E}\frac{B_S}{B_{A,p}}\frac{2}{\gamma+1}} & \text{if } 0 \leq E - qU_p \leq \frac{B_{A,p}}{B_{\max}} E\frac{\gamma+1}{2} \\ 1 - \sqrt{1 - \frac{B_S}{B_{\max}}} & \text{if } E - qU_p > \frac{B_{A,p}}{B_{\max}} E\frac{\gamma+1}{2} \end{cases} \tag{4.31}$$

Where a subscript p was added to take into account the pixel-dependence on E and B, because they are not homogeneous along the analyzing plane. Therefore, in SAMAK there is a slightly different transmission function for each one of the pixels. Also the approximation of $\frac{\gamma+1}{2} = 1.018$ is used, result from evaluating the gamma factor at the endpoint of the spectrum.

For the ring or stacked pixel analyses (see chapter 5), the magnetic and electrostatic fields are averaged for the corresponding pixels (all for stacked pixel, the pixels in the ring for ring analysis) prior to calculating the transmission function.

4.4.2 Energy Loss Function

During the journey of the electrons through the source and until the detector, the most relevant energy loss process is the inelastic scattering of the electrons off molecules in the WGTS. The elastic scattering is not included in neutrino mass search for several reasons:

- the elastic cross section is one order of magnitude smaller than the inelastic one,
- it requires a fine binning in the meV magnitude to include it in the response function,
- and lastly and most important, the systematic shift for ignoring this process is very small and can be absorbed by the systematic budget ($5 \times 10^{-5}\mathrm{meV}^2$) [Kle+18b].

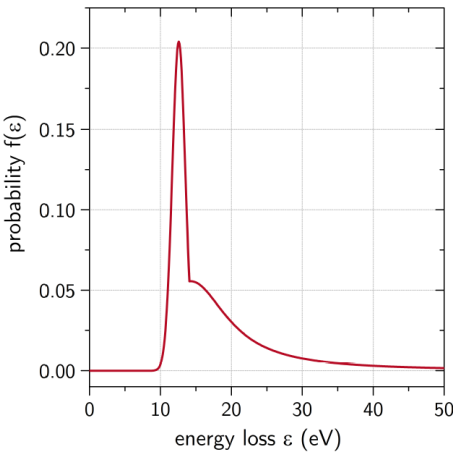

Figure 4.8 | **Energy Loss Function.** Empirical energy loss function calculated by [Ase+00]. Figure from [Kle14].

It was shown in [Gro15] that the scattering angle is minimal and can be neglected. Additionally, the

β-electron kinetic energy dependence of the cross-
section is neglected because the energy range of interest, tens of eVs below the endpoint, is narrow enough [Kle+18b].

The energy loss function was empirically obtained in [Ase+00] and is composed of two parts, a Gaussian for the low energies and a Lorentzian for higher energies.

$$f(\epsilon) = \begin{cases} A_1 \exp\left(-2(\frac{\epsilon-\epsilon_1}{\omega_1})^2\right) & \text{if } \epsilon < \epsilon_c \\ A_2 \frac{\omega_2^2}{\omega_2^2+4(\epsilon-\epsilon_2)^2} & \text{if } \epsilon \geq \epsilon_c, \end{cases} \tag{4.32}$$

being $A_1 = 0.204\ \text{eV}^{-1}$, $A_2 = 0.0556\ \text{eV}^{-1}$, $\omega_1 = 1.85$, $\omega_2 = 12.5$ eV, $\epsilon_2 = 14.30$ eV, $\epsilon_1 = 12.6$ eV, and $\epsilon_c = 14.09$ eV to maintain continuity between the Gaussian and the Lorentzian (fig. 4.8). All of the values just written except ϵ_1 were obtained from a fit using MINUIT and have their respective uncertainties. This is not precise enough for KATRIN, and the function would be remeasured and re-evaluated with high precision e-gun measurements and an elaborate deconvolution technique [Han+17].

If the electrons do not scatter, they do not lose energy and therefore the energy loss function is $f_0(\epsilon) = \delta(\epsilon)$, where the subscript indicates the number of scatterings. For one scattering, $f_1(\epsilon) = f(\epsilon)$ and for subsequent scatterings s, the energy loss function is convoluted s times with itself $f_s(\epsilon) = (f \circledast f)(\epsilon)$.

4.4.3 Scattering Probabilities

To be able to calculate the inelastic scattering probabilities P_i for a certain number of scatterings i, one needs

- the inelastic scattering cross section,
- the starting polar angle,
- and the density distribution of gas inside the WGTS (sec. 3.1.2)

In SAMAK an energy dependent inelastic scattering cross-section $\sigma_{\text{inel}}(E)$ is implemented, whose formula is

$$\sigma_{\text{inel}}(E) = 4\pi r_{\text{B}}^2 Z^2 \frac{E_{\text{Ryd}}}{E} \cdot (1.5487 \ln\left(E/E_{\text{Ryd}}\right) + 2.2212), \tag{4.33}$$

where r_{B} is the Bohr radius in m, Z is the elementary charge of the incident particle ($Z = 1$), E_{Ryd} is the Rydberg energy in keV. Using $E = 18.6$ keV as input, $\sigma_{\text{inel}}(E = 18.6\,\text{keV}) = 3.4501 \times 10^{-22}\ 1/\text{m}^2$.

Being consistent with [Gro15], the number of scatterings can be calculated by a Poisson distribution

$$P_i(z,\theta) = \frac{(\lambda(z,\theta)\sigma_{\text{inel}})^i}{i!} \exp\left(-\lambda(z,\theta)\sigma_{\text{inel}}\right), \tag{4.34}$$

where λ indicates the effective column density, that is to say, the column density seen by an electron depending on the starting angle. It can be obtained by

$$\lambda(z,\theta) = \frac{1}{\cos\theta}\int_{z'=z}^{L}\rho(z')dz', \tag{4.35}$$

the total length of the WGTS being L and having a density distribution along the z-axis, $\rho(z)$. The mean scattering probabilities for an isotropic angular distribution $\sin\theta$ and maximal polar angle $\theta_{\max}$

$$\bar{P}_i(z) = \frac{1}{1-\cos\theta_{\max}}\int_{\theta=0}^{2\pi}P_i(z,\theta)\sin\theta\mathrm{d}\theta. \tag{4.36}$$

Finally to get the probabilities averaged over the complete WGTS tube, an integral over the length is performed[5].

$$\bar{P}_i = \int_0^L \frac{1}{\rho d}\rho(z)\bar{P}_i(z)\mathrm{d}z \tag{4.37}$$

where ρd is the total column density. The default design in SAMAK is to calculate the scattering probabilities up to ten scatterings. The scattering probabilities for nominal settings of KATRIN and for the settings in the First Tritium Campaign are in table 4.1.

Table 4.1 | **Scattering probabilities.** Scattering probabilities for the KATRIN with nominal settings [Col05] and for the First Tritium Campaign.

No. scatterings	Probability Nominal	Probability First Tritium
0	0.4133	0.4474
1	0.2927	0.2957
2	0.1673	0.1550
3	0.0791	0.0665
4	0.0318	0.0241
5	0.0111	0.0076
6	0.0034	0.0021
7	0.0009	0.0005
8	0.0002	0.0001
9	5.5×10^{-05}	2.4×10^{-05}
10	1.2×10^{-05}	4.7×10^{-06}

[5] In SAMAK this is performed in two steps. First, the integrand $f(z)$ is built in a matrix form depending on the binning chosen (in the variable WGTS_ZCells)

$$\frac{1}{\rho d}\rho(z)\bar{P}_i(z).$$

In a later step the matrix is numerically integrated with the Simpsons formula to get the probabilities shown in eq. 4.37.

4.4.4 Response function

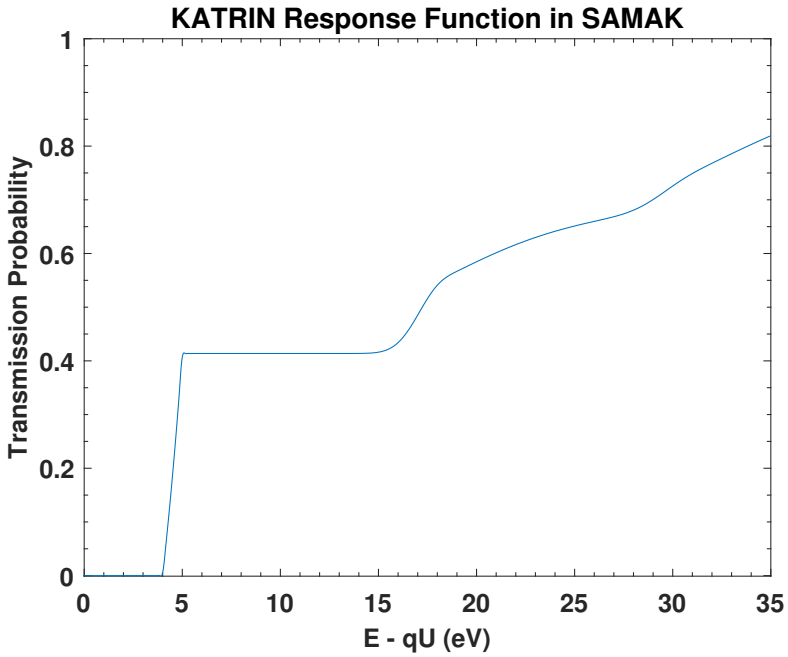

Figure 4.9 | **KATRIN Response Function.** Response Function calculated in SAMAK with Nominal Settings [Col05].

The response function per pixel $\mathcal{R}_p$ in KATRIN is built from the elements exposed in the past sections, and has the form

$$\mathcal{R}_p(E,U) = \mathcal{T}_p(E,U)\cdot P_1 + \int_{\epsilon=0}^{\epsilon=E-qU} \mathcal{T}_p(E-\epsilon,U)F(\epsilon)\mathrm{d}\epsilon, \tag{4.38}$$

where already the angular dependence has been taken care of, and $F(\epsilon)$ is the sum of the convoluted energy loss functions, weighted by the scattering probabilities $F(\epsilon) = \sum_{s=1}^{N} P_s f_s(\epsilon)$, where N is the total number of scatterings considered. The response function for one pixel, calculated with Nominal KATRIN settings [Col05], is in fig. 4.9.

4.4.5 Integral Spectrum

The integral spectrum $\mathcal{IS}$, which is the actual count number measured in the KATRIN Experiment, is constructed by the integration of the combined response function and differential spectrum

$$\mathcal{IS}(U)_p = T_U \int_0^{\infty} (\frac{\mathrm{d}N}{\mathrm{d}t\mathrm{d}E})(E,U)_p \cdot \mathcal{R}_p(E,U)dE. \tag{4.39}$$

where T_U is the measuring time at each retarding potential.

In SAMAK, the integral spectrum is calculated numerically by the use of three-dimensional arrays.

5 Analysis Types

The segmentation of the detector in KATRIN, together with the fact that the measurements are divided in runs, which may use a different measuring time distribution (or MTD[1]), give rise to different ways of analyzing the data presented by KATRIN.

In SAMAK, one of the most commonplace analysis is to fit the tritium model (chapter 4) to the data. This is explained in more detail in chapter 6, but what the reader should have in mind is that normally, there are at least four fitted parameters. Two of them contain some novel information in physics: the neutrino mass and the endpoint; and the other two are nuisance parameters: the background and the overall normalization of the spectrum. The ground and excited final states probabilities can also be fitted.

5.1 Focal Plane Detector Segmentation

The detector has a disc shape and is divided into 148 pixels that see the same tube flux volume. They pixels are arranged in a concentric manner, leaving 4 pixels in the center (bullseye), and then 12 pixels on each of the consecutive rings.

In principle, each pixel acts as an independent detector, and records an independent spectrum. Due to inhomogeneities in the electrostatic and magnetic fields along the analyzing plane, each pixel has a slightly different response function and energy scale, see fig. 5.1. Unfortunately, both fields change both radially and azimuthally, therefore not analyzing the data in a pixel-wise fashion will incur at some point in increasing systematic uncertainties.

5.1.1 No segmentation

In this mode, the assumption that we make is that the detector is made up of only one pixel. Within KATRIN literature, this mode is also called "Uniform Mode" or "Stacked-Pixel Mode". In SAMAK, the approximations done are averaging the retarding potentials and the magnetic fields. The former falls into an average of the energy scale and the latter results in an averaged response function. The uncertainties induced by this averaging can be taken into account by the use of a covariance matrix.

5.1.2 Single-pixel

In the single-pixel analysis mode the four parameters are fitted independently in each of the pixels. It is quite similar to doing the "No segmentation" analysis, but with

[1] A MTD is the way time is distributed among the different qU bins.

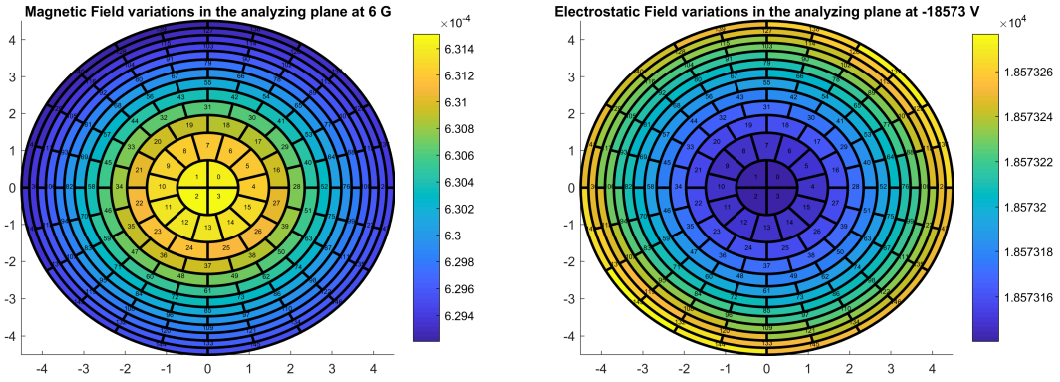

(a) (b)

Figure 5.1 | **Inhomogeneities in the detector.** (a) Magnetic field varying in the analyzing plane at 6 G. (b) Electrostatic field varying in the analyzing plane at -18573 V.

a background and normalization reduced by a factor of 1/148, and using a slightly different energy scale and response function for each pixel. At the end one obtains 148 neutrino masses and 148 endpoints, which will necessitate further statistical treatment as there is only one neutrino mass and one endpoint in nature. Nevertheless, this analysis is useful to identify unforeseen systematic effects or misalignment of the apparatus, and to check the pixel-wise performance of the setup.

5.1.3 Multipixel

This is the analysis mode that makes the best use of all the information available; but, as is often the case in life, the best is also the most expensive.

Here we fit all of the pixels at the same time, having a common neutrino mass squared and endpoint value, but leaving the background and normalization independent pixel-wise. This is done because, in principle, all pixels should see the same endpoint and neutrino mass, but the background and the normalization (see sec. 4.2.3) may be different from one pixel to another. This amounts to 298 parameters being fitted simultaneously. Of course this comes at a computational cost. I will not get into details, but to give a rough idea, the fit of 4 parameters in an ultrabook takes around 1 second, then the single-pixel fit of all pixels takes a few minutes. On the other hand, a multipixel fit with all pixels takes around 30 minutes to complete in the same computer.

The disadvantage of using this method, is that if there are systematic uncertainties, like a shift of the energy scale, affecting differently each of the pixels, it is possible that the fit does not converge, or the results given in a common endpoint are not reliable.

5.1.4 Hybrid Fit

This method arose because the Minuit [Jam94] version for MATLAB® can handle only a maximum of 150 parameters, less than what was needed for the multipixel fit. To overcome this obstacle, a background-only fit was done first, to all of the pixels; these background values were then given as an input, and a multipixel fit was performed using 148 free normalizations, one endpoint and one neutrino mass squared, giving a total of 150 parameters (exactly the maximum allowed!). Since one of the native minimizers in MATLAB®, fminunc [MAT18] is capable of handling all of the 298 parameters needed for the normal multipixel fit, this method has not been revisited as fminunc was implemented.

5.1.5 Ring

Due to the relatively long computation time for the multipixel fit, an interesting compromise was reached. Instead of segmenting the detector in each one of its pixels, we reunite them in rings. Radially dependent effects can still be seen, but the information on azimuthal asymmetries is lost. Although the azimuthal asymmetries are expected to be smaller than the radial asymmetries. As for the approximations, the response function and energy scale are averaged per ring, but there is less loss of information here compared to the "no segmentation" case.

5.2 Multi-run

A run in KATRIN is a complete scan through all retarding potential values stated in the MTD. It is further divided into subruns, which is the time spent at only one retarding potential value. The length of a run is in the range of hours for First Tritium.

There are some parameters that should be kept stable within some tolerance throughout a run to obtain reliable data, examples thereof are the temperature in the source, the magnetic and high voltage values, the tritium concentration in the gas, etc. These are called "slow-control parameters". During the First Tritium Campaign (chapter 9) it was shown that the stability of those parameters comply with the specified requirements during a run [Par18]. Nevertheless, when starting a new run, it is possible that some slow-control parameters vary significantly with respect to values from previous runs, so the best approach is to treat the runs separately.

Fun Fact: A typical length of a run is 3 hours, and KATRIN will take data for three years. That is $3 \times 365.25 \times 24 = 26298$ hours, or around 9000 runs. If we treat each run independently and do a simultaneous multirun-multipixel fit, that would give a total of around 2.5 million parameters to fit simultaneously. Some would say that is quite a challenge.

In the next paragraphs I will first mention the formats for the KATRIN data used in SAMAK, and then what is done with the multiple runs that KATRIN produces.

5.2.1 Run Summary

KATRIN raw data is first processed to build the integral spectrum, then it is available for each collaborator in the Intermediate Data Layer for Everyone (IDLE) in the form of Run Summaries. As indicated in the IDLE Manual [Eno17], Run Summaries are "tree-structured document[s] to store parameters of each run". Run Summaries are a great tool to visualize KATRIN data, owing to the fact that they can be read by humans and condense all relevant information to analyze the data with the analysis tools, see fig. 5.2.

Nonetheless, Run Summaries are not easily read into SAMAK, because they are text-based and a lot of parsing would be needed. Furthermore, the Run Summaries are constantly being updated, so with each new update, the reading mechanism in SAMAK would have to be updated too. At first, the Run Summaries were converted into numerical matrices externally, but currently the solution found was to convert them to HDF5 files.

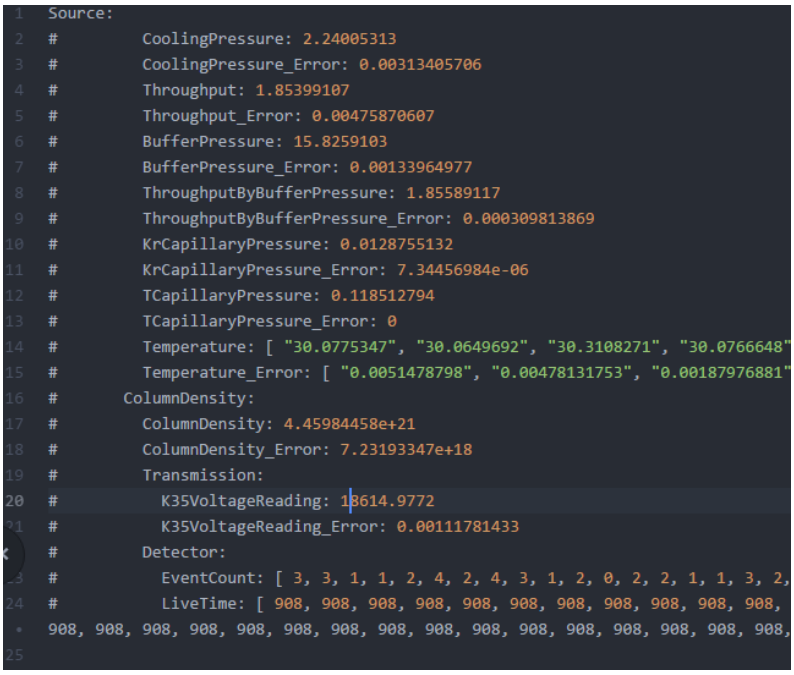

Figure 5.2 | **Run Summary.** Extract from a random Run Summary File of a First Tritium run.

HDF5 Files

Let's take a break here to briefly introduce HDF5 Files. HDF5 stands for Hierarchical Data Format, version 5. According to the HDF Group "HDF5 is a data model, library, and file format for storing and managing data. It supports an unlimited variety of datatypes, and is designed for flexible and efficient I/O and for high volume and complex data." [Gro18]. MATLAB® already includes functions for both high level and

low level reading and writing of HDF5 files. The management is much easier than text files, so updates in the structure of the HDF5 Files with KATRIN information can be adopted effortlessly.

The idea and deployment of the conversion of KTree objects, which are an intermediate step between raw data and Run Summaries, into HDF5 Files was conceived by Christian Karl, a member of the Analysis Team of KATRIN. The reading in SAMAK of the HDF5 Files and further conversion to .mat files (MATLAB Formatted Data), was carried out by me.

5.2.2 Stacking runs

In order perform the analysis and significantly increase the statistics, one must combine the data produced in different runs. There are several idea on how to do this. One of them is to simply append the data in the different runs, and therefore increase the data points. This pursuit, which provokes no added systematic uncertainties, is possible in SAMAK, but has not yet been practiced, as we decided to stack the runs to ease the final fit and treatment of uncertainties.

Simple stacking

Simple stacking means adding the data from different runs which are at the "same" retarding potential, even though from run to run the HV system does not return to exactly the same retarding potential. Some conditions should be met though: the retarding potential difference between runs should not be larger than some set tolerance. At the time of writing the tolerance is 1 V, but that proved to be too large. In fig. 5.4 it can be seen that the retarding potentials are kept within a range of 300 mV for almost all cases. A weighted average based on the measuring time per run is executed on the rest of the slow-control parameters. The systematic uncertainty obtained by stacking is seen on fig. 5.3, calculated using the covariance matrix approach.

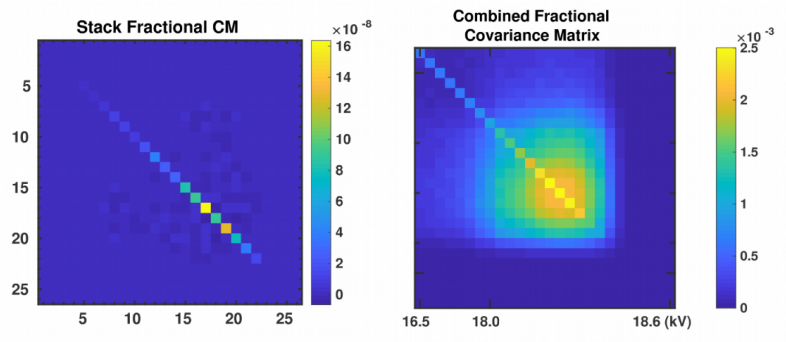

Figure 5.3 | **FT Stack Fractional Covariance Matrix.** Right: Stack fractional Covariance Matrix for First Tritium. Left: Fractional Covariance Matrix including all systematic effects for First Tritium. It can be seen that the effect of stacking the runs is much smaller than the rest of the systematic uncertainties. Figure from [Sch18].

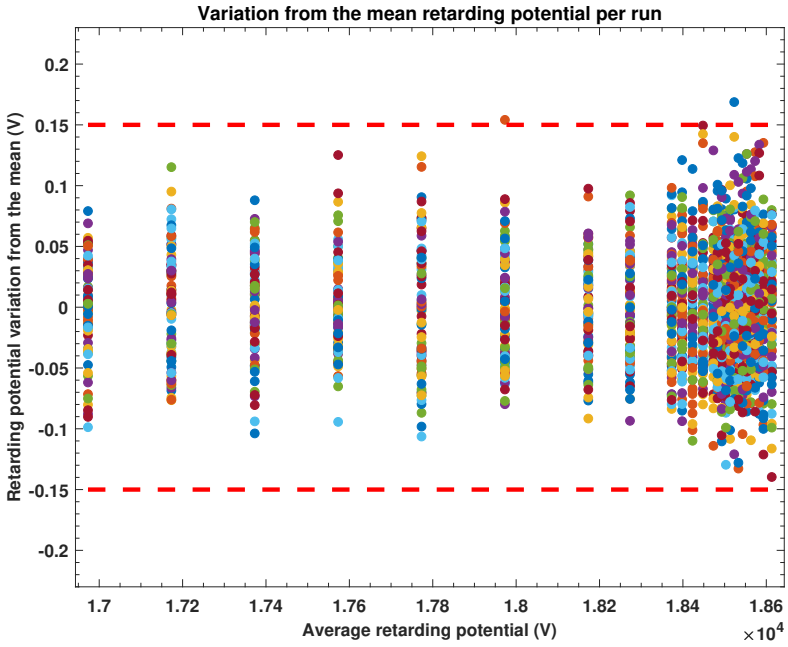

Figure 5.4 | **HV Variation.** Variation of the retarding potential per run with respect to the mean retarding potentials from all runs, for pixel 1 of the detector. Data taken from 85 runs from the First Tritium Campaign.

Advanced stacking proposals

Some stacking proposals that draw less systematic uncertainties have been brought into public knowledge (within the Collaboration). One first proposal was made by Dr. Christian Weinheimer during the Analysis Workshop on July 2018 in Munich. The main idea is to use a polynomial fit on the data to know the number of counts there should be at the retarding potential of interest [Wei18].

One more proposal was done earlier by Dr. Thierry Lasserre, and is similar to the one by Dr. Christian Weinheimer, but instead of using a polynomial fit on the data, the number of counts at the retarding potential of interest is estimated by using the model.

Neither of these proposals have been performed for the studies presented in this work, as they are expected to be relevant with more statistics.

6 Statistical methods implemented in SAMAK

The main goal of KATRIN is to measure the electron antineutrino mass with a sensitivity of 200 meV at 90 % confidence level [Col05]. This means that KATRIN could exclude the null hypothesis of a vanishing neutrino mass if the neutrino mass value is larger than 200 meV.

In this chapter I give a succinct overview of the statistical methods that SAMAK uses to provide best estimators to the physical parameters of interest extracted from the KATRIN data. I focus on the fitting mechanism for the tritium β-decay spectrum and the resulting best fit parameters.

The KATRIN Experiment is limited for providing the true value of the neutrino mass with infinite precision, because of statistical and systematic uncertainties. What KATRIN can do is find a best fit estimator, and establish a confidence interval around it. This would be the so-called frequentist approach, which is one of the main schools in statistics. The Bayesian approach, another school, would give a posterior probability distribution for the neutrino mass, for instance. This process is called parameter inference. Since SAMAK only uses (currently) the frequentist approach, the Bayesian school is not discussed in this work.

6.1 Likelihood and χ^2 statistic

The likelihood function L is how likely a set of parameters Θ_{theo} is, given a set of observations X_{obs}

$$L(\Theta_{\text{theo}}|X_{\text{obs}}), \tag{6.1}$$

and is taken as equivalent to the probability P of making that observation given the set of those parameters

$$L(\Theta_{\text{theo}}|X_{\text{obs}}) = P(X_{\text{obs}}|\Theta_{\text{theo}}) \tag{6.2}$$

In SAMAK, the KATRIN likelihood function consists of the integral tritium β-decay spectrum (chapter 4). In the simplest case, this function depends on four parameters: electron antineutrino mass squared m_ν^2, tritium endpoint energy E_0, the mean background rate B, and the overall normalization C of the signal (tritium activity). In the KATRIN 3-year measurement, the physical parameter of interest is the m_ν^2 and the

other are **nuisance parameters**[1]. In the First Tritium Campaign, m_ν^2 was fixed, and the parameter of interest was taken to be E_0, the rest stayed as nuisance parameters.

For individual measurements (counts in each bin in the KATRIN case) the likelihood function is the product of the likelihoods of each one of the measurements

$$L(m_\nu^2, E_0, B, C|X_{\text{obs}}) = \prod_i p_i(X_{\text{obs},i}|m_\nu^2, E_0, B, C), \tag{6.3}$$

where p_i is the probability of each individual measurement.

The values of Θ that maximize the likelihood function are deemed to be the best estimator values. In practice, both nuisance and main parameters are fitted freely to find the best fit values.

For convenience and computational cost reasons, it is commonplace to *minimize* the negative log likelihhod instead of *maximizing* the likelihood

$$-\ln L = -\ln\left(\prod_i p_i(X_{\text{obs},i}|m_\nu^2, E_0, B, C)\right) = -\sum_i \ln\Big(p_i(X_{\text{obs},i}|m_\nu^2, E_0, B, C)\Big). \tag{6.4}$$

Fitting more parameters

The model and/or the data could depend on other parameters that could also be included as additional fit parameter, i.e. the column density in the First Tritium Campaign, or the exact values of the Final State Distributions.

6.1.1 χ^2 statistic

If the probability distribution for an observation can be approximated by a Gaussian distribution

$$p(X_{\text{obs}}|\Theta) = \Phi(x, \mu, \sigma) = \frac{1}{\sigma\sqrt{2\pi}} \exp\left(-\frac{(x-\mu(\Theta))^2}{\sigma^2}\right), \tag{6.5}$$

where $\mu(\Theta)$ is the expectation value predicted by the model, x is each individual measurement per bin, and σ is the standard deviation. The negative log likelihood distribution acquires the form

$$-2\ln L = -2\prod_i \Phi(x, \mu, \sigma) = \sum_i \left(\frac{x_i - \mu_i(\Theta)}{\sigma_i}\right)^2 + \text{const.} \tag{6.6}$$

If then the $\sigma = \sqrt{\mu}$, eq. 6.6 turns to be the Pearson's χ^2 statistic [Pla83]. This approximation is valid if the probability distribution is Poissonian and the expected value is high enough $\mu \gtrapprox 10$.

[1] Parameters that should be taken into account in the analysis even though they are not the main parameter of interest, due to interference with those main parameters of interest.

6.1.2 Poisson likelihood

One can also use a Poissonian probability distribution, when the statistics are not high enough to use the Gaussian approximation, i.e. when the number of counts in some bins is below 10. Following the work from [BC84], if a Poissonian probability distribution is used in the likelihood

$$L_p(X_{\text{obs}}|\Theta) = \prod_i \exp\big(-\lambda(\Theta)_i\big)\lambda(\Theta)_i^{x_i}/x_i!, \tag{6.7}$$

where $\lambda(\Theta)$ is the number of events in each bin predicted by the model. Applying the likelihood ratio test for the goodness of fit, the resulting χ^2 statistic is

$$\chi^2_p = 2\sum_i (\lambda(\Theta)_i - x_i + x_i \ln\big(x_i/\lambda(\Theta)_i\big)). \tag{6.8}$$

This kind of χ^2 is also be implemented in SAMAK. The disadvantage being that all of the framework of covariance matrices, in which SAMAK relies on for the technical implementation of systematic uncertainties (discussed in the next section), cannot be applied.

6.2 Systematic uncertainties

According to [Sin03] systematic uncertainties (or sometimes called just "systematics") are uncertainties associated with the nature of the measurement apparatus, assumptions made by the experimenter, or the model used to make inferences based on the observed data. In SAMAK they are accounted for through a covariance matrix approach. In the case of First Tritium, this treatment is explained and discussed in the currently unpublished master's thesis of Lisa Schlüter (2019) and the SAMAK Technical Note [Las18].

6.2.1 Covariance Matrix Approach

The covariance matrix M is a 2D array whose element in the i, j position represent the covariance from the i and j elements of a vector of random variables $X = [x_1, x_2, \dots x_n]$

$$M = \begin{bmatrix} \mathrm{V}[x_1] & \mathrm{cov}[x_1, x_2] & \mathrm{cov}[x_1, x_3] & \dots & \mathrm{cov}[x_1, x_n] \\ \mathrm{cov}[x_2, x_1] & \mathrm{V}[x_2] & \mathrm{cov}[x_2, x_3] & \dots & \mathrm{cov}[x_2, x_n] \\ & & \dots\dots\dots\dots\dots\dots & & \\ \mathrm{cov}[x_n, x_1] & \mathrm{cov}[x_n, x_2] & \mathrm{cov}[x_n, x_3] & \dots & \mathrm{V}[x_n] \end{bmatrix}, \tag{6.9}$$

where $\mathrm{cov}[x_i, x_j] = E[x_i, x_j] - E[x_i]E[x_j]$, and $E_[x_i]$ is the expectation value for the random variable x_i. The function $\mathrm{V}[x_i]$ is the variance and is equal to $\mathrm{V}[x_i] = \mathrm{cov}[x_i, x_i]$.

The covariance matrix takes into account bin-to-bin correlation among systematic uncertainties, and can also include uncorrelated systematic and statistical uncertainties

in the main diagonal. It should be noted that the covariance matrix formalism applies only to Gaussian distributed variables, whose errors are propagated linearly. With large statistics and rather low systematics, the KATRIN Experiment complies with both.

6.2.2 Multipixel χ^2 with covariance matrix

As explained in chapter 5, the KATRIN Focal Plane Detector is divided in 148 pixels, and this is taken into account in the χ^2 for the multipixel fit, in which the 148 spectra recorded by the detector are fitted simultaneously (300 parameters: 1 neutrino mass squared, 1 endpoint, 148 overall normalizations, and 148 mean background rates). In addition, the correlated uncertainties are encoded in the covariance matrix. Finally, following [Las18], the χ^2 function to minimize in SAMAK is,

$$\chi^2(\Theta) = \sum_{p}^{n_p} \sum_{i}^{n_i} \sum_{j}^{n_i} (x_i^{(p)} - \mu(\Theta)_i^{(p)}) M_{ij}^{(p)} (X_{\text{obs}}) (x_i^{(p)} - \mu(\Theta)_i^{(p)}), \tag{6.10}$$

where the superscript p refers to the pixel number, and n_p is the total number of pixels analyzed (maximal 148), n_i is the number of energy bins in which the integral β-decay spectrum is divided. The covariance matrix M already contains both statistical uncertainties as well as systematic uncertainties including bin-to-bin correlations.

Generally M depends on Θ, but if the predicted number of events is large, the statistical uncertainty in M can be estimated from the number of measured events

$$M = M_{\text{sys}} + \sqrt{X_{\text{obs}}} \cdot \delta_{ij}, \tag{6.11}$$

where M_{sys} is the covariance matrix that includes only the systematic uncertainties, and δ_{ij} is the Kronecker delta. Likewise, if the systematic variances and covariances are not very sensitive to the values of Θ, then this could be approximated in M by their best-fit prediction. Thus, the dependency on Θ of M can be neglected.

6.2.3 Fitting Procedure

We estimate the values of the fitted parameters Θ by performing a χ^2-fit using eq. 6.10. The parameters for best fit Θ_{bf} are found by minimizing eq. 6.10 as a function of Θ. The $\Delta\chi^2$ statistic is then defined as the exploration of the region around the minimum of said $\chi^2(\Theta)$ function

$$\Delta\chi^2(\Theta) = \chi^2(\Theta) - \chi^2(\Theta_{\text{bf}}). \tag{6.12}$$

In the large sample limit, Θ_{bf} are Gaussian distributed about their true value and the $\Delta\chi^2$ follows a χ^2 distribution with $N_{\text{DoF}} = n_i \cdot n_p - n_\Theta$ degrees of freedom, where n_Θ is the number of parameters fitted. The confidence level is ascertained by the range of values of Θ that make $\Delta\chi^2(\Theta)$ be less than some tabulated value. Moreover, when the predicted number of events in each bin is large enough, the minimum of the χ^2 follows a χ^2 distribution with N_{DoF} degrees of freedom.

7 Sensitivity Studies

One of the applications of SAMAK is to estimate the sensitivity to the physics parameters of interest, based on simulations. In this case those parameters are the electron antineutrino mass and the endpoint of the tritium β-decay spectrum. Here I present three different sensitivity studies.

- A **benchmark study** with the configuration in the Design Report [Col05], to show that SAMAK also confirms the original sensitivity of 0.2 eV for the electron antineutrino mass with 90 % C.L.
- An **updated sensitivity study** for the 3 year measurement, taking into account the current knowledge of the background and a proposal of a new magnet configuration, but keeping the rest as described in the Design Report [Col05]. Recent measurements [Pol18] have shown that the background level is around 400 mcps.
- Yet **another sensitivity study** for the 3 year measurement, with the current background and a new proposal of the magnet configuration, **but** using an **extended measuring time distribution** (MTD). The rest of the parameters are then taken from the Design Report [Col05].

7.1 Sensitivity in Design Report

For this study the model was set up using the benchmark settings specified in table 7.1.

I produced 10,000 different spectra, each one with random statistical fluctuation in the form of

$$S_{B,\text{fluct}}(qU) = (S_{\text{theo}}(qU) + B) + \text{rand}_{qU} \cdot \sqrt{S_{\text{theo}}(qU) + B}, \tag{7.1}$$

where $S_{B,\text{fluct}}$ is the fluctuated integral spectrum including the background at each retarding potential, S_{theo} is the theoretical spectrum model in SAMAK, B is the background taken as constant in each qU bin (independent of the retarding potential), and rand_{qU} is a function that produces an array with random numbers drawn from a Gaussian distribution centered at 0, with an standard deviation of 1. The array size is according to the number of retarding potential bins the spectrum is divided into.

I fit the KATRIN model to each spectra, with four free parameters: neutrino mass squared, endpoint, background and overall normalization (as explained in chapter 6). Then I analyzed the distributions of the 10,000 values of each fitted parameter. For

Table 7.1 | **KATRIN Benchmark Settings.** For the 3 year measurement for the neutrino mass [Col05].

KATRIN 3Y Benchmark Configuration [Col05]	
Total measuring time	3 years
Time Distribution	[-30,+5] eV from E_0 See fig. 7.2
Magnetic Fields	
- Analyzing Plane (B_{ana})	3 G
- Pinch (B_{max})	6 T
- Source (B_s)	3.6 T
Column Density	$5 \times 10^{17}\ \frac{\text{molecules}}{\text{cm}^2}$
TT molecular fraction	90 %
DT molecular fraction	5 %
HT molecular fraction	5 %
Inelastic Scattering Cross Section	$3.45 \times 10^{-22}\ \text{m}^{-2}$
Number of scatterings	10
Mean detector efficiency	0.95
Final States Distribution	
TT	by SAENZ [SJF00]
DT	by DOSS [DT08]
HT	by SAENZ [SJF00]
Theoretical Corrections	
Fermi function	Applied
Radiative corrections	Applied
Screening corrections	Not applied
Finite extension of nucleus	Applied
Weak interaction finite size	Applied
Electron-electron exchange	Applied
Recoil Coulomb	Applied
Synchrotron radiation	Applied
Background	
Background type	flat, 10 mcps
Theoretical Input	
m_ν true value	0 eV
E_0 true value	18575 eV

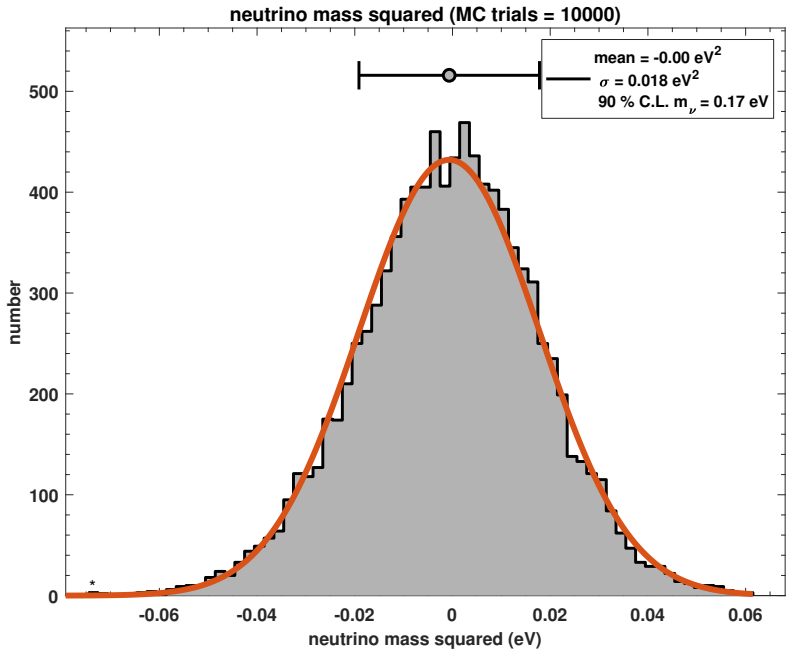

Figure 7.1 | m_ν^2 **dist. DR.** Results from 10,000 Monte Carlo trials using the configuration given in the Design Report [Col05], m_ν^2 distribution.

large samples, I deduce the confidence interval on the neutrino mass by analyzing the frequency of occurrence of the fitted values.

The distribution obtained for the neutrino mass squared can be fitted by a Gaussian distribution with an standard deviation of 0.0185 eV^2 (fig. 7.1). In a Gaussian distribution, the 90 % C.L. will be found at 1.64σ, by the fraction of the distribution such that $|m_\nu^2/\sigma| \leq 1.64$. This means that, including the systematic budget for the neutrino mass calculated in the Design Report [Col05] of 0.017 eV^2, the upper limit of the neutrino mass with 90 % C.L. is at $\sqrt{1.64\sqrt{0.0185^2 + 0.017^2}} = 0.2$ eV. This is the value expected in the Design Report [Col05]. This study validates the simulation in SAMAK.

7.2 Updated sensitivity on the neutrino mass squared and endpoint for 3 years of data taking

In this section I will present the sensitivity studies with the latest KATRIN input for the analysis.

The main KATRIN figures that are used in the model are the same as those in table 7.1, except for two entries: the magnetic field in the analyzing plane is now 9 G instead of 3 G, and the background is ~400 mcps. These settings are pessimistic for several reasons:

- The increased value of B_{ana} would be applied to reduce the flux tube volume, in

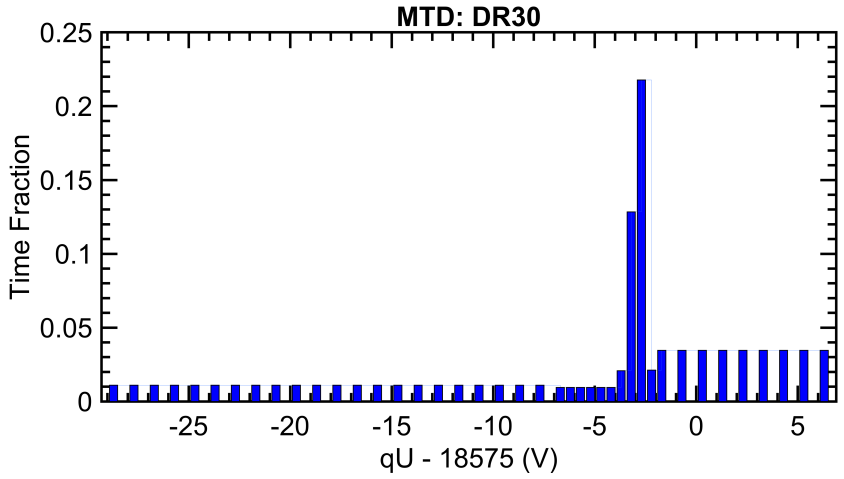

Figure 7.2 | **MTD DR.** Measuring Time Distribution optimized for the Design Report [Col05] settings.

turn reducing the background induced by electrons coming from the inner walls of the main spectrometer vessel.

- Even tough B_{ana} is increased, I assume conservatively that this has no effect in the background. Research is still ongoing on this.
- I use a MTD optimized for a background of 10 mcps, therefore it may not provide the best sensitivity in the current background conditions.

The Focal Plane Detector is treated as a single pixel (unsegmented FPD, chapter 5). Since the uncertainty of the inhomogeneities of the magnetic and electrostatic fields are already taken into account in the systematic uncertainty budget for the squared neutrino mass, there is nothing gained by using a ring or pixel analysis at this simulation stage.

Doing the same procedure as in the previous section (7.1), after three years of data taking, the statistical uncertainty is $\sigma_{\text{stat}} = 0.0958$ eV^2 and the new upper limit that could be set if no neutrino mass is found is 0.396 eV at 90 % C.L. The upper limit was calculated by taking the systematic budget from the Design Report of 0.017 eV^2,$\sigma_{\text{tot}} = \sqrt{0.0958^2 + 0.017^2}$, and $L(90\%\text{C.L.}) = \sqrt{1.64}\sigma_{\text{tot}}$.

In fig. 7.3 the distributions of the effective neutrino mass squared and the effective endpoint of the spectrum are shown. One should not take this estimate as the new KATRIN sensitivity. Again, this study was set under pessimistic conditions, and there are more successful approaches one can take to overcome this adverse situation with the background, like enlarging the qU scanning range.

The rule of thumb given in the Design Report [Col05], is that the statistical accuracy of m_ν^2 scales with the background rate as $\Gamma^{1/5}$. If we have

$$\sigma_\nu(\Gamma = 0.01\,\text{cps}) = \alpha\Gamma^{1/5} = 0.0185. \tag{7.2}$$

where α is the scaling factor and in this case is $\alpha = 0.0465$. The new σ_{stat} is $\sigma_{\text{stat}} = 0.0465 \cdot (0.4065)^{1/5} = 0.04$. That would be an estimate of the sensitivity given that only the background changed. The energy resolution ΔE in the main spectrometer is also worsened by the new B_{ana}. With the new configuration it would be $\Delta E = 2.79$ eV, instead of 0.93 eV, which leads to the current sensitivity obtained with this simulation obtained from the Monte Carlo Experiment.

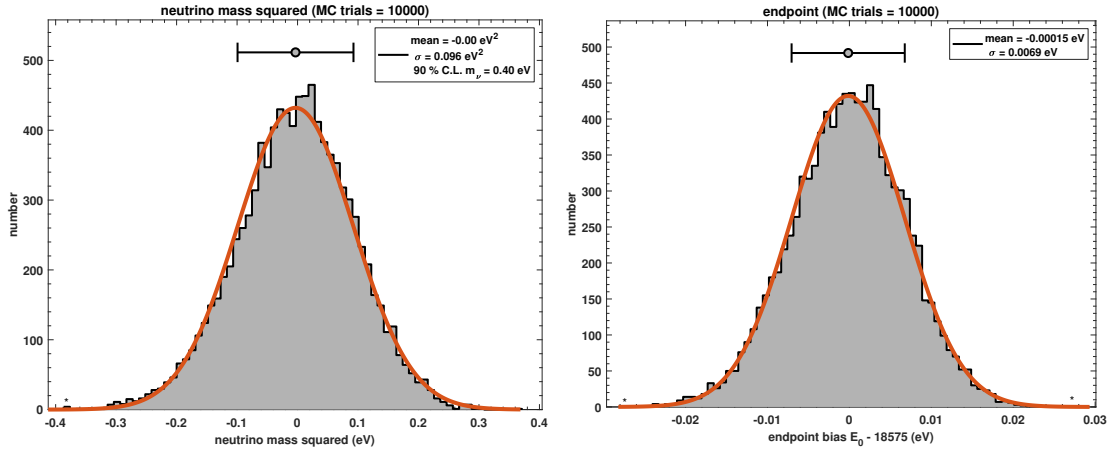

(a) (b)

Figure 7.3 | m_ν^2 **and** E_0 **dists. with current background rate.** Results from 10,000 Monte Carlo trials for the most updated experimental knowledge for KATRIN. (a) Distribution of the fitted neutrino mass squared. (b) Distribution of the fitted endpoint. No anomalies present.

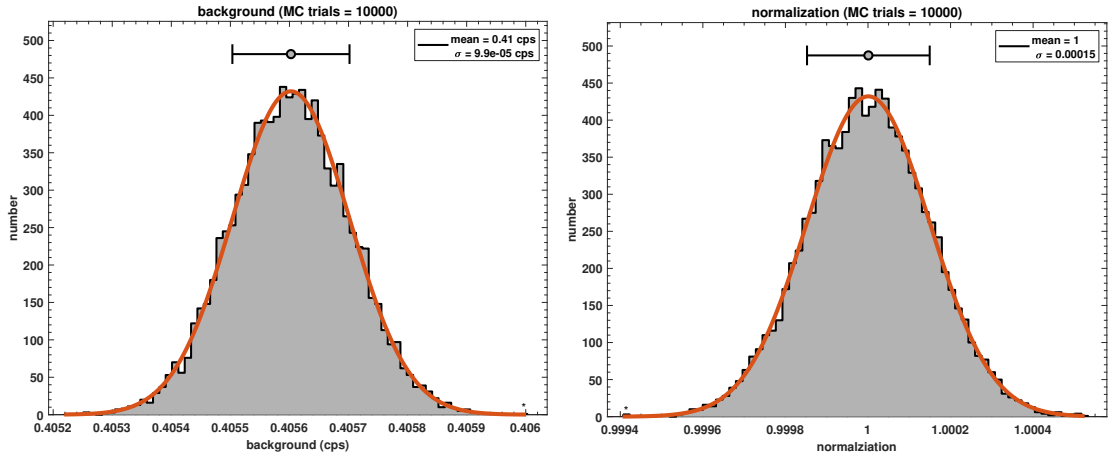

(a) (b)

Figure 7.4 | **Normalization and background dists. with current background rate.** Results from 10,000 Monte Carlo trials. (a) Distribution of the fitted background. (b) Distribution of the fitted normalization. No anomalies present.

The distributions of the other fitted parameters, background and overall normalization,

are also as expected (fig. 7.4), and do not show any anomalies. The background is centered around at its true value of 405.6 mcps, and of course the normalization distribution should peak at 1.

As mentioned, a method to improve the sensitivity under these conditions is to extend the qU scan range and re-optimize the MTD. As the re-optimization of the MTD for this background level is not yet available, I work only with the extension of the scan range in the next section.

7.2.1 Using an extended qU range for the analysis

One way of reducing the statistical uncertainty on the fitted parameters is to increase the energy range; which may lead to an increase in the systematics. Nonetheless, For the following I will assume that the spectrum modeling is equally well known in the extended range of -60 eV below the endpoint as it is in -30 eV below the endpoint, as described in the Design Report [Col05]. The systematic budget for the m_ν^2 had room for unexpected uncertainties already, so I optimistically assume that it is not surpassed.

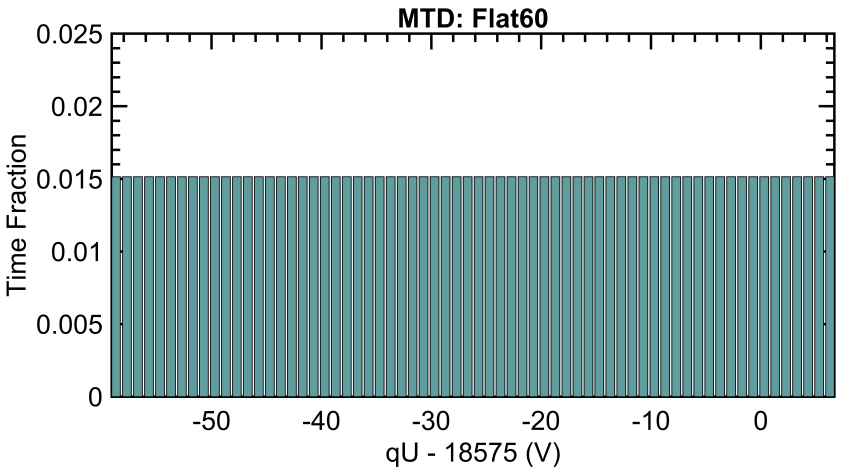

Figure 7.5 Flat 60 MTD
Simple Measuring Time Distribution with an extended range until -60 eV below the endpoint.

Since there is not yet an optimized time distribution for the experimental conditions found out in the First Tritium Campaign, I will use the simple case of a flat distribution. This means that the same time fraction is spent in each retarding potential, and the steps of the retarding potential are unitary between [-18515,-18580] V, see fig. 7.5. Otherwise, the conditions for the Monte Carlo simulations are described in table 7.1, with the exception of the background which is $\sim$400 mcps for this study, and $B_{\text{ana}} = 9$ G. The resulting integral spectrum is in fig. 7.6. On the last bin, at -60 eV, $\sim 3.7 \times 10^8$ counts have accumulated, while $IS(qU = E_0 - 30\,\text{eV}) \approx 3 \times 10^7$ counts. An increase of around one order of magnitude.

The results indicate that the neutrino mass has a statistical uncertainty of $\sigma_{\text{stat}} = 0.0546$ eV^2. That is a bit more than half the value of the uncertainty from the optimized scanning strategy until -30 eV. Taking the same systematic uncertainty as before (0.017 eV^2), the improved upper limit would be 0.3 eV. This value can be further improved by doing an optimized scan of the energy spectrum. The distributions for the neutrino mass and endpoint are in fig. 7.7. It should be noted too that the endpoint in this scenario is known with an statistical uncertainty of 2 meV, still to be checked with the systematic budget for the endpoint, mainly the unknown work funtion on the rear wall (the latest value in the literature for the uncertainty on the endpoint is 70 meV by [Mye+15]).

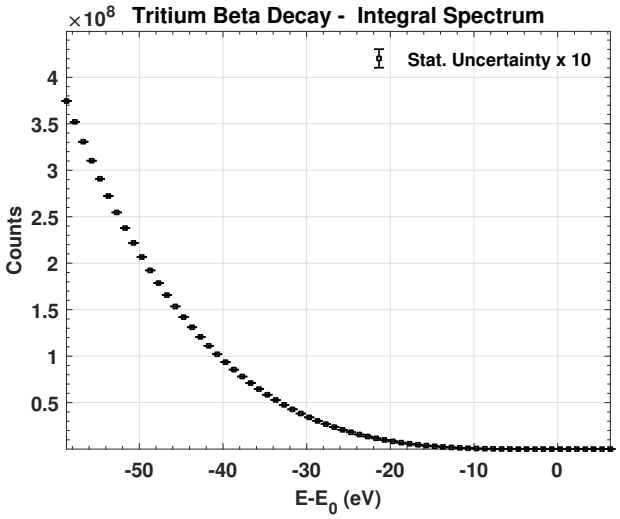

Figure 7.6 | **Integral tritium βspectrum.** Three years of data, flat distribution from [-60,+5] eV in steps of 1 eV.

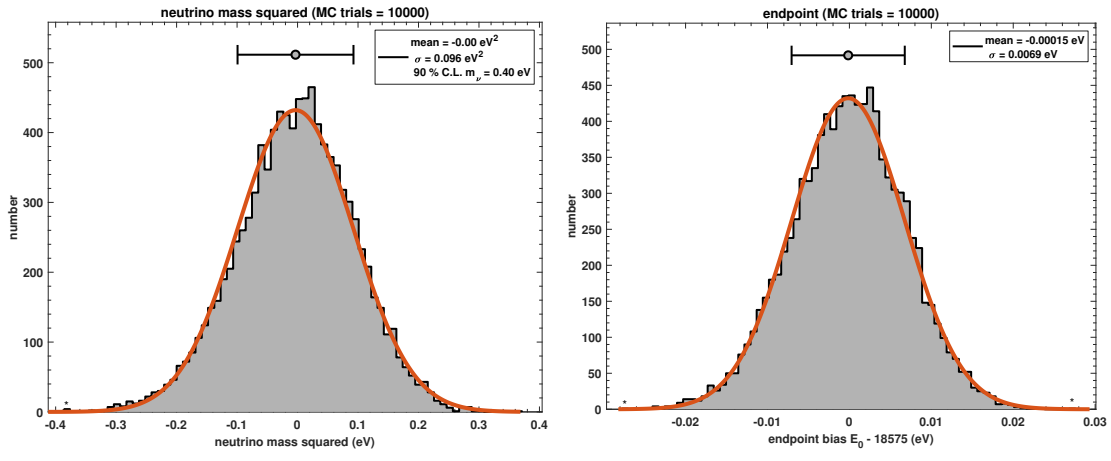

(a) (b)

Figure 7.7 | m_ν^2 **dist. for an extended qU range.** Results from 10,000 Monte Carlo trials for the extended scanned energy range. (a) Distribution of the fitted neutrino mass squared. (b) Distribution of the fitted endpoint.

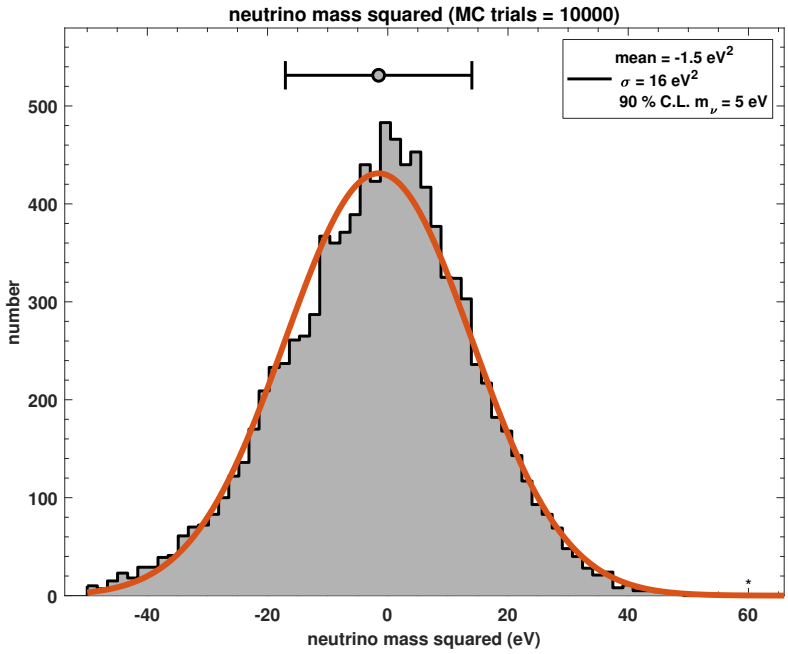

Figure 7.8 | m_ν^2 **dist. FT.** Distribution of fitted neutrino masses squared with the First Tritium settings, but simulated data.

7.3 Sensitivity on the neutrino mass squared in the First Tritium Campaign (Simulation)

The sensitivity to the neutrino mass in the First Tritium Campaign is expected to be poor with respect to the current knowledge, and not competitive with the latest values from the literature [Kra+05] [Lob+01]. However, it is interesting to study the sensitivity using current slow control data and KATRIN settings. In order not to bias the course of the analysis, instead if using real data, I perform a Monte Carlo study as explained in sec. 7.1 using the SAMAK model, which has been proven to reproduce well the data.

To make matters closer to reality, I will exclude in all of the following simulations the two outer rings. They showed a significantly different behavior from the rest, with a very reduced number of counts detected.

The settings used in the SAMAK Model are explained in table 7.2.

The covariance matrix used for this sensitivity study contains the most updated knowledge in SAMAK about the systematic effects of the First Tritium Campaign. More details can be found in table 9.3 in chapter 9.

To account for both systematic and statistical uncertainties, the fluctuated spectrum is built as

$$S_{B,\mathrm{fluct}}(qU) = (S_{\mathrm{theo}}(qU) + B) + \mathrm{rand} \cdot \sqrt{S_{\mathrm{theo}}(qU) + B} + r(R \cdot \vec{1}), \tag{7.3}$$

where everything is the same as in equation 7.1 except for the last additive term, in

Table 7.2 | **Settings for FT sensitivity study.** Settings in the SAMAK Model for the First Tritium Sensitivity Studies, slow-control parameters taken from the Run Summaries.

	KATRIN Configuration
Input	**Value**
Total measuring time	464956 seconds ($\sim$ 5.38 days)
Time Distribution	$[-1600, +40]$ eV from E_0. See fig. 9.1
Magnetic Fields	
- Analyzing Plane	6.302 G
- Pinch	4.2 T
- Source	2.52 T
Column Density mean	$4.598 \times 10^{17} \frac{\text{molecule}}{\text{cm}^2}$
TT molecular fraction	$\sim$ 0.01 %
DT molecular fraction	$\sim$ 1.04 %
HT molecular fraction	$\sim$ 0.05 %
Inelastic Scattering	
Cross Section	$3.45 \times 10^{-22}\,\text{m}^{-2}$
Number of scatterings	10
Mean detector efficiency	0.95
Work Function	0 V
	Final States Distribution
TT	by SAENZ [SJF00]
DT	by DOSS [DT08]
HT	by SAENZ [SJF00]
	Theoretical Corrections
Fermi Function	Applied
Radiative Corrections	Applied
Sychrotron Radiation	Applied
	Background
Background type	flat at 406.5 mcps
	Theoretical Input
Endpoint	18573.7 eV
Neutrino mass	0 eV

which CM is the covariance matrix of First Tritium, R is transpose conjugate of the upper triangular matrix of the Cholesky factorization[1] of the covariance matrix $CM = R^*R$, $\vec{1}$ is a vector of ones, with equal number of elements as there are qU bins, and r is a random number between 0 and 1, from the MATLAB® function randn [MAT18].

First off let us have a look at the sensitivity with the unsegmented FPD. The resulting distribution (fig. 7.8) has a $\sigma = 15.5$ eV^2, which already includes the statistical and the systematic uncertainty. Similarly to the sensitivity studies for the 3-year measurements, making the assumption that the fitted squared neutrino mass values are Gaussian distributed, 90 % of the distribution, lies within approximately 1.64σ from the mean value. Taking the square root of that value would give us the sensitivity to the neutrino mass.

$$\sqrt{1.64\sigma} \approx 5\,\text{eV} \quad \text{C.L.}(90\%) \tag{7.4}$$

This means that neutrino masses above 5 eV could in principle be discarded with the First Tritium data set. That is already an interesting limit, albeit not more precise than the latest experiments from Mainz and Troitsk [Kra+05] [Lob+01], which set the upper limit at 2.3 eV at 95 % C.L.

For completeness:

- I used the "long range" in the analysis ($[-1600, +40]$ eV from E_0), which is actually not fully understood and not perfectly modeled with SAMAK at energies below -200 eV from E_0.
- I simulated the data as if it were taken in just a single run. In reality the data taking is divided into several runs, which leads to small differences in the slow control parameters from run to run. The combination of these runs is not trivial and has been neglected in this study.
- The systematics of the First Tritium Campaign, in spite of an intense dedication to identify them, are still not final (explained in [Las18] and in the unpublished master's thesis of Lisa Schlüter).

[1] The Cholesky factorization of a covariance matrix (or, more generally, any Hermitian positive definite matrix) M is an upper triangular matrix R such that $R^*R = M$. A vector of uncorrelated variables are thus correlated if transformed by the matrix multiplication XR^* [IC82].

8 Data Challenge and Bootcamp

The KATRIN analysis team has developed several independent tools to analyze the data produced by the experiment. From these, there are several which specialize in fitting the data close to the endpoint. Those currently working on the First Tritium data are:

- SSC+KaFit (Source Spectrum Calculation, C++, **official**)
- Fitrium+FitnessStudio (Fit Tritium, C++ and Python)
- BAT+FitnessStudio (Bayesian Analysis Toolkit, C++ and Python)
- SAMAK (Simulation and Analysis with MATLAB® in KATRIN, MATLAB®)

All of these tools are still undergoing upgrades now and then[1], and it is imperative to check that each tool fits the data correctly, and that there were no mistake in the process of upgrading. One way of doing this is through a so called "Data Challenge", which will be explained in the next section.

8.1 Data challenge

In the KATRIN Collaboration, the data challenge is a process in which the same KATRIN data set, either real or simulated, is fitted by each one of the analysis tools, with the goal of obtaining the same results within a predefined tolerance. Up to the time of writing, there have been four data challenges.

- Krypton Data Challenge,
- Tritium Data Challenge,
- Bootcamp with spiked data (First-Tritium-like data), and
- Bootcamp with Monte Carlo data (3-year-measurement-like data).

For the four cases, the data was simulated, and statistical fluctuations were added. The Tritium Data Challenge and the Bootcamp with Monte Carlo Data, in which I took part, will be explained in the next sections.

Figure 8.1 | **KATRIN response function from SSC.** KATRIN response function for the Tritium Data Challenge provided by SSC.

8.2 Tritium Data Challenge

In this challenge, the goal is to test all of the analysis tools against each other. The procedure to successfully participate is the following:

1. Each participant team provides a KATRIN spectrum following the benchmark parameters found in table 8.1.
2. (Optional) Fit 1000 spectra with known true values produced by SSC, and confirm that the distributions of the free parameters were Gaussians centered at the true value. The free parameters are the (electron anti) neutrino mass squared, the endpoint of the β-spectrum, the overall normalization and the background.
3. Each participant team provides a KATRIN spectrum also following table 8.1, but with some differences: first, the addition of Poisson randomized statistical fluctuations; and second, true values for fitted parameters (same as previous point), which the other tools would try to find through a fit. The true values are kept secret until an unblinding meeting.
4. All of the teams fit all of the provided spectra with statistical fluctuations (even their own).
5. All of the teams provide the best values for the fitted parameters together with the corresponding uncertainties, and plots showing the spectrum and the residuals.

In total, four teams participated[2]

[1] Actually the SAMAK package has been significantly upgraded. The SAMAK version used in the data challenges might not be representative of the current version.

[2] At that time, beginning of December 2017, Fitrium and BAT were not sufficiently developed yet.

Table 8.1 | **Data Challenge.** KATRIN model config. for the Tritium Data Challenge.

KATRIN Conf.		**Range for true value**
Total measuting time	3 years	
Time Distribution	Flat [-30,+5] eV from E_0, 1 eV steps	
Magnetic Fields		
- Analyzing Plane	9 G	
- Pinch	6 T	
- Source	3.6 T	
Column Density	$5 \times 10^{17}\ \frac{\text{molecule}}{\text{cm}^2}$	
TT molecular fraction	100 %	
DT molecular fraction	0 %	
HT molecular fraction	0 %	
Inelastic Scattering		
Cross Section	$3.45 \times 10^{-22}\,\text{m}^{-2}$	
Number of scatterings	10	
Mean detector efficiency	0.9	
Final States Distribution		
TT	by DOSS [DT08]	
DT	Not applied	
HT	Not applied	
Theoretical Corrections		
Fermi Function	Applied	
Background type	flat, fitted par.	[200,400] mcps
Response Function	provided by SSC (fig. 8.1)	
Theoretical Input		
m_ν^2	0 eV^2, free par.	[0,0.04] eV^2
E_0	18575 eV, free par.	[18574.7,18575.3] eV

- **SSC/KaFit 1** with Dominik Fuchs
- **SSC/KaFit 2** with Moritz Machatschek, Wonqook Choi, et. al.
- **Susanne's Fitter** with Dr. Susanne Mertens
- **SAMAK** with Pablo I. Morales Guzmán (me)

8.2.1 Results

Fitter →		SAMAK (minuit)		KaFit 1		KaFit 2		Susanne Fit		
Model ↓	**Variable**	**Value**	**Error**	**Value**	**Error**	**Value**	**Error**	**Value**	**Error**	**Unit**
SAMAK	m_ν^2	0.03	5.2E-02	0.03	4.9E-02	-0.03	5.5E-02	0.04	1.0E+00	**eV²**
Pablo	Endpoint	18574.95	3.8E-03	18574.95	3.7E-03	18574.87	4.0E-03	18574.95	1.9E+04	**eV**
	Normal.	1.00	8.4E-05	1.02	3.7E-04	1.02	4.0E-04	1.04	1.0E+00	
	Bckgd.	0.25	9.8E-05	0.25	9.7E-05	0.25	9.9E-02	0.25	1.0E-01	**cps**
	χ^2	32.15	32 (DoF)	31.93	32 (DoF)	31.26	32 (DoF)	50.52	32 (DoF)	
SSC 1	m_ν^2	0.08	8.0E-02	0.07	2.2E-02	0.01	6.5E-03	3069.01	1.5E-01	**eV²**
Dominik	Endpoint	18574.71	5.5E-03	18574.70	2.4E-03	18574.62	1.6E-03	18572.68	9.1E-03	**eV**
	Normal.	0.96	9.1E-05	1.00	3.0E-04	1.00	2.0E-04	1.17	4.9E-04	
	Bckgd.	0.40	1.3E-04	0.40	1.1E-04	0.40	1.1E-01	0.40	1.2E-04	**cps**
	χ^2	22.54	32 (DoF)	22.65	32 (DoF)	23.34	32 (DoF)	9186.13	32 (DoF)	
SSC 2	m_ν^2	0.20	4.4E-02	0.16	2.3E-02	0.10	4.0E-03	0.12	1.5E-03	**eV²**
Moritz	Endpoint	18575.27	3.3E-03	18575.33	2.1E-03	18575.25	1.4E-03	18575.33	3.0E-03	**eV**
Wongqook	Normal.	1.01	8.1E-05	1.00	2.5E-04	1.00	2.0E-04	1.02	3.2E-04	
et al.	Bckgd.	0.22	9.1E-05	0.22	8.5E-05	0.22	8.3E-02	0.22	8.9E-05	**cps**
	χ^2	27.65	32 (DoF)	28.15	32 (DoF)	26.25	32 (DoF)	54.00	32 (DoF)	
Susanne	m_ν^2	0.09	8.6E-03					0.21	4.5E-02	**eV²**
Sim	Endpoint	18575.01	1.4E-03					18575.00	4.8E-03	**eV**
	Normal.	0.97	7.0E-05					1.00	5.4E-04	
	Bckgd.	0.10	5.7E-05					0.10	5.6E-05	**cps**
	χ^2	68.38	32 (DoF)					31.18	32 (DoF)	

Figure 8.2 | **Results of the Tritium Data Challenge.** On the left column are the models and on the top are the fitters. The main diagonal in light green the fitter fitting its own model. The number on the "Error" column is the uncertainty for each parameter, given by the fitter. For the case of the χ^2, this number is the degrees of freedom.

The unblinding meeting took place on the 25th of January 2018. By the time of the unblinding not all teams had the chance to fit all spectra, but the almost complete results were enough to learn something from the event. The true values chosen by the different teams are in table 8.2.

After a first trial, where it was discovered that the uncertainties in KaFit were not being calculated correctly, the final results in tabular form are in fig. 8.2.

		SAMAK	KaFit 1	KaFit 2	Susanne
SAMAK	m_ν^2	0.22	0.11	-0.96	0.02
	Endpoint	0.13	-0.07	-20.00	0.00
	Normal.	-0.18	50.36	50.00	0.04
	Bckgd.	0.66	0.65	0.00	0.00
SSC1	m_ν^2	0.81	2.56	-0.63	19996.32
	Endpoint	0.92	1.70	-49.38	-221.90
	Normal.	-486.72	-1.27	20.00	344.86
	Bckgd.	0.35	0.40	0.00	9.84
SSC2	m_ν^2	3.91	5.72	18.28	57.74
	Endpoint	8.02	41.22	3.57	29.22
	Normal.	152.80	-18.79	0.00	55.46
	Bckgd.	0.26	0.26	0.00	1.01
Susanne	m_ν^2	-10.92			0.68
	Endpoint	3.90			0.04
	Normal.	-494.88			0.01
	Bckgd.	0.83			1.58

Figure 8.3 | **Results of the Tritium Data Challenge.** The number in each space represents how far the fitted value was from the true value in terms of the uncertainty given by the fitter. Values larger than 1 and less than -1 are highlighted in red, meaning the challenge was unsuccessful for that combination of model-fitter-parameter.

For this data challenge, the tolerance chosen to confirm if the data was correctly fitted, was the uncertainty of each fitter. A practical display of the results can be seen in table 8.3. It shows how far away is the fitted parameter in comparison to the true value in terms of the uncertainty of each fitter $p = (X_{\text{fit}} - X_{\text{true}})/\sigma_{\text{fit}}$. If its absolute value was less than one, then the challenge was succeeded, if not, it was failed.

As can be seen in fig. 8.3 there were a lot of discrepancies to be understood. This called for a detailed inspection of the modeling, to see if any of the input given was being overwritten by default settings at some point. It was discovered that the models were using slightly different versions of the KATRIN response function, which could explain the dissimilarities.

On the other side, all fitters could find the true background in all but one case (Susanne fitting SSC1). SAMAK was the code to find the most true values from the other codes, except for the normalization from the SSC models, which is calculated using a completely different approach in both codes, and the endpoint from SSC/KaFit 2.

8.2.2 Follow-up Data Challenge without statistical fluctuations

To alleviate the situation and further investigate the modeling, a small follow-up data challenge was performed. Only two teams participated, SSC and SAMAK. The models

Table 8.2 | **True values.** True values of the parameters m_ν^2, E_0, N, and B, chosen by the different teams participating in the Tritium Data Challenge.

(a)

Truth		
Variable	**Value**	**Unit**
SAMAK		
m_ν^2	0.0225	eV²
Endpoint	18574.95	eV
Normal.	1	
Bckgd.	0.25	cps
SSC1		
m_ν^2	0.0121	eV²
Endpoint	18574.7	eV
Normal.	1	
Bckgd.	0.4	cps

(b)

Truth		
Variable	**Value**	**Unit**
SSC2		
m_ν^2	0.030893	eV²
Endpoint	18575.246	eV
Normal.	1	
Bckgd.	0.222	cps
Susanne		
m_ν^2	0.18	eV^2
Endpoint	18575	eV
Normal.	1	
Bckgd.	0.1	cps

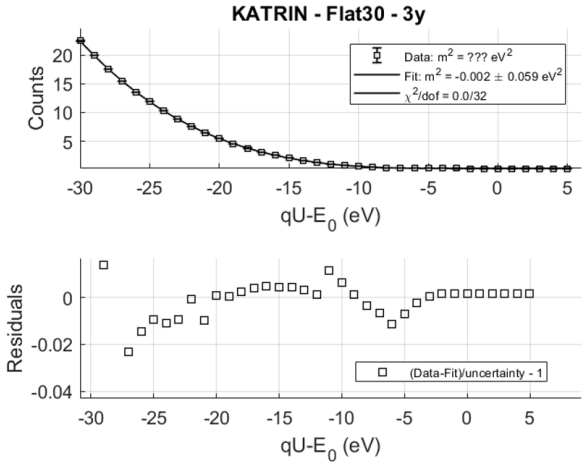

	True	Fit	Error	Unit
m_ν^2	0	-0.002	0.06	eV^2
E_0	18575	18575	0.01	eV
Norm.	1	0.96	0.004	
Bg	0.3	0.3	0.0001	cps
Chi^2	-	0.0025	32	DoF

Figure 8.4 | **Results from the follow-up data challenge.** SAMAK fitting the SSC model. Top left: data from SSC, spectrum from SAMAK. Bottom left: Residuals. Right: True values from SSC and fitted values from SAMAK.

were the same as in table 8.1, except for the fact that statistical fluctuations were not applied, to eliminate any possible biases from the random fluctuations.

The results obtained by SSC, after doing a fit from SAMAK data, are shown in fig. 8.5. Accordingly, the results from SAMAK fitting SSC data are in fig. 8.4. All values where found within uncertainties except for a slight deviation in the normalization, which again, is calculated very differently in both models. The analysis tools were deemed

then ready for the Bootcamp.

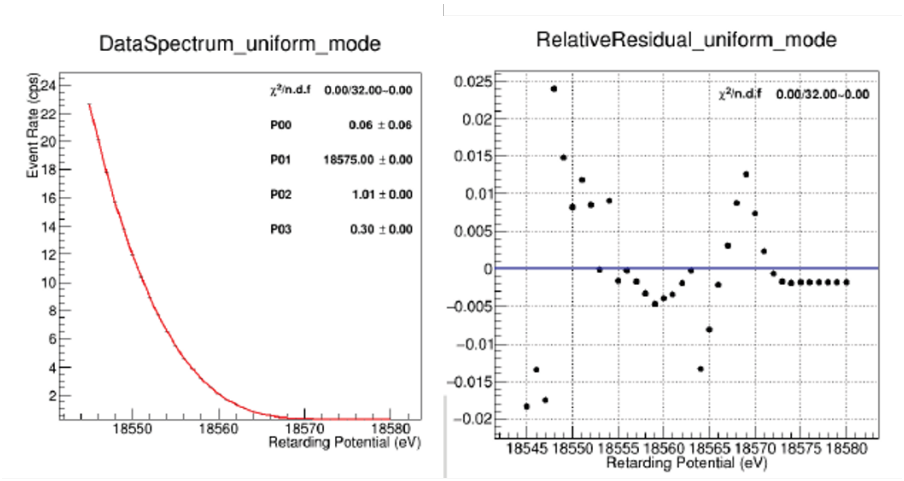

Data: SAMAK	True	Fit Result
Norm. Chi^2	-	8.2e-05
Mnu^2	0.0625	0.0645 +- 0.0576
EndPoint	18575	18574.9997 +- 0.0042
Norm.	1.0	1.0104 +- 0.0004
Bg	0.3	0.3000 +- 0.0001

Figure 8.5 | **Results from the follow-up data challenge.** SSC fitting the SAMAK model. Top left: data from SAMAK, spectrum from SSC. Top right: Residuals. Bottom: True values from SAMAK and fitted values from SSC. Plots and table provided by Wonqook Choi.

8.2.3 Conclusion and Further Work

The Trititum Data Challenge was the first quantitative comparison if the different fitters. It was beneficial in the sense that it made the participating teams more aware of the inner workings of each code. It also showed the importance of understanding the differences among the analysis tools. It was also agreed that the uncertainties provided by minuit with the MIGRAD option could be unreliable as they are approximations using numerical derivatives.

Since the Tritum Data Challenge occurred, there were two other events that enhanced the development of SAMAK and SSC: the Bootcamp, described later, and the First Tritium Campaign. For this reason it is likely that the results from this Data Challenge are no longer relevant. There are also plans to perform new data challenges with data from the First Tritium Campaign and/or simulations, incorporating the new analysis tools that have been developed along the way.

8.3 Bootcamp

The Bootcamp was a preparation event for the first real KATRIN data. Different teams would receive tasks as similar as possible to what would happen on the day of the first data taking. One of these tasks was to analyze the KATRIN data in the form of Run Summaries (sec. 5.2.1). The data in the Run Summaries had a pixel-wise segmentation, that is to say, there was one tritium β-decay spectrum for each pixel in the detector, 148 in total. Until then, SAMAK had not analyzed (simulated nor real) tritium data pixel-wise, so it was an effective boost to incorporate this functionality into SAMAK.

On task was to analyze data for a few hours of measurement, but this had too low statistics to be used for the multipixel case effectively. On the other hand, the task to test the different analysis tools and the analysis of the detector segmentation was to fit one 3-year data set, divided into several Run Summaries, and find the true values hidden in the simulated data. The model for the simulated data was produced by SSC, and it was the same as in table 8.1 with the exception of the magnetic field in the analyzing plane being 6 G instead of 9 G, and the number of scatterings considered being 5 instead of 10.

8.3.1 Results

Each team presented its own results on the last day of the 34th KATRIN Collaboration Meeting (February 24th, 2018). I here present the results obtained by SAMAK. At that time a proper multipixel fit among all the pixels could not be performed, and in its place an iterative single pixel fit was used. In this kind of fit, each pixel is fitted independently and the final answer is a weighted mean among the fitted values, the weights being the inverse square of the uncertainties. The fit was successful[3], but the fitted values were slightly off, due to a combination of using a different modeling in both codes and using a mean response function. The results can be seen in table 8.4.

Table 8.4 | **Bootcamp results.** Fitted values found by SAMAK and true values in simulated data from the Bootcamp Data Challenge. The true value for the background was 0.287 cps for the whole detector, the distribution per pixel was taken from real measurements.

Parameter	Fitted Value	True Value	Unit
m_ν^2	1.285 ± 0.024	0.42	eV^2
E_0	18575.14 ± 0.001	18575	eV
Bckg. per pixel	0.002 ± 0.0	~ 0.002	cps
Norm.	1.21 ± 0.0	1	

Since this was a 3 year measurement, the statistical uncertainty was small ($S_{\text{unc}}/S \approx 2 \times 10^{-4}$ at -30 eV from the endpoint, where S_{unc} is the uncertainty on the counts and S the number of counts), so every known effect that could alter the spectrum should be taken into account. Contrary to this, SAMAK used only one KATRIN response function

[3]Which at that time was already a good accomplishment.

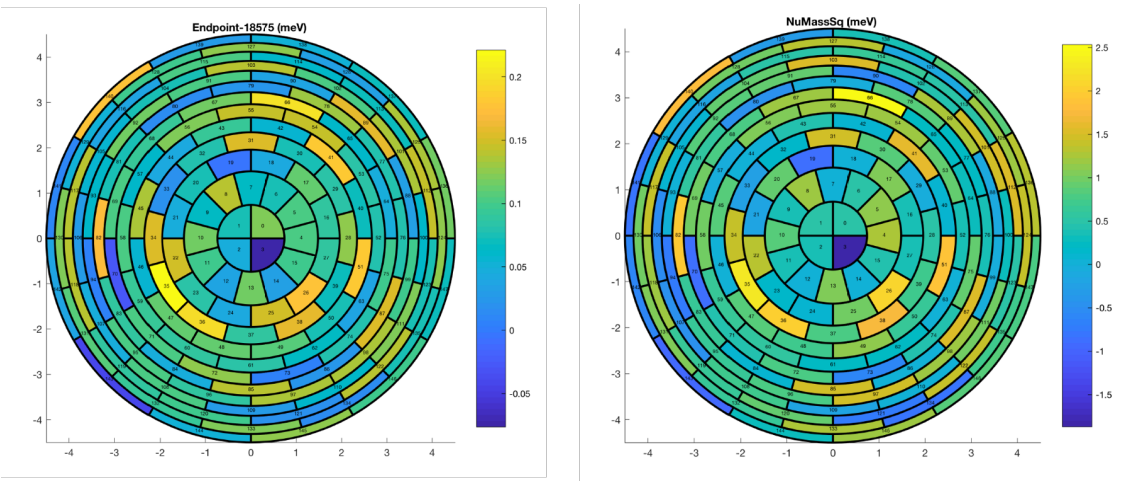

Figure 8.6 | **Bootcamp results FPD.** Left: FPD View of the bias of the fitted E_0 from 18575 eV. Right: fitted m_ν^2. The correlation between the two parameters is visible in the similar patterns both plots present.

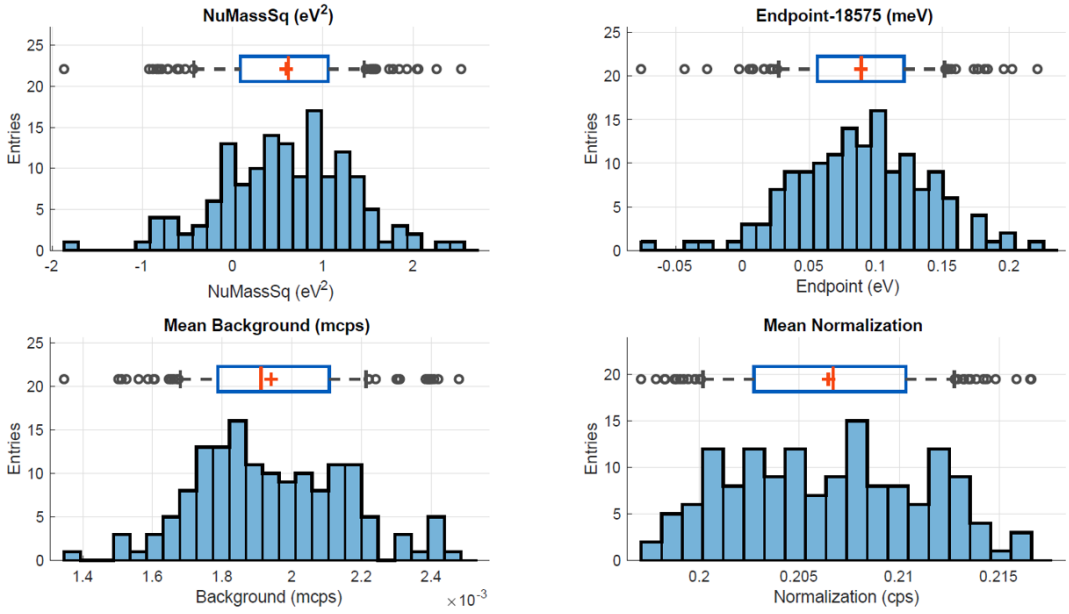

Figure 8.7 | **Bootcamp results dist..** Distribution of the four fitted parameters in the Bootcamp Data Challenge with the 3-year data set per pixel: m_ν^2, E_0, overall norm. and background.

for all pixels, where it is a pixel-dependent function. This was done because the response function was provided in a file by SSC.

A preliminary version of the multipixel fit was also tested, and more work will be necessary to guarantee the robustness of the analysis. It consisted in fitting first the 148 backgrounds (one per pixel), then giving them as a fixed input for a second fit which

looked for the neutrino mass squared, the endpoint, and the 148 normalizations (one per pixel). The fitted neutrino mass for such a fit was $m_{\nu,\text{fit}} = 0.57 \pm 0.04$ eV^2, which is much closer to the true value. As can be seen, the fitting strategy does play a role in this case.

In fig. 8.6 one can see the Focal Plane Detector "heat-map" view of the fitted endpoint and neutrino mass squared for the iterative single pixel fit. The correlation between both parameters can be appreciated qualitatively as one follows the pattern from the other. Fig. 8.7 shows the distribution of the fitted parameters for all pixels. It can already be detected that there were some anomalies with the fit as the distributions cannot be recognized at a glance. Especially the normalization and the background show this problem. This could again be explained, at least partially, by the use of only one response function in SAMAK, or differences in the modeling. The value fitted for the normalization at that Data Challenge is $1 + N_{\text{fit}}$, which meant SAMAK needed ~ 20 % more counts to reach the count number given by SSC. This was due because of the modeling of the normalization. At that time SAMAK relied on some tabulated values to calculate the cumulative fraction, which were not updated regularly because the normalization is a free fitted parameter in any case, as the activity of tritium is not known precisely. Currently this normalization is calculated according to the settings for each model, and is not read from a table anymore (sec. 4.2.3).

8.3.2 Conclusion and Further Work

We focused afterwards on the preparation to analyze real first tritium data, including a response function per pixel and per retarding potential calculated within SAMAK. Also, currently it is possible to perform multipixel fits with all of the parameters (300+) simultaneously, which would make use of all the information available in the data. This event was nevertheless fruitful because it kickstarted the development of more advanced fitting techniques that incorporated the segmentation in the KATRIN detector, the reading and converting of KATRIN data in a format usable by SAMAK, and highlighted the importance of understanding the difference between the different analysis tools in KATRIN.

A new data challenge is being planned, to deal with the First Tritium data, and will be tied with the testing of different data blinding schemes.

9 First Tritium Analysis

The "First Tritium Campaign" in KATRIN is, as the name suggests, the first time when tritium was injected into the WGTS and qU-scans were performed to measure the first integrated tritium spectrum and test the almost final set-up of whole the experiment[1]. There are some differences with respect to the KATRIN nominal settings though, the most important of those being the fact that DT was used instead of TT, and its molecular fraction was 1 %. The column density (sec. 3.1.2) was close to the nominal column density. In the next section more details about the experimental set-up are given.

The First Tritium Campaign started on the 5th of June and ended on the 18th of the same month. During this campaign, the data was collected and distributed in 119 runs[2]. From those runs, 24 were 1-hour runs, 64 were 1.5-hours runs, and 31 were 3-hours runs.

Some of the runs can also be used with the purpose of giving an estimate on the column density with the data, the value of which is paramount in the data analysis for KATRIN, for it is needed to accurately estimate the inelastic scatterings of electrons off atoms in the gaseous source (that are inside the computation of the KATRIN response function, see sec. 4.4.4). Currently, the absolute value can only be approximated by the buffer vessel pressure and/or the throughput of the WGTS loop system [Hei18]. This will not be the case for future data-taking, as an electron gun will be installed to measure the column density with high precision, by measuring the response function at different points, then applying a sophisticated deconvolution process.

9.1 KATRIN set-up and configuration for the First Tritium measurements

For the first tritium measurements, the nominal KATRIN setting was disfavored; in its place, a less risky configuration was chosen, just 1 % molecular fraction of DT was injected in the WGTS. This occurred in order to, among other things, mitigate the impact of any unexpected incident with tritium, which indeed did not occur. The main settings needed for the SAMAK model are stated in table 9.1.

The time distribution was design to be multi-purpose. Contrary to the Nominal KATRIN settings in which the spectrum is scanned down to -30 eV (or -60 eV) below the endpoint, for the First Tritium Campaign, the range was enlarged to -1.6 keV below E_0. One of the reasons for the largely extended range was to increase the overall statistics.

[1] Actually the very first time was during the "Very First Tritium Campaign", but the statistics from the First Tritium Campaign are much higher and so, only results from the latter are shown in this work.

[2] There were a few more runs (127) but some had issues and were left out of this analysis.

Table 9.1 | **SAMAK configuration for First Tritium.** SAMAK configuration for First Tritium for the data analysis and modeling.

Input	Value	Comment
	KATRIN Configuration	
Time Distribution	See fig. 9.1	obtained from Run Summary
Magnetic Fields		
- Analyzing Plane	6 G	obtained from Run Summary
- Pinch	4.2 T	obtained from Run Summary
- Source	2.52 T	obtained from Run Summary
Column Density	$\sim 4.5 \times 10^{17} \frac{\text{molecule}}{\text{cm}^2}$	obtained from Run Summary
TT concentration	~ 0 %	obtained from Run Summary
DT concentration	~ 1 %	obtained from Run Summary
HT concentration	~ 0 %	obtained from Run Summary
Inelastic Scattering		
Cross Section	$3.45 \times 10^{-22}\,\text{m}^{-2}$	
Number of scatterings	10	
Mean detector efficiency	0.95	fitted in the overall normalization
Work Function	0 V	Unknown
	Final States Distribution	
TT	by SAENZ [SJF00]	
DT	by DOSS [DT08]	
HT	by SAENZ [SJF00]	
	Theoretical Corrections	
Fermi Function	Applied	Relativistic
Radiative Corrections	Applied	
Screening	Not applied	
Finite Extension of Nucleus	Not applied	
Weak interaction finite size	Not applied	
Electron-Electron Exchange	Not applied	
Recoil Coulomb	Not applied	
Sychrotron Radiation	Applied	
Doppler Broadening	Not applied	
	Background	
Background type	flat	Free parameter in fit
	Theoretical Input	
Endpoint	18573.7 eV	Free parameter in fit
Neutrino mass	0 eV	Fixed parameter

With just 1 % of DT and a few days of measurements, the results of scanning until -30 eV below the endpoint would not have been as meaningful. This enlarged range also serves to test KATRIN with large statistics, which is also useful of the TRISTAN project, which will look for sterile neutrinos in the keV range. A plot of the time fraction spent in each retarding potential can be seen in fig. 9.1. Due to normal operating procedures, the measurement time changed by several seconds from run to run and subrun to subrun, compared to the established MTD. Anyways, this is taken into account when doing the analysis.

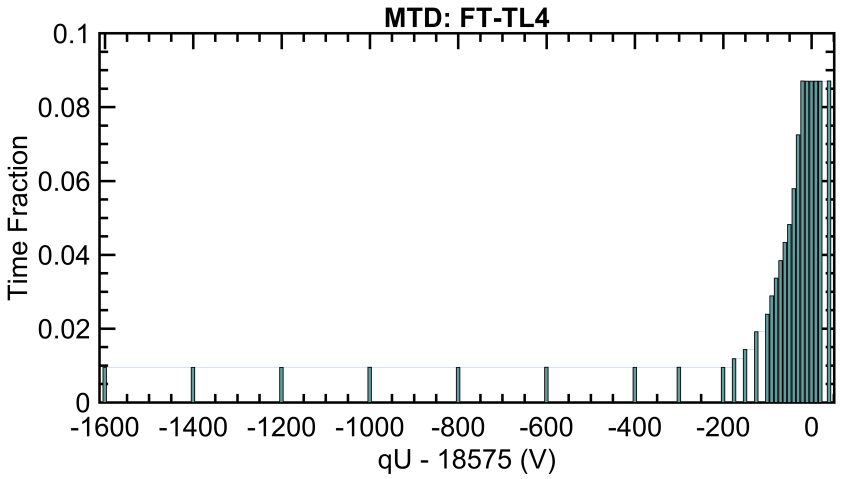

Figure 9.1 | **FT MTD.** Measuring Time Distribution used in the First Tritium Campaign.

The SAMAK framework is optimized to simulate the tritium β-decay spectrum close to the endpoint, and therefore systematic uncertainties are expected to increase as one considers data further away below the endpoint. The following systematic uncertainties are currently under investigation

- the backscattering of the detector,
- the efficiency of the detector at high rates[3],
- the Final Excited States Distribution,
- the absolute uncertainty on the column density,
- and the magnetic reflection of β-electrons.

For the following analyses I use the three ranges shown in chapter 5, where the statistical uncertainty starts to be relevant in the range from 0 to approx. -200 eV below E_0, and dominate only in the range 0 to -50 eV. Further away below the endpoint, the uncertainties are dominated by systematics, as seen in fig. 9.2.

The run numbers I use for the following sections are in table 9.2. The column density in them was $\sim 4.5 \times 10^{17} \frac{\text{molecules}}{\text{cm}^2}$. They are 71 runs which add up to a total measuring time of 449,911 seconds ($\sim$ 5.2 days).

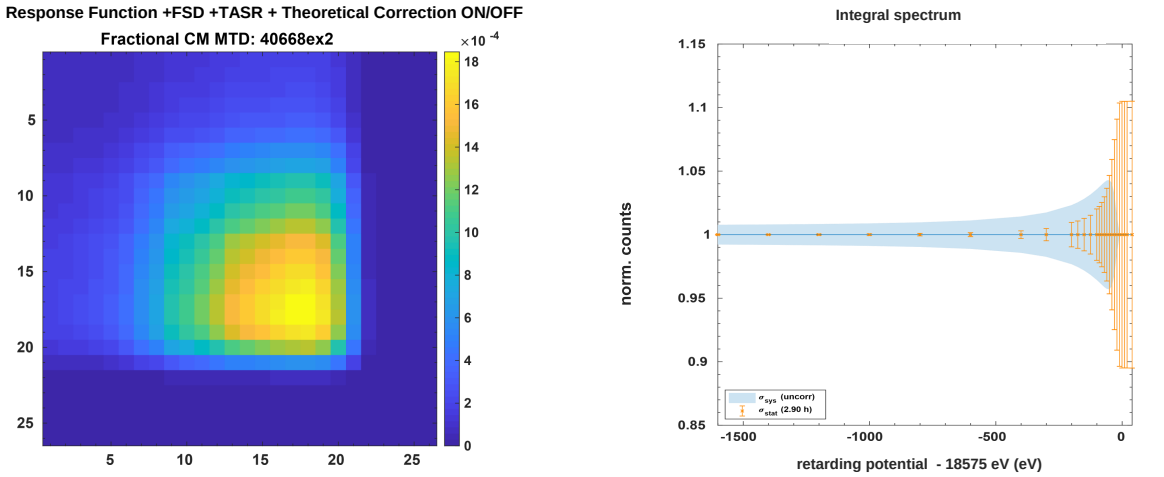

Figure 9.2 | **Statistical and systematic uncertainties FT.** Right: covariance matrix used in SAMAK for the First Tritium Campaign. "FSD" means Final States Distribution and "TASR" is the tritium activity per sub run. Right: statistical and systematic uncertainties for the 3-hour run 40668. Approximately around -50 eV below the endpoint both uncertainties have the same magnitude normalized to the counts. Below that point, systematics dominate, and above, statistics dominate. Plot by Lisa Schlüter.

9.2 Systematic uncertainties for the First Tritium Campaign

Table 9.3 shows the systematic uncertainties applied in SAMAK as the time of writing of this thesis [Las18]. It is important to note that there are several systematics that are not perfectly understood far away from the endpoint:

- The Final Excited States distribution is known only up to energies of $\sim$ 200 eV, and it is still not clear what is the uncertainty on the distribution used in SAMAK.
- The absolute value of the column density is estimated and has an estimated uncertainty of 8 %. This becomes relevant when fitting only with the statistical uncertainty, because it becomes small[3] at low retarding potentials. Therefore, any deviations of the model from the data could lead to an increased value of the goodness-of-fit statistic. If correct, this approach means that these points at low retarding potentials could have a large influence on the fitted results. More information on the column density in sec. 9.5.
- The detector system was designed to measure rates of β-electrons with energies close to the endpoint. As the energies accepted are lower, the rate increases

[3]There are around 8 million events in the whole detector when the retarding potential is at ≈ -17 kV in a 3-hour run, which means $\sim$ 600 counts per second per pixel, with a relative statistical uncertainty of $\sim$ 0.3 permille.

Table 9.2 | **First Tritium runs used for the analysis.** I used the runs with 100 % column density which were scanned up or down, but not the ones with the random scan.

Run numbers used in the First Tritium analysis

Up scan								
40541	40543	40604	40611	40613	40667	40669	40671	40673
40675	40677	40679	40681	40683	40685	40687	40689	40691
40977	40980	40983	40986	40989	40992	40995	41002	41005
41011	41014	41019	41022	41026	41029	41032	40693	41008
Down scan								
40531	40540	40542	40603	40668	40670	40672	40674	
40676	40678	40680	40682	40684	40686	40688	40690	40692
40979	40982	40985	40988	40991	40994	40997	41007	41013
41016	41017	41020	41023	41025	41028	41031	41010	40976

significantly[3], and, even with the correction presented in sec. 9.4.2, the efficiency of the detector is not totally understood at such high rates.

Table 9.3 | **Preliminary Samak Systematics Effects.** The uncorrelated parameters were drawn from a Gaussian distribution independent from other parameters, when applying the multisim method (unpublished master's thesis of Lisa Schlüter and [Las18]).

Effect	Parameter	Rel. error (%)	Correlation	Method	Comment
Response Function					
Magnetic fields	B_WGTS	2 %	uncorrelated		
	B_Max	2 %	uncorrelated		
	B_AP	2 %	uncorrelated		
Column density	rho.d	8 %	uncorrelated	Multisim	overestimated
z-profile		0 %			not included yet
IS cross section	ISCS	2%	uncorrelated	Multisim	overestimated
Energy loss	A1	0.50%	uncorrelated	Multisim	may be correlated
	A	0.54 %	uncorrelated	Multisim	may be correlated
	w1	1.10 %	uncorrelated	Multisim	may be correlated
	w2	0.80 %	uncorrelated	Multisim	may be correlated
	eps1	0.00 %	uncorrelated	Multisim	may be correlated
	eps2	0.14 %	uncorrelated	Multisim	may be correlated
Av. over pixels					not included yet
Av. over rings					not included yet
DT Final State Distributions					
Ground st. prob.	P_{gs}	3%	with P_{es}	Multisim	overestimated
Excited st. prob.	P_{es}		$P_{gs} + P_{es} = 1$	Multisim	

Continued on next page

Table 9.3 – *Continued from previous page*

Effect	Parameter	rel. error	correlation	method	comment
Excitation prob.	Pi	3%	uncorrelated	Multisim	overestimated
		Theoretical Corrections			
Radiative corr.				on/off	overestimated
All but rad. corr.				on/off	overestimated
Doppler				on/off	negligible
Synchrotron				on/off	negligible
		Background			
Rate				Fit	
Shape			deviation from flat		data driven
		Run Stacking			
				Multisim	data driven

9.3 Stability of slow control parameters

One of the challenges of KATRIN is to maintain stability on certain parameters in order to achieve the desired precision in the neutrino mass measurement. The First Tritium Campaign was the perfect opportunity to test this in some of the key parameters, i.e. column density (defined in sec. 9.5), tritium purity (defined in sec. 4.2.3), and retarding potential. The stability of the latter is already covered in sec. 5.2.2, the rest is discussed in the next paragraphs.

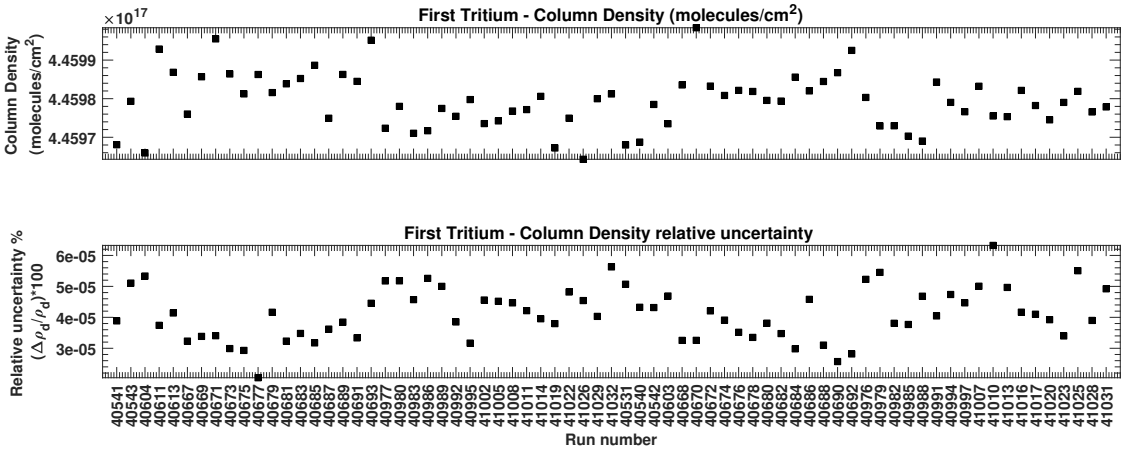

Figure 9.3 | **Column density stability.** Top: Column density values per run. Bottom: Relative uncertainty of the column density within one run.

As a reminder, in the Design Report [Col05] the limit on the relative uncertainty of the

column density is $\frac{\Delta\rho d}{\rho d} = 0.1$ %. For the runs with column density $\sim 4.5 \times 10^{17} \frac{\text{molecules}}{\text{cm}^2}$, the average of this relative uncertainty is 0.004 ± 0.001 % (fig. 9.3), which is well below the value stated in the Design Report. The column density was estimated from the buffer vessel pressure [Hei18] and its true value and its absolute uncertainty are only known with a ~ 8 % uncertainty. What is plotted in fig. 9.3 is the change of this estimated value within one run.

Although the LARA system (sec. 3.1.2) was designed to measure the concentrations of the isotopologues of tritium in a column density of $\sim 5 \times 10^{17} \frac{\text{molecules}}{\text{cm}^2}$, with molecular fractions around 95 % for TT, and 5 % for DT and HT. However, the only isotopologue used was DT, in about 1 % molecular fraction of the gas in the WGTS, which is far below the designed working point. The stability of it within each run is seen, as given at the time of writing by the LARA team, in fig. 9.4, together with its relative uncertainty. The LARA team communicated in the Analysis Workshop[4] in Munich July 2018, that the DT concentration calculation was being corrected, specially improving the absolute uncertainty associated with the DT concentration. As it is now, the relative uncertainty is 0.97 ± 0.2 %, which does not meet the requirement of 0.1 % relative precision, but again, the operating conditions of KATRIN in the First Tritium were not was LARA was design to measure [KZa18]. It was also informed at that meeting that the absolute uncertainty given for each DT measurement was overestimated, and a better estimate of that uncertainty was being calculated.

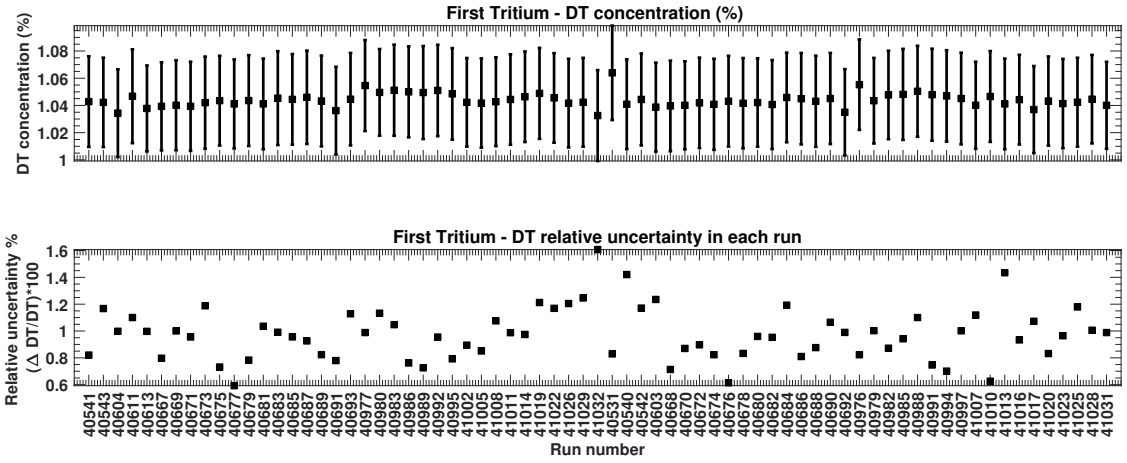

Figure 9.4 | **DT molecular fraction stability.** Top: DT molecular fraction (concentration) and its absolute uncertainty provided by the LARA Team. The error bars are overestimated at this stage. Bottom: Relative uncertainty of the DT concentration within one run.

[4]URL: https://indico.mpp.mpg.de/event/5918/

9.4 First endpoint limits of the tritium β-decay spectrum

In this section I use the different analysis types in SAMAK (chapter 5) to constrain the value of the tritium β-decay endpoint. The slow-control parameters for the model are taken from the Run Summaries. In the case of the simple stacking, a weighted average from the stacked runs is used, where each slow control parameter is weighted by the measurement time of its respective run.

Furthermore, the squared neutrino mass value is not fitted because the sensitivity to it given the First Tritium configuration is not relevant. It is fixed at a value of 0 eV in the model.

The data sets for the unsegmented detector, ring, and single pixel segmentations were fitted using Minuit [Jam94], the data set for the multipixel study was fitted with the MATLAB® minimizer fminunc [MAT18].

9.4.1 DT expected endpoint estimate

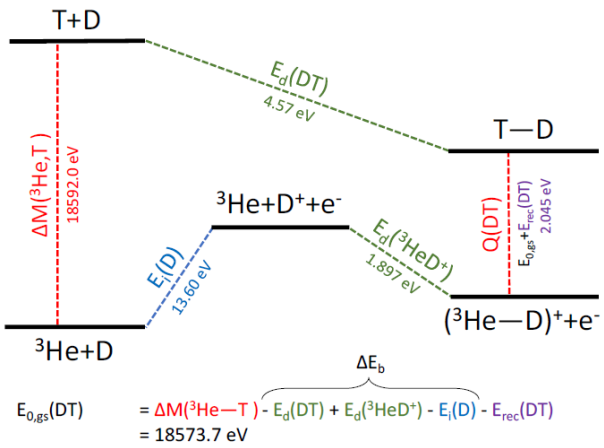

Figure 9.5 | **DT expected endpoint.** Estimation of the expected endpoint DT for the ground state of the daughter molecule. Figure from [Las18].

The endpoint fitted for any run or combination of runs for the First Tritium Campaign is the endpoint for tritium as part of the DT (deuterium-tritium) molecule. As seen in sec. 4.1, taking into account the recoil energy of the daughter nucleus E_{rec} and assuming that it is produced in the ground state ($V_j = 0$), the endpoint $E_{0,gs}$ of the tritium β-decay spectrum is

$$E_{0,gs} = Q - E_{\text{rec}}. \tag{9.1}$$

In the case of the DT molecule, Q, the energy released in the decay, is given by the mass difference of the tritium and helium atoms, minus the electronic binding energy of

the mother-daughter pair

$$Q = \Delta M(^3\mathrm{He}, \mathrm{T}) - \Delta E_b \tag{9.2}$$

The binding energy, ΔE_b, can in turn be calculated by the use of the dissociation energies (E_d) of DT and $^3\mathrm{HeD}^+$ and ionizing energies E_i of D,

$$\Delta E_b = E_d(\mathrm{DT}) - E_d(^3\mathrm{HeD}^+) + E_i(\mathrm{D}). \tag{9.3}$$

The dissociation energy of $^3\mathrm{HeD}^+$ is still under investigation, and for now the value for TT is taken: $E_d(^3\mathrm{HeD}^+) = 1.897$ eV [Las18]. Combining eqs. 9.1, 9.2, and 9.3, and using the values from fig. 9.5, the endpoint value is calculated to be

$$E_{0,gs} = 18573.7\,\mathrm{eV}. \tag{9.4}$$

Furthermore, there is an unknown work function at the rear wall, estimated to be in the hundreds of millivolts, and being independent for each pixel (See also 4.1). So the effective endpoint fitted is

$$E_{fit}(DT, W) = E_{0,gs}(DT) + W. \tag{9.5}$$

9.4.2 Comment on data

Invalid pixels

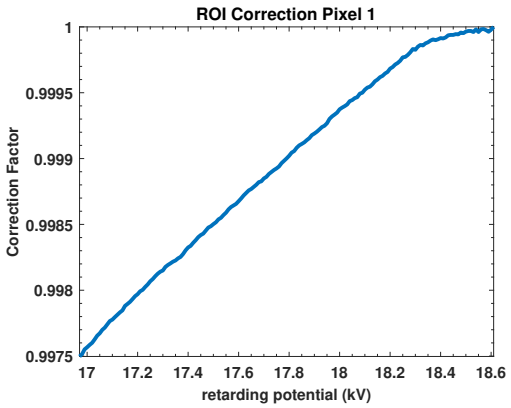

Figure 9.6 | **ROI correction factor for pixel 1.** The corrections amounts to a maximal difference of 0.25 % in the measurement bin furthest from the endpoint.

There was an issue with some of the pixels during First Tritium. Many pixels from the two rings closer to the edge of the detector showed a very small number of counts compared to the rest of the pixels. For this reason, they were removed from the analysis. More exactly, for the stacked pixels and ring studies, the last two rings are excluded; and for the pixel-wise analyses, pixels 112 and 123-148 are excluded.

ROI Correction Factor

There is also a correction due to the region of interest (ROI) cuts, that is dependent on both retarding potential and pixel. The function encoding this correction was provided by S. Enomoto. As can be seen in fig. 9.6, the correction becomes more important as the retarding potential goes farther away from the endpoint, and it does not

exceed 0.03 %. In SAMAK, to get the best estimate for the correction factor value at the retarding potential of interest, an interpolation using cubic splines is done.

9.4.3 Weighted mean

Due to the nature of some studies, sometimes not one but several fitted values are given as a result. Talking about the endpoint more specifically these studies have several fitted endpoint values.

- Stacked pixels all runs: one endpoint per run
- Ring study stacked runs: one endpoint per ring
- Single pixel study, stacked runs: one endpoint per pixel.

In all cases described in the previous list, to summarize the fitted values in just one value, I used a weighted average,

$$< E_0 >= \sum_{i=1}^{n} w_i E_{0,i}, \tag{9.6}$$

where the subscript i represents each run, ring, or pixel, n the total number of runs, rings, or pixels respectively, and the weights w_i are the inverse squared if the uncertainties σ_i of each fitted value

$$w_i = \frac{1}{\sigma_i^2}. \tag{9.7}$$

The new uncertainty to this average can be shown to be

$$< \sigma >= \frac{1}{\sqrt{\sum_{i=1}^{n} w_i}}. \tag{9.8}$$

9.4.4 Representative Endpoint for fit with systematics

Due to the correlation between the uncertainties from run to run or pixel to pixel, the simple weighted mean presented in sec. 9.4.3 cannot be used. In its place, the following procedure is applied.

We assume that the systematic uncertainties are fully correlated. One can then build a covariance matrix with the fitted endpoints as

$$M_{nn} = \begin{bmatrix} \sigma_{11} + s_{11} & s_{12} & s_{13} & \dots & s_{1n} \\ s_{21} & \sigma_{22} + s_{22} & s_{23} \dots & s_{2n} & \\ & \dots\dots\dots\dots\dots\dots & & & \\ s_{n1} & x_{n2} & s_{n3} & \dots & \sigma_{nn} + s_{nn} \end{bmatrix}, \tag{9.9}$$

where $s_{xx} = \sqrt{\sigma^2_{\text{x,total}} - \sigma^2_{\text{x,stat}}}$ and n is the total number of runs used in the analysis. With this covariance matrix one can then perform a fit on the endpoint using the values of each of the runs,

$$\chi^2 = \sum_{ij}^{n} (E_{0,i} - < E_0 >) M_{ij}^{-1} (E_{0,i} - < E_0 >), \tag{9.10}$$

and minimize with respect to $< E_0 >$. The $< E_0 >$ at which the minimum is found is considered to be the representative E_0 for the set of runs, and the uncertainty on $< E_0 >$ of the fit is the correct uncertainty including correlations. In this process the systematic uncertainties are considered to be fully correlated.

9.4.5 Effective endpoint fit summary table

Here are all the results condensed in a single table 9.4.

Table 9.4 | **Effective endpoint fit summary.** Results of the different kinds of analyses possible in SAMAK for the tritium β-decay endpoint, of tritium embedded in DT.

Segm.	(eV)	Stat.	χ^2	Stat.+Sys.	χ^2
NO	Runs Av.				
	Sh.	18573.7 ± 0.08	See fig. 9.8	18573.9 ± 0.63	See fig. 9.10
	Med.	18573.44 ± 0.04	See fig. 9.8	18574.4 ± 0.56	See fig. 9.10
	L.	18573.33 ± 0.02	See fig. 9.8	18574.8 ± 0.18	See fig. 9.10
	Stacked Runs				
	Sh.	18573.8 ± 0.07	32.73/15	18573.8 ± 0.64	27.85/15
	Med.	18573.44 ± 0.04	60.48/17	18574.5 ± 0.41	33.2/17
	L.	18573.34 ± 0.02	102.99/23	18574 ± 0.3	36.67/23
Ring	Stacked Runs				
	Sh.	18573.7 ± 0.07	See fig. 9.11	18573.9 ± 0.67	See fig. 9.12
	Med.	18573.44 ± 0.04	See fig. 9.11	18575.3 ± 0.48	See fig. 9.12
Single Pix.	Stacked Runs				
	Sh.	18573.7 ± 0.07	See fig. 9.13	18573.7 ± 0.66	See fig. 9.14
	Med.	18573.13 ± 0.04	See fig. 9.13	18573.2 ± 0.75	See fig. 9.14
Multi Pix.	Stacked Runs				
	Sh.	18573.8 ± 0.07	2149.94/1970	18573.7 ± 0.09	2104.34/1970
	Med.	18573.14 ± 0.04	6707.9/2216	18573 ± 0.08	6555.07/2216
	TOTAL	18573.4 ± 0.01			

9.4.6 Stacked Pixel Analysis (Uniform Mode)

As a short reminder, stacked pixel means that the counts from all pixels (in this case excluding the last two rings) are summed and the detector is treated as if it were just one pixel.

All runs

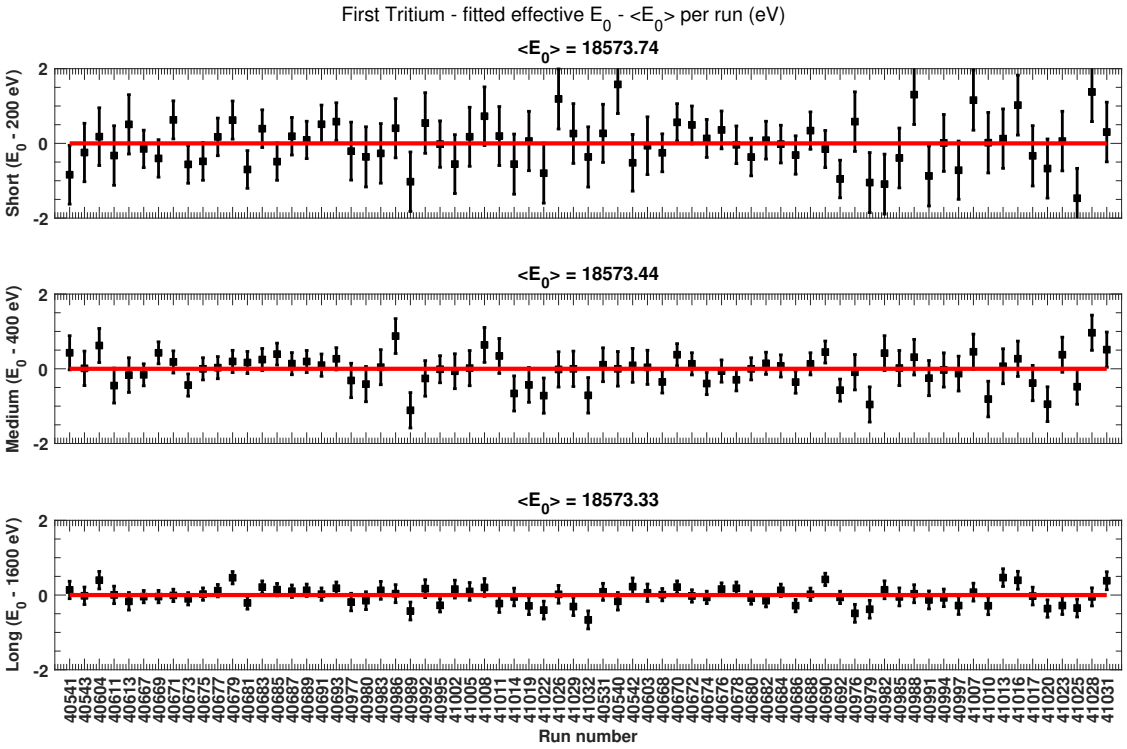

Figure 9.7 | **Effective E_0 statistical uncertainties all runs.** Value of the fitted endpoint minus the weighted mean endpoint for all runs analyzed from the First Tritium Campaign, using only statistical uncertainties.

Statistical uncertainty only First of all, the results of fitting the endpoint per run in the three ranges are shown in fig. 9.7.

As expected, the uncertainty on the fitted value is smaller as the range analyzed is larger. As the analyzed range increases the fitted endpoint strives away from the expected value, starting in 18573.74 ± 0.043 eV for the short range, and ending in 18573.33 ± 0.024 eV for the long range. Also, the fitted values for the three ranges are not the same within statistical uncertainties, which calls for the inclusion of systematics in the analysis.

The distribution of the test statistic is shown in fig. 9.8. It is clear that the distribution of the goodness of fit test parameter resembles a χ^2 distribution, although not perfectly.

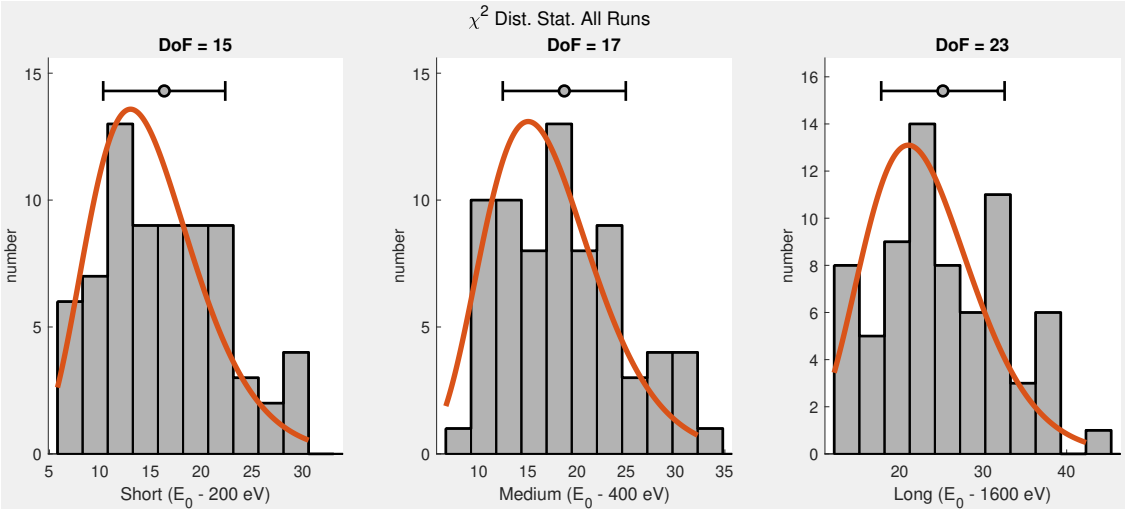

Figure 9.8 | χ^2 **dist. statistical all runs.** Distribution of the test statistic for the three ranges for all runs, using only statistical uncertainties. Left: short range (up to -200 eV from E_0). Middle: Medium range (-400 eV from E_0). Right: Long range (-1600 eV from E_0).

In this case, even for the long range, the statistical uncertainty is large enough for the minimizer to find a minimum close to the degrees of freedom of the fit.

Statistical and systematic uncertainty Performing the fit with the aid if the covariance matrix leads immediately to a larger uncertainty of the fitted endpoints. Now the values are less spread, and are the same within uncertainty. The fig. 9.9 shows again the development of the endpoint depending on the run, this time with systematics. In the short range, the main pattern is maintained because this range is dominated by statistics.

In fig. 9.10 it is visible that the distribution of the test statistic is slightly perturbed by the inclusion of the covariance matrix in the short and medium ranges, but in the long range, that distribution looks much closer to a χ^2 distribution, when compared to the case with statistics only. The weighted mean for the medium and especially long range, are above most measurements due to the fully correlation of the systematic uncertainties. This was done as a first approach, but it could be improved by adding the information on the correlation coefficient between the systematic uncertainties, and separating the uncertainty due to tritium activity fluctuations as it is uncorrelated.

Stacked runs

Statistical uncertainty only The fitted values for the case where all runs are stacked follow the trend given by the mean endpoint values of the analysis of all the runs, as well as the uncertainties. Actually, up to 0.01 eV precision, the uncertainties are the same, meaning that the effect of stacking with this level of statistics does not affect the results significantly. One can also see clearly, looking at the χ^2 value, that the model

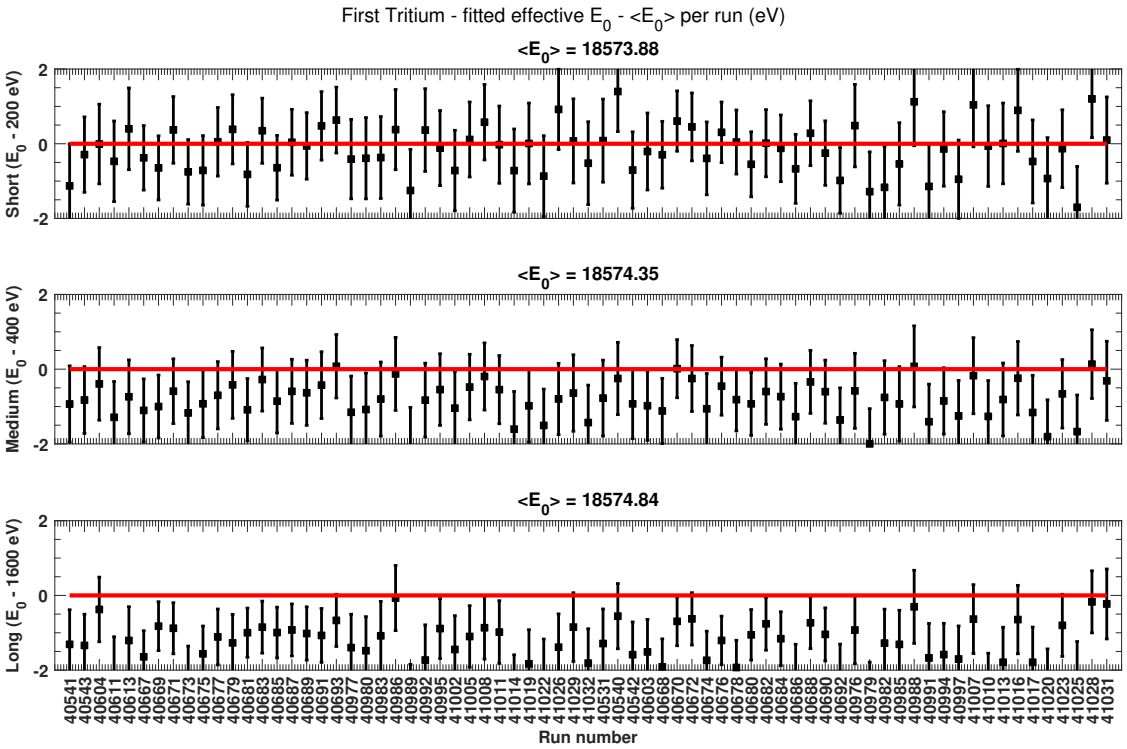

Figure 9.9 | **Effective E_0 statistical and systematical uncertainties all runs.** Value of the fitted endpoint minus the weighted mean endpoint for all runs analyzed from the First Tritium Campaign, using statistical and systematic uncertainties.

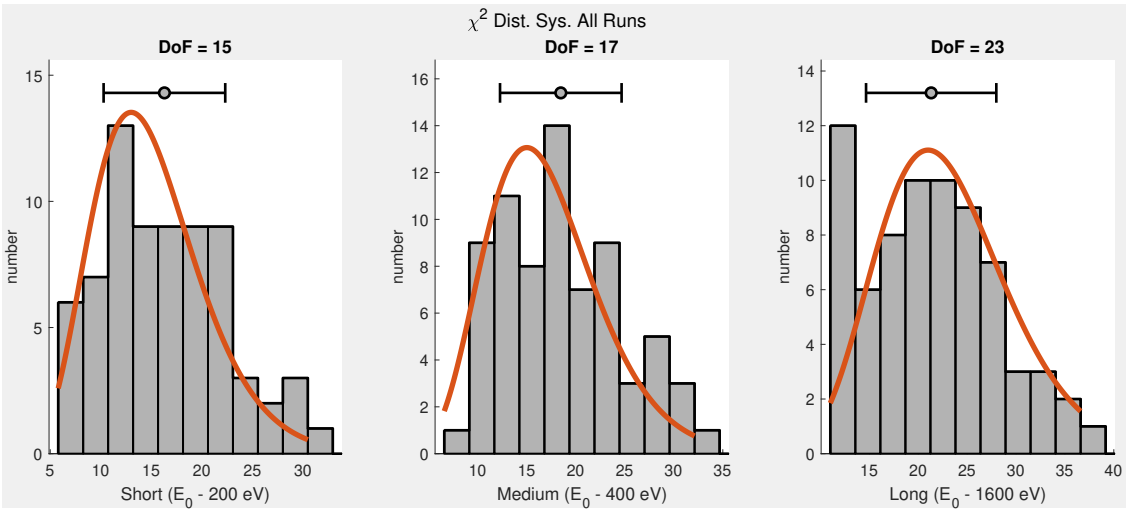

Figure 9.10 | **χ^2 dist. statistical all runs.** Distribution of the test statistic for the three ranges for all runs, using statistical and systematic uncertainties. Left: short range (up to -200 eV from E_0). Middle: Medium range (-400 eV from E_0). Right: Long range (-1600 eV from E_0).

looks less and less like the data, within statistical uncertainty. This also confirms that there are still effects that need to be understood at ranges further away than -200 eV.

Statistical and systematic uncertainty Although still not perfect, the minimizer finds a χ^2 value much closer to the degrees of freedom in the fit. One of the reason for this is that the differences in qU due to the simple stacking are taken into account by the systematic treatment. Nevertheless, seeing that the p-value of the long range fit is $p = 0.035$, one might think of it as an indicator that there is still work to do in the investigation of the systematics of First Tritium.

9.4.7 Stacked Ring Analysis

Statistical uncertainty only The first division of the segmentation brings no surprises in terms of the values fitted, as it follows quite closely the trend presented so far, up to the precision shown[5]. The long range was excluded because of the lack of knowledge we have on the model, explained earlier.

The effect on averaging the electrostatic and magnetic field inhomogenities within a ring has not yet been accounted for in a covariance matrix. Nevertheless, one can already give some comments about it observing at the results. The spread of the retarding potential among different runs does not exceed 300 meV. In the case of the electrostatic potential inhomogenities, that spread among pixels is lower than 150 meV. So this averaging of retarding potentials when stacking the pixels has an effect smaller than the spread resulting from stacking the runs. The averaging of the magnetic field inhomogenities apparently has an small impact, too. In fig. 9.11 one can see the fitted values per ring and the χ^2 distribution for the ranges analyzed.

There is no radial dependency on the endpoint value, as expected, but the pattern is different for the short and medium ranges. This difference could be explained if the extra data points taken into account in the medium range have more importance for the fit, than the rest of the points.

Statistical and systematic uncertainty An important comment here is that there is no dedicated covariance matrix for the ring analysis, so the covariance matrix for the stacked pixels stacked runs was used, with the appropriate statistics for each ring.

By adding the systematic uncertainty in the fit, fig. 9.12. The test statistic distribution in the medium range follows better a χ^2 distribution than with only statistics. As in the case of applying the "correlated" weighted mean to the fitted endpoint of the individual runs, the full correlation of the systematical uncertainties shifts the weighted mean endpoint to higher values, outside of the range of the individual endpoints per ring.

[5]Not shown in this work: if one takes more digits, they do become different.

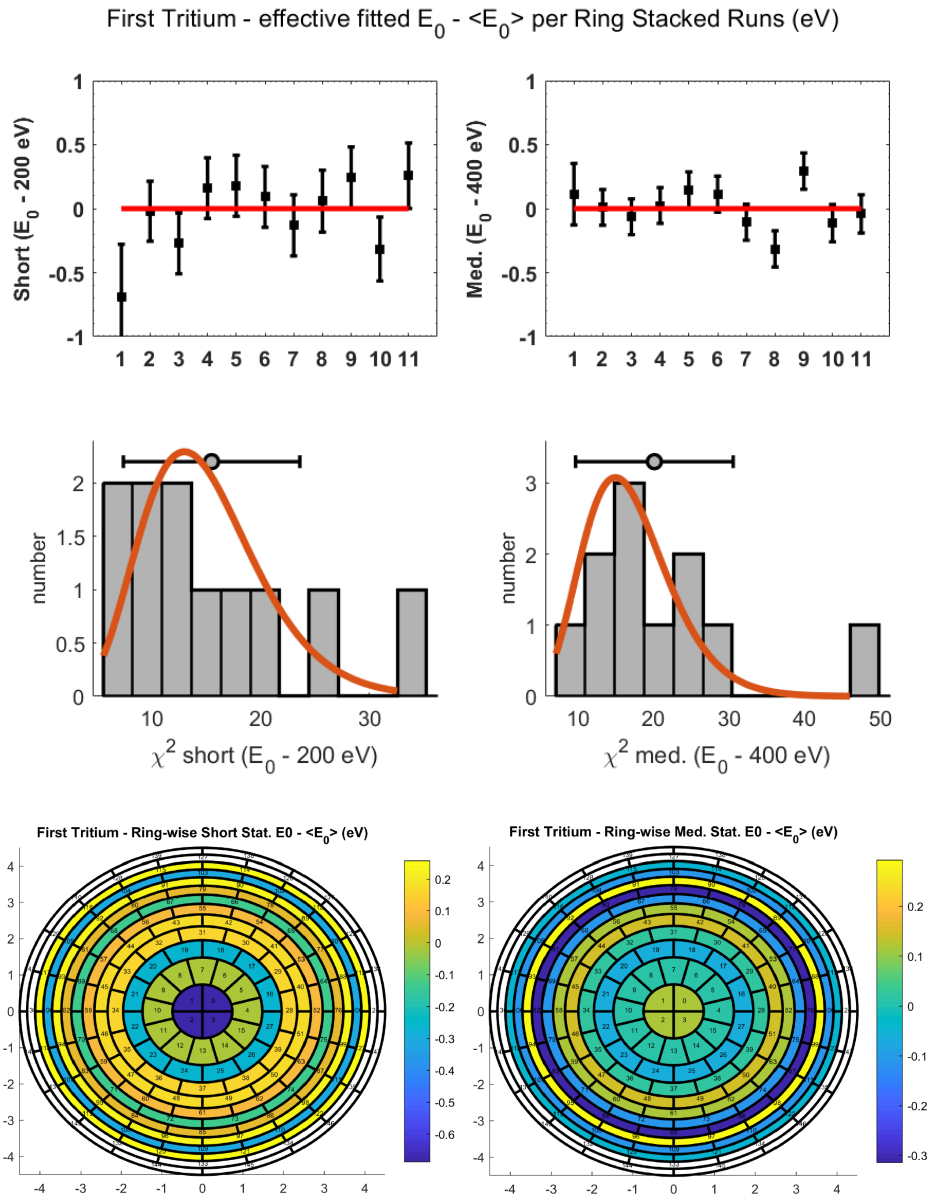

Figure 9.11 | **Effective E_0 statistics per ring.** Top: fitted endpoint per ring short range (left) and medium range (right), using only statistical uncertainties. Middle: test statistic distribution short range (left) and medium range (right). Bottom: FPD view of the fitted values in each ring short range (left) and medium range (right).

9.4.8 Single-pixel Analysis

Statistical uncertainty only A further segmentation of the detector again brings no new information on the discussion to the fit values. Let us have a look at the FPD Viewer

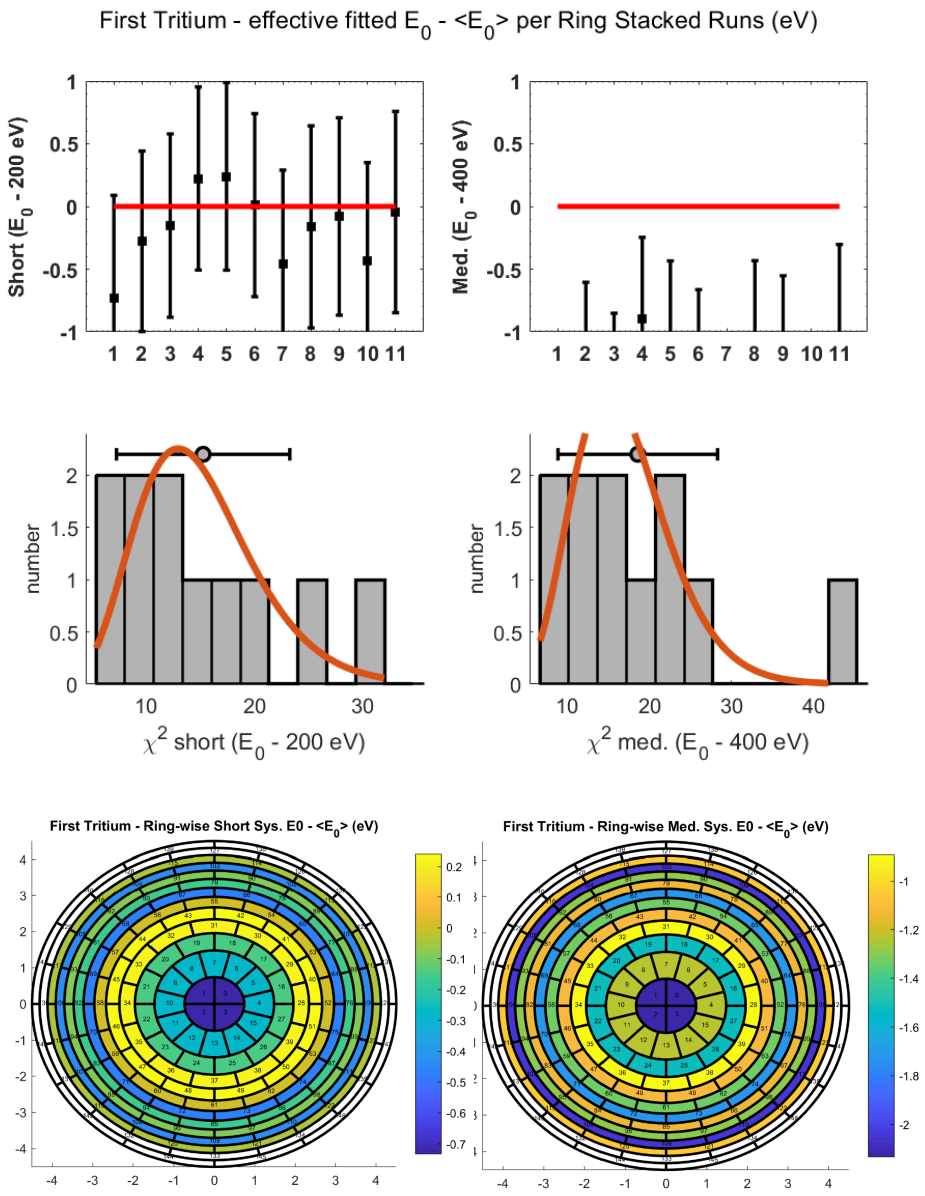

Figure 9.12 | **Effective E_0 statistics + systematics per ring.** Top: fitted endpoint per ring short range (left) and medium range (right), using statistical and systematic uncertainties. Middle: test statistic distribution short range (left) and medium range (right). Bottom: FPD view of the fitted values in each ring short range (left) and medium range (right).

and χ^2 distribution in fig. 9.13.

A remarkable feature is that the test statistic distribution does not follow a χ^2 distribution for the degrees of freedom in the medium range, highlighting the need of a

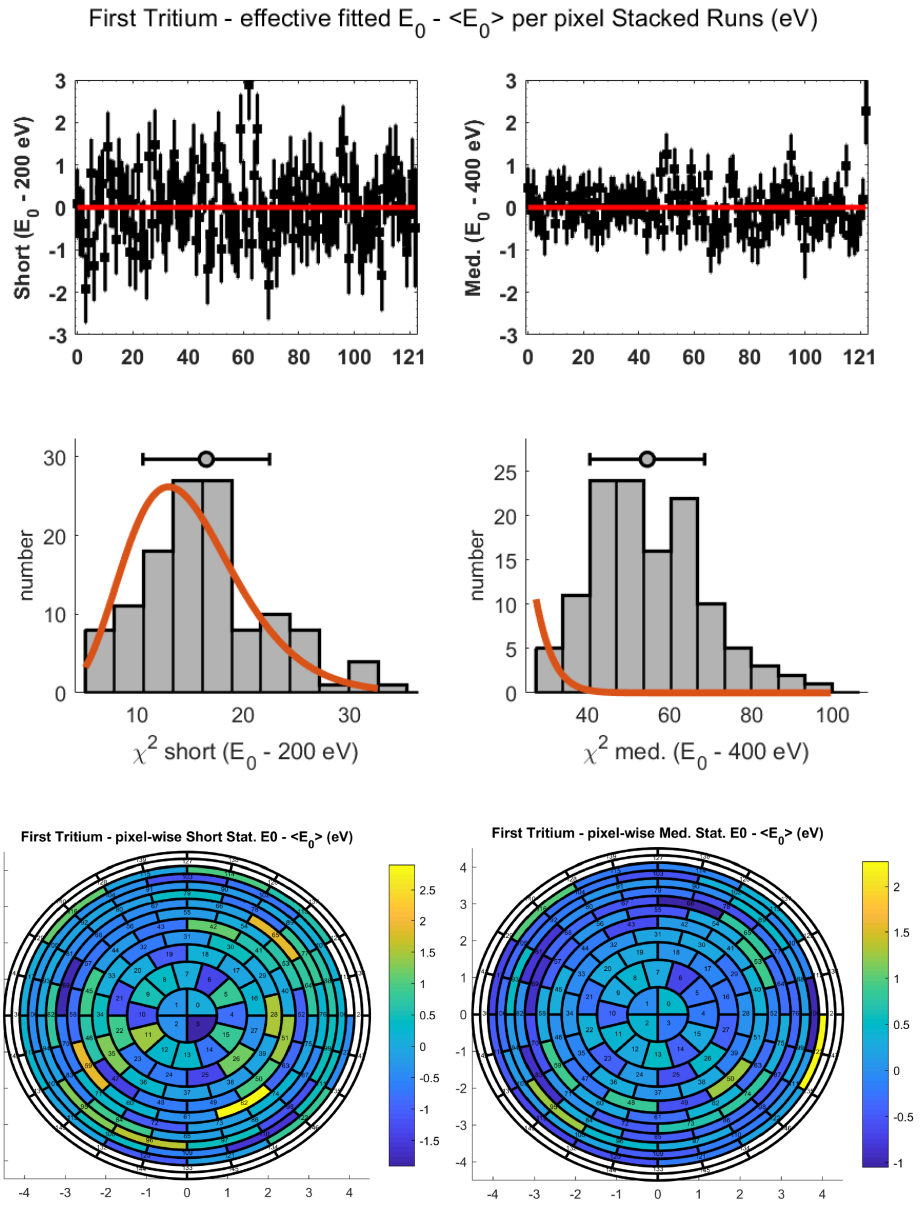

Figure 9.13 | **Effective E_0 statistics per pixel.** Top: fitted endpoint per pixel short range (left) and medium range (right), using only statistical uncertainties. Middle: test statistic distribution short range (left) and medium range (right). Bottom: FPD view of the fitted values in each pixel short range (left) and medium range (right).

better understanding of the data in ranges longer than -200 eV below the endpoint, and improved stacking techniques. Some of the pixels in the FPD view maintain the same relative value compared to the rest of the pixels (6, 50, 59, 95, and 116), but others do

change (62, 66, and 122). Nevertheless, no pattern can be distinguished in any of the two cases.

It should be noted that the minimizer is dealing with very low statistics in the zone close to the endpoint. The order of magnitude of counts from $[-30, 40]$ eV from E_0 is 10^2 per pixel, with an statistical uncertainty of ~ 10. This leads to difficulties for the minimizer to find the background precisely.

Statistical and systematic uncertainty Similarly to the ring analysis, there is no pixel-wise covariance matrix. Again the covariance matrix from the stacked pixels stacked runs was used, with the correct statistics for each pixel. In the future the plan is to have a covariance matrix that one can use in each pixel individually, and that includes correlations among pixels.

In this case, fig. 9.14, the covariance matrix did little to change the results. There are more similarities in the FPD Viewer in both ranges, but the χ^2 distributions remains almost unchanged. It is possible that the systematic effects act differently on each pixel individually, than in the detector as a whole. This calls for a more intensive look into the systematics of the experiment, and for the elaboration of covariance matrices that incorporate possible correlations among pixels.

9.4.9 Multi-pixel Analysis

Statistical uncertainty only Finally, the fit that incorporates all of the information in the data, whose results are in table 9.4. The χ^2 value for the short range is of course the better of the two, but its p-value of 0.002 is rather low, indicating that the model does not match well the data. The values fitted do not deviate from the trend of the other analyses, and in this case, the added segmentation does not provide more precision, as the uncertainty on the fitted parameters is the same.

This fit uses the same data as the single pixel fit, but in a different way. Therefore, similar low statistics issues could arise in this study.

Building on the premise that the segmentation and the stacking are not the most significant source of error, the values obtained from the fit are expected, as the same quantity of statistics is analyzed in each case. What changes is just the granularity of the segmentation of the detector, which can be translated in different response functions for each pixel (or ring). The response functions in turn are only differentiated by the inhomogenities if the magnetic and electrostatic fields.

Statistical and systematic uncertainty Once more, the covariance matrix from the stacked pixel stacked runs was applied to each pixel. Adding the systematics decreases the χ^2 value slightly, but in this case the covariance matrix was not able to make the fitted values be in the same range within uncertainties. This confirms the need of a deeper understanding of the systematics pixel-wise, and again a dedicated covariance matrix for the Single and Multi-pixel analyses.

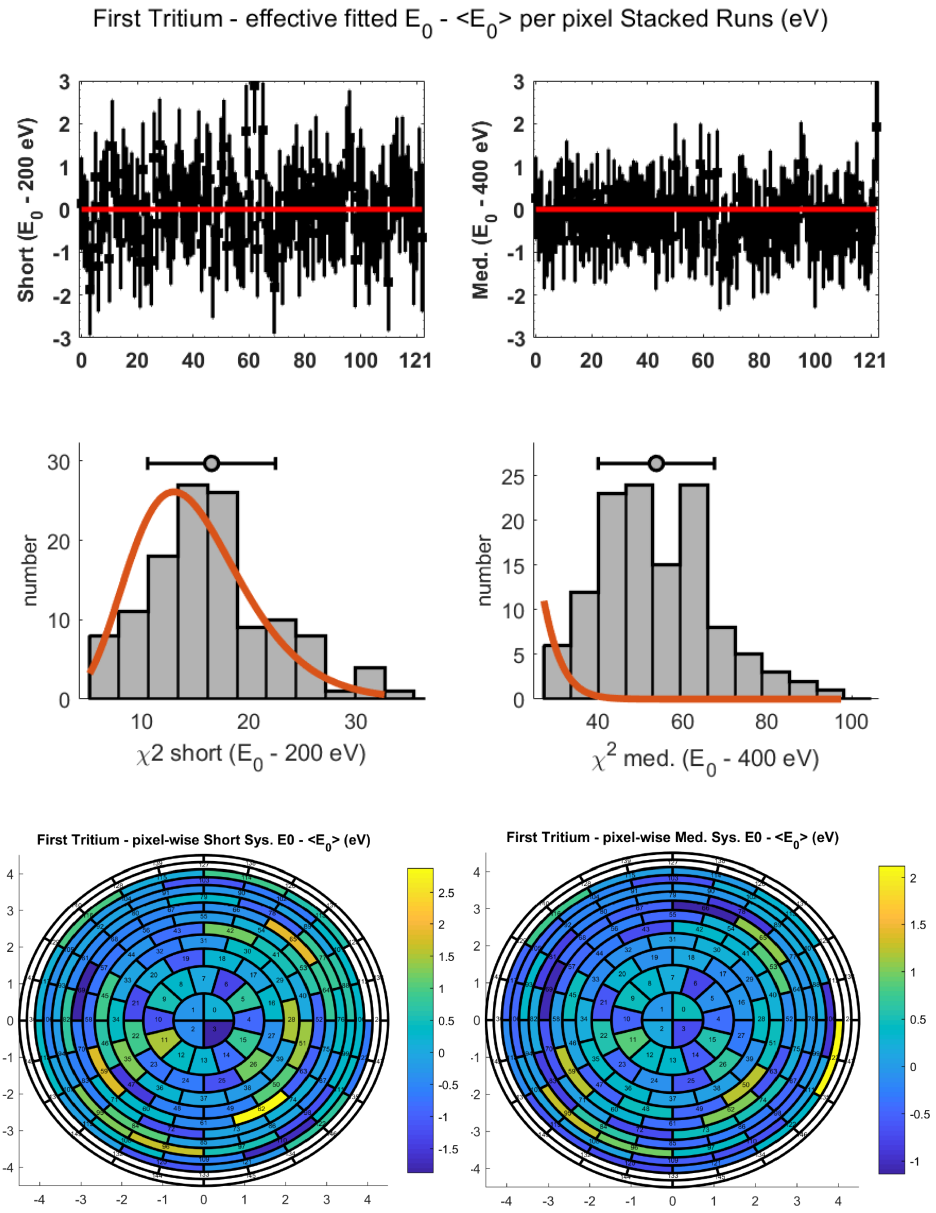

Figure 9.14 | **Effective E_0 statistics + systematics per pixel.** Top: fitted endpoint per pixel short range (left) and medium range (right), using statistical and systematic uncertainties. Middle: test statistic distribution short range (left) and medium range (right). Bottom: FPD view of the fitted values in each pixel short range (left) and medium range (right).

9.4.10 Summary Endpoint Fits

In fig. 9.15 is the plot with the information about the fits discussed in the previous sections. The most relevant remarks is that the accounting of systematics is critical

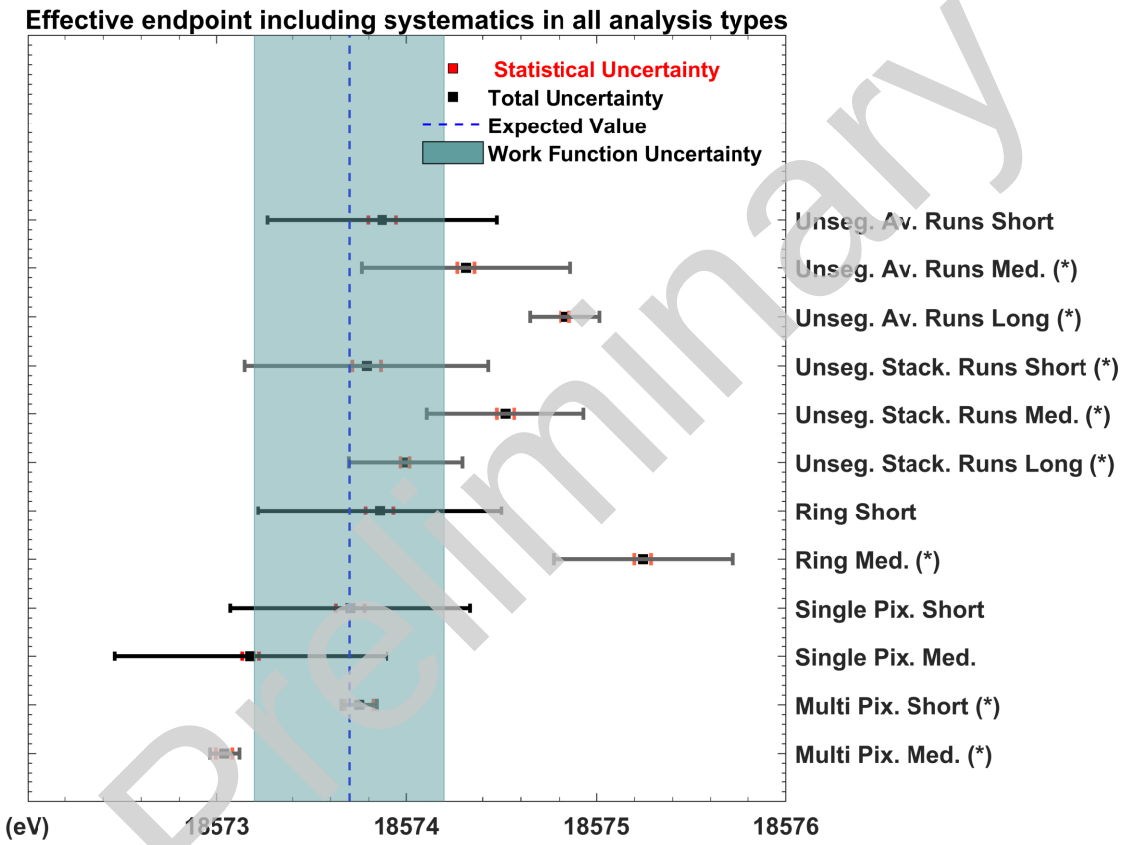

Figure 9.15 | **Effective endpoint summary.** Effective endpoints fitted per analysis mode with statistical and total uncertainties. The systematic uncertainties are fully correlated. (*) The labels marked with (*) means that the p-value of the fit was smaller than 0.05, indicating that the model does not match well the data, and therefore may not be reliable.

to analyze the data, specially going lower than -200 eV away from the endpoint. The tools to analyze the spectrum were for years developed for a range that would not exceed more than -100 eV from the endpoint, and therefore there is still work ongoing in the understanding of the data in the medium and long ranges. In this respect, the systematics treatment through the covariance matrix has proven to be a useful in improving the fit and bringing realistic uncertainties on the fitted parameters.

The low statistics per pixel/per ring makes it necessary to stack the runs, and with the simple stacking mechanism currently used in SAMAK, we incur in a mistake as the data is not taken under the same slow-control conditions run after run. This is already taken into account in the covariance matrix for the unsegmented FPD, but it still has to be seen if there is a need of a dedicated covariance matrix for the stacking of the pixels or rings. Also, there are better stacking mechanisms that minimize the mistake done with the stacking.

9.5 Column density handle

9.5.1 Column density scan

Since the E-gun for a precise measurement of the column density is not available yet, the value of the column density has been investigated by other means, i.e. with the buffer vessel pressure and the throughput of the WGTS loop system [Hei18]. Another method available is treating the column density as a free fit parameter. The greatest challenge of this new fit, is the computational time it would take to perform the minimization. An average fit of the First Tritium Data with the MATLAB® minimizer needs tens of thousands of function evaluations (using numerical derivatives), fitting just the neutrino mass squared, endpoint, background and overall normalization. When the minimizer explores new column density values, new response functions should be calculated for each model, and due to the long range analyzed and fine binning of the response function, this can be time consuming. So although possible, with the resources at hand it was impractical to attempt to do so.

A workaround to the previously exposed problem is to "scan" over the column density, which we call ρd scan in what follows. This is done by initializing the model with a certain value of the column density and performing a fit. The values are discrete and are chosen uniformly within a predefined range, normally between 50 % to 150 % of the value given in the Run Summary, going in steps of 10 %. At each stage, all other fit parameters are free to converge to any value.

A parabola around the minimum is then formed with the χ^2 values at each column density. But since the points are spread out, the minimum of this parabola is very probably between two of the points. To obtain this minimum, we take the 4 points closer to the point with the lowest value (inclusively, so 5 points in total), and fit a parabola with the function polyfit [MAT18] from MATLAB®.

$$\chi^2 = a \cdot (\rho d)^2 + b \cdot (\rho d) + c. \tag{9.11}$$

After fitting the coefficents a, b, and c, we find the column density value where the minimum χ^2 is located,

$$CD_{\text{min}} = -\frac{b}{2a}, \tag{9.12}$$

and also that minimum χ^2_{min}

$$\chi^2_{\text{min}} = y(CD_{\text{min}}). \tag{9.13}$$

Using also the χ^2 values, the asymmetric errors are computed by calculating the intersection of a line, parallel to the horizontal axis at $\chi^2_{min} + 1$, with the parabola. The column density value left to CD_{min} is the lower bound on the uncertainty, and the value right of CD_{min} is the upper bound.

9.5.2 Special set of runs at different column densities

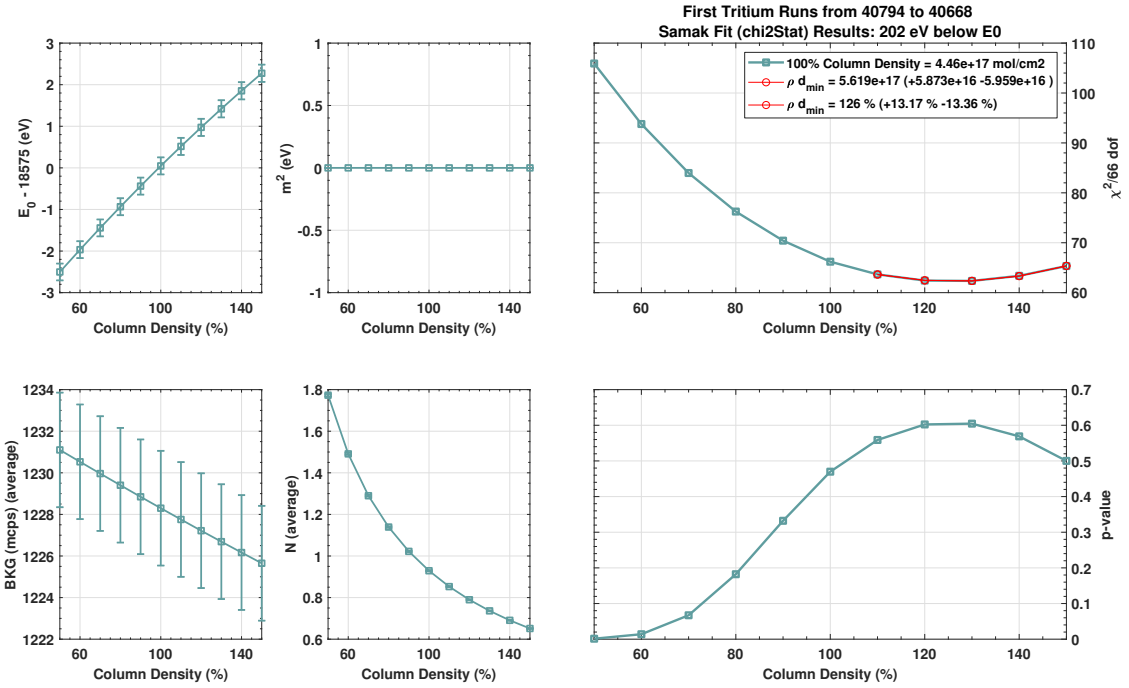

Figure 9.16 | ρd **scan.** ρd scan using 4 data sets of runs at 24 %, 48 %, 71 % and 100 % column density, analyzed in the short range.

During the First Tritium, same runs were done at different column densities. For this study, column densities are normally given in percentage, where 100 % corresponds to the column density of run 40668, which is $\rho d(40668) = 4.4598 \times 10^{17}$ molecules/cm^2.

- 11 runs at 24 % column density (40794 to 40804),
- 4 runs at 48 % column density (40763 to 40766)
- 10 runs at 71 % column density (40926 to 40935)
- 1 runs at 100 % column density (40668)

With this data set, a simultaneous ρd scan is performed, using four different sets of ρd. The absolute value of the column density is poorly known, but the relative values are known precisely by the estimation made with the buffer vessel pressure and the throughput of the WGTS loop system [Hei18], and we use this information to better constrain the absolute value of the ρd. A model is made such that it has the properties of the stacked runs of each data set (four models in total).

The neutrino mass is not fitted and is maintained at 0 eV, the endpoint is common for all data sets, but the normalization and background can be fitted independently. In

total, 13 parameters are fitted: 1 endpoint, 4 normalizations and 4 background values (flat over the energy range of interest).

The minimized function is then

$$\chi^2 = \sum_{n=1}^{4} \sum_{t,q} (N_{n,q}^{\text{data}} - N_{n,q}^{\text{model}}(\mathrm{X})) M_{t,q}^{n} (N_{n,q}^{\text{data}} - N_{n,q}^{\text{model}}(\mathrm{X}))^{\intercal}) \tag{9.14}$$

where the subscript n stands for each one of the datasets, and X is the vector with the 13 fitted parameters. $M_{t,q}^{n}$ contains both statistical and systematic uncertainties in the integral spectrum, including bin to bin correlations. For the case of only statistical uncertainties, the content of X is the counts of the electron events at each retarding potential in the main diagonal.

At first we perform a fit using only the statistical uncertainties in the short range (up to -200 eV from the endpoint).

9.5.3 Scanned Column Density

The result of such a fit is in fig. 9.16. The best value found with this manual search is $5.62^{+0.59}_{-0.6} \times 10^{17}\ \frac{\text{molecules}}{\text{cm}^2}$, which is $126^{+13.2}_{-13.4}$ % from the value given in run 40668. This means that the value in the Run Summary is underestimated. One should have in mind the limitations of this value, where the fit was done without systematics and with stacked runs and stacked pixels.

A similar study using the medium range, gives a CD_{min} value of $116^{+4.43}_{-5.8}$ %, and on the long range $CD_{\text{min}} = 104^{+3.9}_{-3.1}$ %. Even tough the value of the fitted column density gets closer to the value proposed in the Run Summary, it is still outside of the range given by the uncertainties of the scan, and it is always underestimated.

The scan was also done in the long range, and using the covariance matrix to account for the systematics. The results are summarized in table 9.5. In all cases the same trend is followed, the CD_{min} is lower as the range increases. In the case of the study with statistical and systematic uncertainties, the results agree with each other. That is not the case for the statistical only study. In all cases, according to the results, the column density value given in the Run Summary was underestimated.

At the time of writing there is no way to assess if the Column Density values obtained in this way are more correct than the ones estimated through the buffer vessel pressure or throughput. However, this is one method to investigate the Column Density value by using the spectrum itself.

Table 9.5 | **Column Density handle.** Values of the column density where the minimum χ^2 is found, for the special data set described in the text.

ρd scan	100 % = 4.46×10^{17} $\frac{\text{molecules}}{cm^2}$
Stat.	CD_{min}
Sh.	$126^{+13.17}_{-13.36}$
Med.	$116^{+4.43}_{-5.8}$
L.	$104^{+3.91}_{-3.13}$
Stat.+Sys.	
Sh.	$135^{+26.24}_{-21.67}$
Med.	$121^{+11.6}_{-12.9}$
L.	$115^{+7.3}_{-7.2}$

10 Conclusion

In this thesis, SAMAK, a new analysis software to analyze KATRIN data, was presented. SAMAK is a MATLAB® based software which has a detailed model of the tritium β-decay spectrum. It also includes, through the KATRIN response function, the effects of the experimental settings of KATRIN. In addition, SAMAK can fit real data produced by KATRIN, using Minuit [Jam94] or the MATLAB® minimizer fminunc [MAT18], both gradient based. Systematic uncertainties are treated through the covariance matrix approach in SAMAK.

The SAMAK code was validated by recovering the sensitivity of KATRIN for the electron antineutrino mass for the 3-year measurement with the nominal settings from the Design Report [Col05]. Afterwards, it was applied to calculate the sensitivity to m_ν considering the most updated background experimental information from the First Tritium Campaign. A flat measuring time distribution extended to -60 eV below the endpoint was used to obtain a sensitivity of 0.3 eV for the neutrino mass, which could be further improved by optimized scanning strategies.

SAMAK also participated in several data challenges, which are events designed to compare and harmonize the results among different analysis tools. A deeper understanding of each of the analysis tools was gained by figuring out the differences among the models used. Since the analysis codes are under constant development, having periodic data challenges help minimize the possibility of having unnoticed mistakes in the code.

A special framework in SAMAK was developed, dedicated to analyzing the data coming from the First Tritium Campaign. That framework is prepared to read in the KATRIN data in the form of HDF5 files, and analyze it using the different analysis modes available for the First Tritium. The analysis modes are the possible combinations of the segmentations of the Focal Plane Detector (uniform mode, ring, single pixel and multipixel), the qU scan ranges (short -200 eV below E_0, medium -400 eV below E_0, long -1600 eV below E_0), and the stacking of the runs.

Using such framework the effective[1] endpoint of the tritium β-decay spectrum was analyzed, with the current status of the systematic uncertainties. A final value for the physical endpoint cannot be given yet, most of the values in the different analysis mode lie around the expected value of 18573.7 eV for DT [Las18].

One more study with the KATRIN First Tritium data was done to have a new handle on the column density (density of the gas in the Windowless Gaseous Tritium Source of KATRIN), since currently it is poorly known, with an uncertainty of 8 %. This study

[1] E_0 + work function

made use of a set of runs with different column density and of the fact that, although the absolute value of the column density is not precisely known, the relative values are known. The results of this study indicates that, if correct, the column density was underestimated, and the correct absolute value, depending on the qU range considered for the analysis, could be between 101 % and 160 % of the value given in the Run Summaries.

The SAMAK software is under development, and new features and components are added continuously. After finishing the First Tritium analysis, SAMAK will continue giving valuable information to the KATRIN Collaboration in the 3-year measurement phase and beyond.

List of Figures

List of Tables

Bibliography

[AB18] N. M. AB. *All Nobel Prizes in Physics. NobelPrize.org*. 2018. URL: https://www.nobelprize.org/prizes/uncategorized/all-nobel-prizes-in-physics/ (visited on 08/16/2018).

[Abd+02] J. N. Abdurashitov, E. P. Veretenkin, V. M. Vermul, V. N. Gavrin, S. V. Girin, V. V. Gorbachev, P. P. Gurkina, G. T. Zatsepin, T. V. Ibragimova, A. V. Kalikhov, T. V. Knodel, I. N. Mirmov, N. G. Khairnasov, A. A. Shikhin, V. E. Yants, T. J. Bowles, W. A. Teasdale, J. S. Nico, J. F. Wilkerson, B. T. Cleveland, S. R. Elliott, and SAGE Collaboration. "Solar neutrino flux measurements by the Soviet-American gallium experiment (SAGE) for half the 22-year solar cycle." In: *Journal of Experimental and Theoretical Physics* 95.2 (Aug. 2002), pp. 181–193. ISSN: 1090-6509. DOI: 10.1134/1.1506424.

[Abe+11] K. Abe et al. "Solar neutrino results in Super-Kamiokande-III." In: *Phys. Rev.* D83 (2011), p. 052010. DOI: 10.1103/PhysRevD.83.052010. arXiv: 1010.0118 [hep-ex].

[Abe+12a] Y. Abe et al. "Indication of Reactor $\bar{\nu}_e$ Disappearance in the Double Chooz Experiment." In: *Phys. Rev. Lett.* 108 (2012), p. 131801. DOI: 10.1103/PhysRevLett.108.131801. arXiv: 1112.6353 [hep-ex].

[Abe+12b] Y. Abe et al. "Indication of Reactor $\bar{\nu}_e$ Disappearance in the Double Chooz Experiment." In: *Phys. Rev. Lett.* 108 (2012), p. 131801. DOI: 10.1103/PhysRevLett.108.131801. arXiv: 1112.6353 [hep-ex].

[Ada+11] P. Adamson, C. Andreopoulos, R. Armstrong, et al. "Measurement of the Neutrino Mass Splitting and Flavor Mixing by MINOS." In: *Phys. Rev. Lett.* 106 (18 May 2011), p. 181801. DOI: 10.1103/PhysRevLett.106.181801.

[Ago+13] M. Agostini, M. Allardt, E. Andreotti, et al. "Results on Neutrinoless Double-β Decay of ^{76}Ge from Phase I of the GERDA Experiment." In: *Phys. Rev. Lett.* 111 (12 Sept. 2013), p. 122503. DOI: 10.1103/PhysRevLett.111.122503.

[Ahm+02] Q. R. Ahmad, R. C. Allen, T. C. Andersen, et al. "Direct Evidence for Neutrino Flavor Transformation from Neutral-Current Interactions in the Sudbury Neutrino Observatory." In: *Phys. Rev. Lett.* 89 (1 June 2002), p. 011301. DOI: 10.1103/PhysRevLett.89.011301.

[Ahn+12] J. K. Ahn et al. "Observation of Reactor Electron Antineutrino Disappearance in the RENO Experiment." In: *Phys. Rev. Lett.* 108 (2012), p. 191802. DOI: 10.1103/PhysRevLett.108.191802. arXiv: 1204.0626 [hep-ex].

[Alt+05] M. Altmann, M. Balata, P. Belli, E. Bellotti, R. Bernabei, E. Burkert, C. Cattadori, R. Cerulli, M. Chiarini, M. Cribier, S. d'Angelo, G. D. Re, K. Ebert, F. von Feilitzsch, N. Ferrari, W. Hampel, F. Hartmann, E. Henrich, G. Heusser, F. Kaether, J. Kiko, T. Kirsten, T. Lachenmaier, J. Lanfranchi, M. Laubenstein, K. Lützenkirchen, K. Mayer, P. Moegel, D. Motta, S. Nisi, J. Oehm, L. Pandola, F. Petricca, W. Potzel, H. Richter, S. Schoenert, M. Wallenius, M. Wojcik, and L. Zanotti. "Complete results for five years of GNO solar neutrino observations." In: *Physics Letters B* 616.3 (2005), pp. 174–190. ISSN: 0370-2693. DOI: https://doi.org/10.1016/j.physletb.2005.04.068.

[Ara+05] T. Araki, K. Eguchi, S. Enomoto, K. Furuno, K. Ichimura, H. Ikeda, K. Inoue, K. Ishihara, T. Iwamoto, T. Kawashima, et al. "Measurement of neutrino oscillation with KamLAND: Evidence of spectral distortion." In: *Physical Review Letters* 94.8 (2005), p. 081801.

[Ase+00] V. Aseev, A. Belesev, A. Berlev, E. Geraskin, O. Kazachenko, Y. Kuznetsov, V. Lobashev, R. Ostroumov, N. Titov, S. Zadorozhny, Y. Zakharov, J. Bonn, B. Bornschein, L. Bornschein, E. Otten, M. Przyrembel, C. Weinheimer, and A. Saenz. "Energy loss of 18 keV electrons in gaseous T and quench condensed D films." In: *The European Physical Journal D - Atomic, Molecular, Optical and Plasma Physics* 10.1 (Mar. 2000), pp. 39–52. ISSN: 1434-6079. DOI: 10.1007/s100530050525.

[BC84] S. Baker and R. D. Cousins. "Clarification of the use of chi-square and likelihood functions in fits to histograms." In: *Nuclear Instruments and Methods in Physics Research* 221.2 (1984), pp. 437–442.

[Boy+18] A. Boyarsky, M. Drewes, T. Lasserre, S. Mertens, and O. Ruchayskiy. "Sterile Neutrino Dark Matter." In: (2018). arXiv: 1807.07938 [hep-ph].

[Cle+98] B. T. Cleveland, T. Daily, J. Raymond Davis, J. R. Distel, K. Lande, C. K. Lee, P. S. Wildenhain, and J. Ullman. "Measurement of the Solar Electron Neutrino Flux with the Homestake Chlorine Detector." In: *The Astrophysical Journal* 496.1 (1998), p. 505.

[Col+14] P. Collaboration, P. Ade, N. Aghanim, C. Armitage-Caplan, et al. "Planck 2013 results. XVI. Cosmological parameters." In: *Astron. Astrophys* 571 (2014), A16.

[Col+18] I. Collaboration et al. "Multimessenger observations of a flaring blazar coincident with high-energy neutrino IceCube-170922A." In: *Science* 361.6398 (2018), eaat1378.

[Col05] K. Collaboration. *KATRIN design report 2004*. Tech. rep. 51.54.01; LK 01; Auch: NPI ASCR Rez EXP-01/2005; MS-KP-0501. Forschungszentrum, Karlsruhe, 2005. 245 pp.

[Cow+56] C. L. Cowan, F. Reines, F. B. Harrison, H. W. Kruse, and A. D. McGuire. "Detection of the Free Neutrino: A Confirmation." In: *Science* 124.3212 (1956), pp. 103–104. ISSN: 00368075, 10959203.

[Dan+62] G. Danby, J. Gaillard, K. Goulianos, L. Lederman, N. Mistry, M. Schwartz, and J. Steinberger. "Observation of high-energy neutrino reactions and the existence of two kinds of neutrinos." In: *Physical Review Letters* 9.1 (1962), p. 36.

[Dav87] G. David. *Introduction to elementary particles*. John Wiley and Sons, 1987.

[DeC+89] D. DeCamp, B. Deschizeaux, J.-P. Lees, et al. "Determination of the number of light neutrino species." In: *Physics Letters B* 231.4 (1989), pp. 519–529. ISSN: 0370-2693. DOI: https://doi.org/10.1016/0370-2693(89)90704-1.

[Dre+13] G. Drexlin, V. Hannen, S. Mertens, and C. Weinheimer. "Current direct neutrino mass experiments." In: *Advances in High Energy Physics* 2013 (2013).

[DT08] N. Doss and J. Tennyson. "Excitations to the electronic continuum of 3 HeT in investigations of T 2 beta-decay experiments." In: *Journal of Physics B: Atomic, Molecular and Optical Physics* 41.12 (2008), p. 125701.

[Eno17] S. Enomoto. *IDLE: Intermediate Data Layer for Everyone*. 2017. URL: http://katana.npl.washington.edu/~sanshiro/doc/IDLE/IdleManual.html (visited on 08/16/2018).

[Est+17] I. Esteban, M. C. Gonzalez-Garcia, M. Maltoni, I. Martinez-Soler, and T. Schwetz. "Updated fit to three neutrino mixing: exploring the accelerator-reactor complementarity." In: *Journal of High Energy Physics* 2017.1 (Jan. 2017), p. 87. ISSN: 1029-8479. DOI: 10.1007/JHEP01(2017)087.

[Fer34] E. Fermi. "Versuch einer Theorie der β-Strahlen. I." In: *Zeitschrift für Physik* 88.3-4 (1934), pp. 161–177.

[Fer50] E. Fermi. *Nuclear physics: a course given by Enrico Fermi at the University of Chicago*. University of Chicago Press, 1950.

[Fuk+96] Y. Fukuda, T. Hayakawa, K. Inoue, K. Ishihara, H. Ishino, S. Joukou, T. Kajita, S. Kasuga, Y. Koshio, T. Kumita, K. Matsumoto, M. Nakahata, K. Nakamura, K. Okumura, A. Sakai, M. Shiozawa, J. Suzuki, Y. Suzuki, T. Tomoeda, Y. Totsuka, K. S. Hirata, K. Kihara, Y. Oyama, M. Koshiba, K. Nishijima, T. Horiuchi, K. Fujita, S. Hatakeyama, M. Koga, T. Maruyama, A. Suzuki, M. Mori, T. Kajimura, T. Suda, A. T. Suzuki, T. Ishizuka, K. Miyano, H. Okazawa, T. Hara, Y. Nagashima, M. Takita, T. Yamaguchi, Y. Hayato, K. Kaneyuki, T. Suzuki, Y. Takeuchi, T. Tanimori, S. Tasaka, E. Ichihara, S. Miyamoto, and K. Nishikawa. "Solar Neutrino Data Covering Solar Cycle 22." In: *Phys. Rev. Lett.* 77 (9 Aug. 1996), pp. 1683–1686. DOI: 10.1103/PhysRevLett.77.1683.

[Gro+11] S. Grohmann, T. Bode, H. Schön, and M. Süßer. "Precise temperature measurement at 30K in the KATRIN source cryostat." In: *Cryogenics* 51.8 (2011), pp. 438–445. ISSN: 0011-2275. DOI: https://doi.org/10.1016/j.cryogenics.2011.05.001.

[Gro15] S. Groh. "Modeling of the response function and measurement of transmission properties of the KATRIN experiment." PhD thesis. 2015.

[Gro18] T. H. Group. *HDF5*. 2018. URL: https://portal.hdfgroup.org/display/HDF5/HDF5 (visited on 08/16/2018).

[Han+17] V. Hannen, I. Heese, C. Weinheimer, A. S. Riis, and K. Valerius. "Deconvolution of the energy loss function of the KATRIN experiment." In: *Astroparticle Physics* 89 (2017), pp. 30–38. ISSN: 0927-6505. DOI: https://doi.org/10.1016/j.astropartphys.2017.01.010.

[Hei18] F. Heizmann. "Calculations of column densities from throughput, RunSummary. etc.." Analysis Workshop Munich 2018. 2018.

[Hen16] R. Henning. "Current status of neutrinoless double-beta decay searches." In: *Reviews in Physics* 1 (2016), pp. 29–35. ISSN: 2405-4283. DOI: https://doi.org/10.1016/j.revip.2016.03.001.

[IC82] R. L. Iman and W. J. Conover. "A distribution-free approach to inducing rank correlation among input variables." In: *Communications in Statistics - Simulation and Computation* 11.3 (1982), pp. 311–334. DOI: 10.1080/03610918208812265. eprint: https://doi.org/10.1080/03610918208812265.

[Jam94] F. James. "MINUIT Function Minimization and Error Analysis: Reference Manual Version 94.1." In: (1994).

[KAT99] KATRIN. *Transport Section*. 1999. URL: http://www.katrin.kit.edu/768.php (visited on 08/16/2018).

[Kle+18a] M. Kleesiek et al. "β-Decay Spectrum, Response Function and Statistical Model for Neutrino Mass Measurements with the KATRIN Experiment." In: (2018). arXiv: 1806.00369 [physics.data-an].

[Kle+18b] M. Kleesiek et al. "β-Decay Spectrum, Response Function and Statistical Model for Neutrino Mass Measurements with the KATRIN Experiment." In: (2018). arXiv: 1806.00369 [physics.data-an].

[Kle14] M. Kleesiek. "A Data-Analysis and Sensitivity-Optimization Framework for the KATRIN Experiment." PhD thesis. 2014.

[Kod+01] K. Kodama, N. Ushida, C. Andreopoulos, N. Saoulidou, G. Tzanakos, P. Yager, B. Baller, D. Boehnlein, W. Freeman, B. Lundberg, J. Morfin, R. Rameika, J. Yun, J. Song, C. Yoon, S. Chung, P. Berghaus, M. Kubantsev, N. Reay, R. Sidwell, N. Stanton, S. Yoshida, S. Aoki, T. Hara, J. Rhee, D. Ciampa, C. Erickson, M. Graham, K. Heller, R. Rusack, R. Schwienhorst, J. Sielaff, J. Trammell, J. Wilcox, K. Hoshino, H. Jiko, M. Miyanishi, M.

Komatsu, M. Nakamura, T. Nakano, K. Niwa, N. Nonaka, K. Okada, O. Sato, T. Akdogan, V. Paolone, C. Rosenfeld, A. Kulik, T. Kafka, W. Oliver, T. Patzak, and J. Schneps. "Observation of tau neutrino interactions." In: *Physics Letters B* 504.3 (2001), pp. 218–224. ISSN: 0370-2693. DOI: https://doi.org/10.1016/S0370-2693(01)00307-0.

[Kra+05] C. Kraus, B. Bornschein, L. Bornschein, J. Bonn, B. Flatt, A. Kovalik, B. Ostrick, E. W. Otten, J. P. Schall, T. Thümmler, and C. Weinheimer. "Final results from phase II of the Mainz neutrino mass searchin tritium β decay." In: *The European Physical Journal C - Particles and Fields* 40.4 (Apr. 2005), pp. 447–468. ISSN: 1434-6052. DOI: 10.1140/epjc/s2005-02139-7.

[KZa18] B. Krasch, G. Zeller, and et al. "Laser Raman spectroscopy at KATRIN." Analysis Workshop Munich 2018. 2018.

[Las18] T. Lasserre. "Simulation and Analysis of the First KATRIN Tritium Data wirh Samak (Technical Note)." Analysis Workshop Munich 2018. 2018.

[Lob+01] V. Lobashev, V. Aseev, A. Belesev, A. Berlev, E. Geraskin, A. Golubev, O. Kazachenko, Y. Kuznetsov, R. Ostroumov, L. Rivkis, B. Stern, N. Titov, C. Zadoroghny, and Y. Zakharov. "Direct search for neutrino mass and anomaly in the tritium beta-spectrum: Status of "Troitsk neutrino mass" experiment." In: *Nuclear Physics B - Proceedings Supplements* 91.1 (2001). Neutrino 2000, pp. 280–286. ISSN: 0920-5632. DOI: https://doi.org/10.1016/S0920-5632(00)00952-X.

[LP06] J. Lesgourgues and S. Pastor. "Massive neutrinos and cosmology." In: *Physics Reports* 429.6 (2006), pp. 307–379. ISSN: 0370-1573. DOI: https://doi.org/10.1016/j.physrep.2006.04.001.

[LP12] J. Lesgourgues and S. Pastor. "Neutrino mass from Cosmology." In: *Adv. High Energy Phys.* 2012 (2012), p. 608515. DOI: 10.1155/2012/608515. arXiv: 1212.6154 [hep-ph].

[LU00] L. L. Lucas and M. P. Unterweger. "Comprehensive review and critical evaluation of the half-life of Tritium." In: *Journal of research of the National Institute of Standards and Technology* 105.4 (2000), p. 541.

[Mas+07] S. S. Masood, S. Nasri, J. Schechter, M. A. Tórtola, J. W. F. Valle, and C. Weinheimer. "Exact relativistic β decay endpoint spectrum." In: *Phys. Rev. C* 76 (4 Oct. 2007), p. 045501. DOI: 10.1103/PhysRevC.76.045501.

[MAT18] MATLAB. *version 9.4.0.813654 (R2018a)*. Natick, Massachusetts: The MathWorks Inc., 2018.

[Mer+15] S. Mertens, T. Lasserre, S. Groh, G. Drexlin, F. Glueck, A. Huber, A. W. P. Poon, M. Steidl, N. Steinbrink, and C. Weinheimer. "Sensitivity of Next-Generation Tritium Beta-Decay Experiments for keV-Scale Sterile Neutrinos." In: *JCAP* 1502.02 (2015), p. 020. DOI: 10.1088/1475-7516/2015/02/020. arXiv: 1409.0920 [physics.ins-det].

[Mye+15] E. G. Myers, A. Wagner, H. Kracke, and B. A. Wesson. "Atomic Masses of Tritium and Helium-3." In: *Phys. Rev. Lett.* 114 (1 Jan. 2015), p. 013003. DOI: 10.1103/PhysRevLett.114.013003.

[NAS15] NASA. *What Is Pluto?* 2015. URL: https://www.nasa.gov/audience/forstudents/5-8/features/nasa-knows/what-is-pluto-58.html (visited on 08/16/2018).

[Nav16a] R. Nave. *Fermi Theory of Beta Decay*. 2016. URL: http://hyperphysics.phy-astr.gsu.edu/hbase/quantum/fermi2.html (visited on 08/16/2018).

[Nav16b] R. Nave. *Neutral Currents and the Z0*. http://hyperphysics.phy-astr.gsu.edu/hbase/Particles/neucur.html. 2016.

[Par18] D. Parno. *KATRIN: Toward a High-Precision Neutrino-Mass Determination with Tritium*. June 2018. DOI: 10.5281/zenodo.1287933.

[Pau] W. Pauli. "Pauli letter collection: letter to Lise Meitner." Typed copy.

[Pla83] R. L. Plackett. "Karl Pearson and the chi-squared test." In: *International Statistical Review Revue Internationale de Statistique* (1983), pp. 59–72.

[Pol18] A. Pollithy. "First Tritium Background." Analysis Workshop Munich 2018. 2018.

[Pon57] B. Pontecorvo. "Mesonium and antimesonium." In: *Zhur. Eksptl'. i Teoret. Fiz.* 33 (Aug. 1957).

[PR15] H. Päs and W. Rodejohann. "Neutrinoless double beta decay." In: *New Journal of Physics* 17.11 (2015), p. 115010.

[PW65] A. A. Penzias and R. W. Wilson. "A measurement of excess antenna temperature at 4080 Mc/s." In: *The Astrophysical Journal* 142 (1965), pp. 419–421.

[Rei+60] F. Reines, C. L. Cowan, F. B. Harrison, A. D. McGuire, and H. W. Kruse. "Detection of the Free Antineutrino." In: *Phys. Rev.* 117 (1 Jan. 1960), pp. 159–173. DOI: 10.1103/PhysRev.117.159.

[Roc18] F. Rocatti. "Novel simulation techniques for a sterile neutrino search with KATRIN." MA thesis. Technische Universität München, Ludwig-Maximilians-Universität, 2018.

[RW83] W. W. Repko and C.-e. Wu. "Radiative corrections to the end point of the tritium β decay spectrum." In: *Phys. Rev. C* 28 (6 Dec. 1983), pp. 2433–2436. DOI: 10.1103/PhysRevC.28.2433.

[SBN06] N. Severijns, M. Beck, and O. Naviliat-Cuncic. "Tests of the standard electroweak model in nuclear beta decay." In: *Reviews of Modern Physics* 78.3 (2006), p. 991.

[Sch18] L. Schlüter. *First Tritium -Stacking Runs-*. June 2018.

[Sco35] F. A. Scott. "Energy Spectrum of the Beta-Rays of Radium E." In: *Phys. Rev.* 48 (5 Sept. 1935), pp. 391–395. DOI: 10.1103/PhysRev.48.391.

[Sin03] P. K. Sinervo. "Definition and treatment of systematic uncertainties in high energy physics and astrophysics." In: *Proc. Conf. on Statistical Problems in Particle Physics, Astrophysics and Cosmology (PHYSTAT 2003), Stanford, CA, 8–11 September*. Citeseer. 2003, pp. 122–129.

[Sir67] A. Sirlin. "General Properties of the Electromagnetic Corrections to the Beta Decay of a Physical Nucleon." In: *Phys. Rev.* 164 (5 Dec. 1967), pp. 1767–1775. DOI: 10.1103/PhysRev.164.1767.

[SJF00] A. Saenz, S. Jonsell, and P. Froelich. "Improved Molecular Final-State Distribution of $HeT+$ for the β-Decay Process of $T2$." In: *Phys. Rev. Lett.* 84.2 (Jan. 2000), pp. 242–245. DOI: 10.1103/PhysRevLett.84.242.

[Sle16] M. Slezák. "Monitoring of the energy scale in the KATRIN neutrino experiment." In: (2016).

[Sta+12] D. Stancil, P. Adamson, M. Alania, L. Aliaga, M. Andrews, C. A. Del Castillo, L. Bagby, J. Bazo Alba, A. Bodek, D. Boehnlein, et al. "Demonstration of communication using neutrinos." In: *Modern Physics Letters A* 27.12 (2012), p. 1250077.

[Tur16] S. Turck-Chièze. "The standard solar model and beyond." In: *Journal of Physics: Conference Series*. Vol. 665. 1. IOP Publishing. 2016, p. 012078.

[Wei18] C. Weinheimer. "Bias through stacking for different values of qUi." Analysis Workshop Munich 2018. 2018.

[Wen+10] R. Wendell et al. "Atmospheric neutrino oscillation analysis with subleading effects in Super-Kamiokande I, II, and III." In: *Phys. Rev.* D81 (2010), p. 092004. DOI: 10.1103/PhysRevD.81.092004. arXiv: 1002.3471 [hep-ex].

[Wil91a] D. H. Wilkinson. "Small terms in the beta-decay spectrum of tritium." In: *Nucl. Phys.* A526 (1991), pp. 131–140. DOI: 10.1016/0375-9474(91)90301-L.

[Wil91b] D. Wilkinson. "Small terms in the beta-decay spectrum of tritium." In: *Nuclear Physics A* 526.1 (1991), pp. 131–140. ISSN: 0375-9474. DOI: https://doi.org/10.1016/0375-9474(91)90301-L.

[Win13] W. Winter. "Neutrino mass hierarchy determination with IceCube-PINGU." In: *Phys. Rev.* D88.1 (2013), p. 013013. DOI: 10.1103/PhysRevD.88.013013. arXiv: 1305.5539 [hep-ph].